Mollo, S., Forni, F., Bachmann, O., Blundy, J. D., De Astis, G., & Scarlato, P. (2016). Trace element partitioning between clinopyroxene and trachy-phonolitic melts: A case study from the Campanian ignimbrite (campi flegrei, Italy). *Lithos*, *252-253*, 160-172. https://doi.org/10.1016/j.lithos.2016.02.024

Trace element partitioning between clinopyroxene and trachy-phonolitic melts: A case study from the Campanian Ignimbrite (Campi Flegrei, Italy)

S. Mollo[1,2], F. Forni[3], O. Bachmann[3], J. D. Blundy[4], G. De Astis[2], P. Scarlato[2]

[1]Dipartimento di Scienze della Terra, Sapienza-Università di Roma, P.le Aldo Moro 5, 00185 Roma, Italy

[2] Istituto Nazionale di Geofisica e Vulcanologia, Roma, Italy

[3] Department of Earth Sciences, Institute of Geochemistry and Petrology, ETH, Zurich, Switzerland

[4] School of Earth Sciences, University of Bristol, Bristol, United Kingdom

Corresponding author:
Silvio Mollo
Sapienza-Università di Roma
Dipartimento di Scienze della Terra
P.le Aldo Moro 5
00185 Roma, Italy
e-mail silvio.mollo@uniroma1.it

Abstract

The partitioning of trace elements between crystals and melts provides an important petrogenetic tool for understanding magmatic processes. We present trace element partition coefficients measured between clinopyroxene phenocrysts and trachy-phonolitic magmas at the Campi Flegrei (Italy), whose late Quaternary volcanism has been characterized by two major caldera-forming events (Campanian Ignimbrite at ~39 ka, and the Neapolitan Yellow Tuff at ~15 ka). Our data indicate that the increase of trivalent rare earth elements and yttrium into the crystal lattice M2 site is facilitated by the charge-balancing substitution of Si^{4+} with Al^{3+} on the tetrahedral site. Higher concentrations of tetravalent and pentavalent high field strength elements on the M1 site are also measured when the average charge on this site is increased by the substitution of divalent cations by Al^{vi}. In contrast, due to these charge balance requirements, divalent transitional elements become less compatible within the crystal lattice. On the basis of the lattice strain theory, we document that the incorporation of rare earth elements and yttrium in clinopyroxene is influenced by both compositional and physical parameters. Data from this study allow to update existing partitioning equations for rare earth elements in order to construct a self-consistent model for trachy-phonolitic magmas based on the lattice strain theory. The application of this model to natural products from the Campanian Ignimbrite, the largest caldera-forming eruption at the Campi Flegrei, reveals that the complex rare earth element pattern recorded by the eruptive products can be successfully described by the stepwise fractional crystallization of clinopyroxene and feldspar where the clinopyroxene-melt partition coefficient changes progressively as a function of the physicochemical conditions of the system.

Keywords: clinopyroxene-melt trace element partitioning; lattice strain theory; trachy-phonolitic magmas; Campi Flegrei.

Introduction

Clinopyroxene is one of the most important constituents of igneous rocks and its crystallization behaviour impacts significantly the composition of magmas. The partitioning of trace elements between clinopyroxene and melt is frequently used in petrological and geochemical studies to better understand magma differentiation processes, such as fractional or equilibrium crystallization, assimilation, and partial melting. For simplicity, the clinopyroxene-melt partition coefficient [$D_i = {}^{xls}(I)/{}^{melt}(I)$ on a weight basis] is generally assumed to be constant for magma modelling. However, this simple approximation does not take into account for the effects of crystal and melt compositions, as well as the physical conditions of the system on trace element partitioning. Wood and Blundy (1997) showed for the first time that partition coefficients of rare earth elements (REE) can be modelled as a function of composition of the crystal (X_{Mg}^{M1}), *Mg*-number of the melt [$Mg\#^{melt} = X_{Mg}^{melt}/(X_{Fe}^{melt} + X_{Mg}^{melt})$], pressure (*P*) and temperature (*T*). Crystal chemistry influences both the dimensions of the M2 site, into which REE partition, and the molar fraction of the hypothetical REE end-member, such as $REEMgAlSiO_6$. Blundy et al. (1998) and Bennett et al. (2004) also argued that D_{REE} is dependent on X_{Na}^{M2} due to the higher incorporation of Na^+ in M2 with increasing *P*, for example via the hypothetic end-member $Na_{0.5}REE_{0.5}MgSi_2O_6$. Furthermore, Hill et al. (2000), Wood and Trigila (2001) and Wood and Blundy (2001) documented a close relationship between REE partitioning and the concentration of tetrahedrally-coordinated aluminum in clinopyroxene, as required for charge balance. Sun and Liang (2012) derived a predictive model in which D_{REE} is positively correlated with X_{Al}^{iv} and X_{Mg}^{M2}, and negatively correlated with *T* and H_2O dissolved in the melt. Gaetani et al. (2003) attributed the decrease of D_{REE} with increasing H_2O to the depolymerizing effect of water on the melt structure. Moreover, complementary studies of Gaetani (2004) and Huang et al. (2006) pointed out that the melt structure becomes dominantly important

below a threshold value of the number of non-bridging oxygens per tetrahedral cations *(NBO/T*) corresponding to 0.4. As a whole, results from previous works highlight that the partitioning of trace elements between clinopyroxene and melt is governed by complex mechanisms whose effects and magnitudes on D_i depend on specific compositional and physical parameters that are still poorly understood for a significant number of natural cases.

In this study, we present a new set of apparent partition coefficients calculated for clinopyroxene phenocrysts in equilibrium with trachytic and phonolitic compositions from the Campi Flegrei (Italy). Despite the highly explosive nature of these magmas and their common involvement in hazardous volcanic settings, little attention has been given to the most important parameters that influence the partitioning of trace elements (however, see Pappalardo et al., 2008; Fedele et al., 2009). On the basis of the lattice strain theory derived by Blundy and Wood (1994), it has been determined to what extent the physicochemical conditions of the system may influence the partitioning of trace elements. Through an improved version of the predictive equations of Wood and Blundy (1997), we have also modelled the complex trace element compositions of several rock samples from the Campanian Ignimbrite, one of the largest late Quaternary volcanic eruptions in Europe.

Geological background

The Campi Flegrei, located within the Campanian Plain, belong to the potassic alkaline volcanic province of central Italy. Volcanism is still active, as demonstrated by fumarolic and seismic activity, and by recurrent episodes of unrest in the past 30 years (Orsi et al., 1999 and references therein). The highly explosive behaviour of magmas represents a continuous threat to more than one million people living in the city of Naples and its densely inhabited suburbs. This makes the Campi Flegrei one of the most dangerous volcanic systems in the world.

The caldera is a resurgent nested structure formed during two major collapses related to the eruptions of the Campanian Ignimbrite (CI) and the Neapolitan Yellow Tuff (NYT). Seismic reflections indicate the presence of a discontinuity at 7.5 km depth, where seismic velocities are consistent with values expected for a magma body set in a densely fractured volume of rock (Zollo et al., 2008). Petrological and melt inclusion studies suggest that differentiated alkaline melts formed dominantly through fractional crystallization from a more mafic parental magma, likely emplaced at depths between 4 and 8 km, with little assimilation of surrounding crust (Signorelli et al., 2001; Webster et al., 2003; Marianelli et al., 2006; Pabst et al., 2008; D'Antonio, 2011).

The Campanian Ignimbrite eruption (~39 ka; De Vivo et al., 2001) is regarded as the dominant event in the history of the Campi Flegrei with an initial areal distribution of ~30,000 km^2 (Rolandi et al., 2003). It consists of ~200 km^3 of pyroclastic-fall and pyroclastic-flow deposits (Civetta et al., 1997). The composition of the erupted products changed from trachyte to phonolite during the eruption. Phase equilibria data, geothermometry, and fluid inclusion analysis, suggest an overall thermal path of the magma from 840 to 1,080 °C (Fulignati et al., 2004; Marianelli et al., 2006; Fowler et al., 2007; Fedele et al., 2009; Masotta et al., 2013). Melt inclusion measurements and hygrometric predictions indicate a melt-water concentration ranging from 3 to 6 wt.% (Signorelli et al., 2001; Webster et al., 2003; Marianelli et al., 2006; Mollo et al., 2014). On the basis of these heterogeneous petrological information, it has been proposed that the CI magma evolved in a thermally and chemically zoned magmatic reservoir (Pappalardo et al., 2008; Pappalardo and Mastrolorenzo, 2012).

The Neapolitan Yellow Tuff eruption (~15 ka ; Deino et al., 2004) was the second more recent phreatoplinian event in the history of the Campi Flegrei. It erupted ~40 km^3 of pyroclastic-fall and pyroclastic-flow deposits dispersed over an area of more than ~1,000 km^2 (Orsi et al. 1992). The erupted products are characterized by latitic to trachytic compositions. The vent for the NYT eruption was located inside the caldera formed during collapse of the CI eruption, resulting in a final caldera that covered an area of ~90 km^2 (Orsi et al., 2009).

Analytical methods

Field emission gun scanning electron microscope (FE-SEM) images and electron probe micro analyses (EPMA) of twelve clinopyroxenes were collected at the HPHT Laboratory of Experimental Volcanology and Geophysics of the Istituto Nazionale di Geofisica e Vulcanologia (INGV) in Rome, Italy. Images were obtained through the backscattered electron (BSE) mode of a JEOL 6500F FE-SEM equipped with an energy-dispersive spectrometer (EDS) detector. Microprobe analyses were performed with a JEOL-JXA8200 EPMA equipped with five spectrometers. The beam diameter was ~1 μm with a counting time of 20 and 10 s on peaks and background respectively. The following standards were used: jadeite (Si and Na), corundum (Al), forsterite (Mg), andradite (Fe), rutile (Ti), orthoclase (K), barite (Ba), apatite (P), spessartine (Mn) and chromite (Cr). Sodium and potassium were analyzed first to prevent alkali migration effects. The precision of the microprobe was measured through the analysis of well-characterized synthetic oxides and minerals. Data quality was ensured by analyzing standard materials as unknowns. Based on counting statistics, analytical precision was better than 5% for all cations.

Major and trace elements of whole-rocks, and trace elements of clinopyroxene phenocrysts were measured at the Institute of Geochemistry and Petrology of the ETH Zürich, Switzerland. For the whole-rock analyses 1.5 g of powdered sample was heated to 950 °C for 2 h in a chamber furnace and then weighed to determine the loss on ignition (LOI). The ignited material was charged in a Pt-Au crucible and fused with a 1:5 Lithium-Tetraborate mixture using a Claisse M4® fluxer. The fused disk was analysed for major elements using a wave-length dispersive X-ray fluorescence spectrometer (WD-XRF; Axios PANanalytical) equipped with five diffraction crystals. Calibration was based on thirty certified international standards of predominantly igneous and metamorphic rocks. Trace element analyses of both whole-rock disks and clinopyroxene phenocrysts were performed through a 193 nm excimer laser coupled with a second generation two-volume constant

geometry ablation cell (Resonetics:S-155LR) and a high-sensitivity, sector-field inductively-coupled plasma mass spectrometer (ICP-MS; Thermo:Element XR). Points with a spot size of 45 μm were set on chemically homogeneous portions of the material (i.e., clinopyroxene cores) previously analyzed by EPMA, and ablated with a pulse rate of 10 Hz and an energy density of 3.5 J/cm^3 for 40 sec. The isotopes were analyzed relative to an internal standard of known composition (i.e., NIST612). A second standard (i.e., GSD-1G) was used as an unknown to check the quality of data during each analytical run. ^{43}Ca or ^{29}Si were used as internal standards for clinopyroxene and whole-rock analyses, respectively, in order to recover the concentrations of light and heavy rare earth elements (REE divided in LREE and HREE), high field strength elements (HFSE), large ion lithophile elements (LILE) and transition elements (TE). The precision of individual analyses varied depending upon a number of factors, e.g., the element and isotope analyzed as well as the homogeneity of the ablated material. However, the 1 sigma errors calculated from variations in replicate analyses of crystals and whole-rock disks were invariably several times larger than the fully integrated 1 sigma errors determined from counting statistics alone.

Sample description

Sampled rocks belong to twelve pyroclastic deposits at the Campi Flegrei characterized by variable proportions of juvenile material (i.e., pumices, scoriae, spatter clasts, fiamme and obsidians), variably porphyritic textures (10-25 vol.% of phenocrysts), and the ubiquitous occurrence of clinopyroxene, biotite, K-feldspar, plagioclase, opaques, and rare apatite. Samples were collected from different outcrops in order to fully characterize the compositions of clinopyroxene phenocrysts and host magmas of pre-CI, CI, post-CI, NYT, and post-NYT eruptions (see Table 1S for the locations). Major and trace element concentrations measured for crystals and melts are reported in Tables 1S and 2S, respectively. We present our data in comparison with those of Pappalardo et al. (2008) and Fedele et al. (2009) that provided a complete dataset comprising whole-rock analyses,

clinopyroxene chemistries, apparent partition coefficients for REE, and lattice strain parameters (see below) of four additional rock samples from the Campanian Ignimbrite eruption.

Whole-rock analyses show increasing SiO_2 contents (57-62 wt.%) with decreasing CaO (1.8-5.3 wt.%) and $Mg\#^{melt}$ (16-40). All compositions are also rich in alkali (Na_2O+K_2O = 11-14 wt.%). In the TAS (total alkali vs. silica; Le Bas et al., 1986) diagram, samples are classified as trachytes and phonolites, in agreement with most of the differentiated alkaline products at Campi Flegrei (Fig. 1a). Whole-rocks exhibit a variable degree of differentiation that, in terms of trace element concentrations, reproduces well the evolutionary behaviour of magmas (Fig. 1b). The increase of REE is commonly associated with a significant increase in Th, U, Nb, Ta, Zr and Hf, and decrease in Sr testifying to an increased plagioclase fractionation (Table 2S).

Clinopyroxenes occur as euhedral phenocrysts (longest size dimensions > 0.3 mm) with diopsidic compositions (Morimoto, 1988). Al^{iv} (0.05-0.13 apfu) is positively correlated with Ti^{+4} (0.01-0.04 apfu) and negatively correlated with $Mg\#^{cpx}$ (0.73-0.84). The ratio of octahedrally-coordinated to tetrahedrally-coordinated aluminium cations is less than 1 in all phenocrysts, indicating preferential incorporation of Al^{iv} at low pressure crystallization conditions (Muñoz and Sagredo, 1974; Putirka, 1996; Mollo et al., 2011b). The ratio of Fe^{3+}/Fe^{2+} in clinopyroxenes, as calculated from stoichiometry, ranges between 0 and 0.5 with values identical to those experimentally-derived for magmas at Campi Flegrei equilibrated at NNO+1 and NNO+2 oxygen fugacity (Fabbrizio and Carroll, 2008; Masotta et al., 2013). Diopside vs. hedenbergite (Fig. 1c) and Ce vs. Y (Fig. 1d) diagrams suggest that major and trace elements of our clinopyroxenes capture most of the geochemical evolution of phenocrysts at Campi Flegrei.

Apparent trace element partition coefficients were measured for pre-CI, CI, post-CI, NYT, and post-NYT samples using clinopyroxene core and whole-rock analyses that were found to be in equilibrium (see below) and are reported in Table 3S. The most important changes of D_i can be summarized as follows: (i) LREE (e.g., $D_{La} \leq 0.27$) are more incompatible than HREE (e.g., $D_{Dy} \leq 1.67$); (ii) TE are always compatible within clinopyroxene (e.g., $D_{Co} \leq 10.07$); (iii) pentavalent

207 HFSE cations are more incompatible (D_{Nb} and $D_{Ta} \leq 0.05$) that tetravalent HFSE cations (D_{Zr} and
208 $D_{Hf} \leq 0.87$) and; (iv) LILE are generally incompatible (e.g., $D_{Sr} \leq 0.8$) with the exception of one
209 sample ($D_{Sr} = 1.39$ for PM2).
210
211 **Assessment of equilibrium crystallization conditions**
212
213 Laboratory investigations of clinopyroxene-melt partition coefficients are generally designed to
214 guarantee the achievement of equilibrium between crystals and melts. The initial rate of cooling and
215 the time duration of experiments are set to ensure that the melt supplies nutrients at equilibrium
216 proportions to the growing crystals. The experimental charges are then quenched at very fast
217 cooling rates and the system is almost instantaneously "frozen-in" (e.g., quenching rate of
218 2,000 °C/min; Freda et al., 2008). Due to the use of rapid quenching conditions, disequilibrium
219 processes may only operate at the nanometre scale, leading to the formation of a diffusive boundary
220 layer with thickness orders of magnitude lower that the analytical spot size used for major and trace
221 element measurements (e.g., Mollo et al., 2012). On the other hand, apparent partition coefficients
222 obtained from natural samples measuring the compositional ratios between bulk phenocrysts and
223 host lavas (i.e., whole-rock analyses) are potentially biased by contamination or disequilibrium
224 processes. Even when single point analyses are carried out at the crystal-melt interface, the
225 compositional zoning of minerals and surrounding glasses can make the accurate determination of
226 D_i extremely difficult. The entrapment of melt in rapidly growing crystals may increase the value of
227 D_i by up to 3 orders of magnitude (Kennedy et al., 1993). Additionally, rapid crystal growth
228 conditions are not necessary accompanied by detectable melt entrapments or crystal discontinuities
229 and, under such circumstances, disequilibrium values of D_i can exhibit variations in the same order
230 of magnitude of equilibrium data (Mollo et al., 2013a).
231 For the purpose of this study, we have accurately inspected each phenocryst and coexisting
232 glass using SEM and EPMA, in order to make sure that the occurrence of melt inclusions, crystal

zoning and/or melt diffusion phenomena were kept to a minimum. Clinopyroxenes are generally euhedral with well-defined edges and without evident zoning patters (Fig. 2a). However, microprobe compositional profiles reveal the occurrence of chemical heterogeneities at the crystal-melt interface (Fig. 2b and Table 5S). A diffusive boundary layer occurs into the glass next to clinopyroxene surface. This thin diffusive boundary layer is enriched in chemical species less compatible in clinopyroxene crystal lattice (e.g., Al and Na). Concentration–dependent partitioning produces crystal growth layers that respond to the chemical gradients in the melt, producing Al and Na enrichments in clinopyroxene that are identical to those experimentally documented by cooling rate studies (Lofgren et al., 2006; Mollo et al., 2013b). Compositional perturbations at the crystal rim also suggest that, at the closure temperature of the crystal growth (i.e., $T_{final} << T_{liquidus}$), the free energy difference between the crystal surface and the liquid was large enough that diffusion became the rate-controlling process (Watson and Muller, 2009). Due to the high explosivity of eruptions at Campi Flegrei, phenocrysts underwent typically high degrees of undercooling during magma ascent in the volcanic conduit and eruption to the surface (Pappalardo and Mastrolorenzo, 2012 and references therein). Mollo et al. (2013b) proposed an equilibrium model based on the difference (Δ) between diopside+hedenbergite (DiHd) components predicted for clinopyroxene via regression analyses of clinopyroxene-liquid pairs in equilibrium conditions, with those measured in the analyzed phenocrysts. Mollo and Masotta (2014) successfully tested this model on trachytic and phonolitic compositions obtained at both equilibrium and disequilibrium conditions. Calculations performed using clinopyroxene rim and coexisting melt compositions yield values of 0.11-0.16 (Fig. 2b) that are considerably higher than those measured at near-equilibrium conditions (ΔDiHd $\leq$ 0.02). This suggests that D_i values measured at the crystal-melt interface results from disequilibrium partitioning due to the effect of rapid magma decompression and degassing at the time of eruption (e.g., Lanzafame et al., 2013; Mollo et al., 2015a). On the other hand, it is reasonable to infer that, over the timescale of magma chamber evolution and in absence of perturbation phenomena (e.g., magma mixing), early-formed clinopyroxene phenocrysts may have crystallized in equilibrium with

259 the host magma, despite the occasional occurrence of chemical heterogeneities or melt inclusions in
260 crystal that tend to reduce the accuracy of D_i calculations. In light of this, apparent trace element
261 partition coefficients have been calculated by the analyses of bulk phenocrysts and whole-rock
262 compositions (e.g., Schnetzler and Philpotts 1970; Nagasawa and Schnetzler 1971; Nagasawa 1973;
263 Mahood and Hildreth 1983; Lemarchand et al. 1987; Villemant 1988).

264 Experiments and thermodynamic studies have clearly documented that clinopyroxene is the
265 liquidus phase of trachytic and phonolitic melts (Fowler et al., 2007; Fabbrizio and Carroll, 2008;
266 Masotta et al., 2013, Del Bello et al., 2014). Under such circumstances, near-liquidus crystals are
267 represented by early-formed cores of large phenocrysts that likely equilibrated with the host magma
268 (i.e., whole-rock analysis) in terms of major and trace element concentrations (see for example the
269 studies of Armienti et al., 2007; Masotta et al., 2010; Mollo et al., 2011a; Lanzafame et al., 2013;
270 Scarlato et al., 2014). In this respect, Fig. 2b shows the development of an almost homogeneous
271 plateau composition at the clinopyroxene core that suggests near-equilibrium crystallization and
272 excludes chemical perturbations in the original magma. Tests conducted with the model of Mollo et
273 al. (2013b) yield ΔDiHd values between 0 and 0.02 testifying to equilibrium or near-equilibrium
274 conditions between phenocryst core and whole-rock data that were therefore used for our D_i
275 calculations (see also ΔDiHd values reported in Table 1S).

276 As stated above, the differentiation of magmas mostly occurs at shallow crustal levels (100-
277 300 MPa) where the effect of pressure on near-liquidus clinopyroxene-melt partition coefficients is
278 expected to be minimal. Thermodynamic data derived by the lattice strain model indicate that the
279 influence of P on D_i can be considered negligible at pressures lower than 500 MPa (Blundy and
280 Wood, 2003). It could be argued that REE partitioning is also sensitive to sodium in clinopyroxene,
281 which in turn varies with pressure (Blundy et al., 1995; Bennett et al., 2004). However, the control
282 of Na^+ on D_{REE} is dominant only at mantle pressures ($\geq$ 3 GPa) where sodium concentration (Na_2O
283 = 2.2-13.5 wt.%; data from Klemme et al., 2002; Bennett et al., 2004; Marks et al., 2004) is one to
284 two order of magnitude higher than that measured in our phenocrysts (Na_2O = 0.15-0.56 wt.%;

285 Table 1S). Therefore, in terms of physical parameters, temperature is likely the most important
286 variable that can influence D_i at the crystallization conditions of magmas. To estimate the
287 equilibration temperatures and pressures of clinopyroxene-melt pairs from this study (Table 1S), we
288 have used the thermometers and barometers of Masotta et al. (2013) specifically calibrated for
289 trachytic and phonolitic compositions. A melt-water content of 3 wt.% has been set in the model, in
290 agreement with most of the water concentrations measured by melt inclusion studies on Campi
291 Flegrei (Signorelli et al., 2001; Webster et al., 2003; Marianelli et al., 2006). We have established
292 that a water change of ±2 wt.% produces temperature and pressures variations of only ±12 °C and
293 ±15 MPa, which are well below the errors of estimate of the thermometer (±24 °C) and barometer
294 (±114 MPa). Results from calculations indicate that our clinopyroxenes crystallized at temperatures
295 and pressures of 840-1,020 °C and 85-309 MPa (Table 1S), in close correspondence with those
296 (840-1,080 °C and 20-300 MPa) derived for trachy-phonolitic products belonging to the Campanian
297 Ignimbrite eruption (Fedele et al., 2009; Masotta et al., 2013).
298
299 **Discussion**
300
301 Trace element partition coefficients
302
303 The dependence of trace element partition coefficient on tetrahedrally-coordinated aluminium has
304 been the focus of many studies on clinopyroxene (Lindstrom 1976; Ray et al. 1983; Hart and Dunn
305 1993; Forsythe et al. 1994; Lundstrom et al. 1994, 1998; Skulski et al. 1994; Blundy et al. 1998;
306 Hill et al. 2000; Wood and Trigila 2001; Sun and Liang, 2012; 2013; Mollo et al., 2013a; Yao et al.,
307 2013; Scarlato et al., 2014). In Fig. 3, the close correspondence between D_i and Al^{iv} for
308 representative HFSE, REE and TE, is confirmed and extended to trachytic and phonolitic magmas.
309 Note that the gray fields in Fig. 3 indicate that our D_i values are consistent with those previously
310 calculated for magmas at Campi Flegrei (data from Pappalardo et al., 2008 and Fedele et al., 2009).

From a crystallochemical point of view, HFSE enter the smaller M1 octahedral site, and the correlation between D_{HFSE} and Al reflects the increasing charge on this site with increasing $CaAl_2SiO_6$ and $CaFeAlSiO_6$ substitution, i.e., with increasing replacement of Mg^{2+} by Fe^{3+} and Al^{3+} (Wood and Trigila, 2001). Thus, entry of +4 and +5 ions into M1 is enabled by the substitution of Al^{+3} for Si^{+4} in the tetrahedral site (Hill et al., 2000; Mollo et al., 2013a). In the case of trivalent trace elements, REE and Y enter the large M2 site that, apart from minor amounts of Na^{+}, is almost exclusively occupied by Ca^{2+}, Mg^{2+}, and Fe^{2+}. Data plotted in Fig. 3 show a clear positive correlation between D_{La} and Al^{iv} that has been extensively documented under both equilibrium and disequilibrium crystal growth conditions (Gaetani and Grove, 1995; Blundy et al., 1998; Mollo et al., 2013a; Scarlato et al., 2014). The dependence of REE partitioning on tetrahedral aluminium reflects an increased ease of locally balancing the excess charge at M2 as the number of surrounding Al^{iv} atoms increases. For example, the concentration of La in our clinopyroxenes progressively increases from 8 to 46 ppm as the molar Al/Si ratio decreases from 0.11 to 0.05 (Tables 1S and 2S). This matches with the consideration that clinopyroxenes can accommodate REE simply by adjusting their Al/Si ratios, without producing an energetically unfavourable vacancy (Hill et al., 2000; Wood and Trigila, 2001). The importance of site charge for achieving local charge balance is provided by the different behaviour of Sr and Co as divalent cations entering M2 and M1 sites, respectively. Since charge on the M2 site is the same in both $CaMgSiO_2$ and $CaAl_2SiO_6$, no correlation is found between D_{Sr} and tetrahedrally-coordinated aluminum (cf. Hill et al., 2000). In contrast, the M1 site requires an increased net charge (2+ to 3+) to balance the increase in Al substitution for Si (cf. Mollo et al., 2013a), such that Co becomes less compatible as $CaAl_2SiO_6$ content increases (Fig. 3).

The lattice strain model

Fig. 4 shows that our apparent partition coefficients for REE and Y lie on parabola-like curves of Onuma diagrams (Onuma et al., 1968), resembling the regular trajectories found by Pappalardo et al. (2008) and Fedele et al. (2009) for magmas at Campi Flegrei. The height of the parabola depends on the crystal composition (Matsui et al., 1977; Blundy and Wood, 1994; 2003) and the physical conditions of the system (Blundy and Wood, 2001; Sun and Liang, 2012). Blundy and Wood (1994) provided a quantitative model for the parabolic trend of an isovalent series of cations with radius, r_i, entering crystal lattice site M, where the partition coefficient, D_i, can be described in terms of (i) the radius of the site, r_0, (ii) the elastic response of that site, E (as measured by Young's Modulus), to lattice strain caused by cations that are larger or smaller than r_0, and (iii) the strain-free partition coefficient, D_0, for a (fictive) cation with radius r_0:

$$D_i = D_0 \exp\left(\frac{-4\pi E N_A \left(\frac{r_0}{2}(r_i - r_0)^2 + \frac{1}{3}(r_i - r_0)^3 \right)}{RT} \right) \quad (1)$$

In Eqn. (1), N_A is Avogadro's number (6.022×10^{23} mol^{-1}), R is the universal gas constant (8.3145 J mol^{-1} K^{-1}), and T is the temperature (in Kelvin). The effective use of the lattice strain model requires partition coefficients for a large range of isovalent cations of appropriate ionic radii for substitution into the M site. Therefore, to obtain reliable estimates and minimize the standard error, we focused on r_0, D_0, and E for the partitioning of trivalent REE and Y cations (Table 3S), as they form the largest group of isovalent elements in our analytical dataset. Except for one sample with $D_0^{3+} \approx 1$, we observe that, as a general rule, the peak position of our partitioning parabolas corresponds to $D_0^{3+} \geq 1$ when $Al^{iv} \geq 0.09$ apfu and $T \leq 950$ °C (Tables 1S and 3S and Fig. 4). Otherwise, the peak position can be alternatively higher or lower than 1 as a function of Al^{iv} and T, in agreement with the observation that these parameters have opposing effects on trace element partitioning (cf. Sun and Liang, 2012). Fitting of the parabolic trends indicates a good agreement between modelled and

360 measured values of D_0^{3+} (Table 4S and Fig. 4), suggesting the attainment of a thermodynamic
361 equilibrium between phenocrysts and host magmas.

362 At first, D_0^{3+} and D_{REE} were taken to be independent of the Al^{iv} content in clinopyroxene
363 due to assumed complete short-range order between REE on M2 site and Al in T site in the
364 molecule $REEMgAlSiO_6$ (e.g., Wood and Blundy, 1997). Subsequently, this assumption has since
365 been found to be an oversimplification (Wood and Trigila, 2001; Hill et al., 2000; Tuff and Gibson,
366 2007, Mollo et al., 2013a; Scarlato et al., 2014), probably due to more complex charge-balance
367 mechanisms than simple short-range order (Wood & Blundy, 2001). In Fig. 5, lattice strain-free
368 partition coefficients for clinopyroxenes in trachy-phonolitic melts are compared with those
369 obtained by previous studies on ultramafic, mafic and silicic compositions. D_0^{3+} increases
370 significantly with increasing tetrahedral aluminium, providing clear evidence of the effect of crystal
371 composition on REE and Y partitioning. Importantly, three different trends are depicted in Fig. 5 for
372 different bulk melt chemistries. The value of D_0^{3+} and the slope of each single trend increase as a
373 function of the melt composition (i.e., SiO_2), suggesting that the control of Al^{iv} on D_0^{3+} is mediated
374 by the increasing silicic character of the bulk melt (Fig. 5). Gaetani (2004) observed that the
375 magnitude of the partition coefficient correlates with the degree of melt polymerization due to a
376 melt structural influence on trace element partitioning. The complementary results from Gaetani
377 (2004) and Huang et al. (2006) noted that melt structure affects the trace element compatibility only
378 if $[NBO/T]^{melt} < 0.4$. This is confirmed by our data showing a somewhat higher D_0^{3+} for a lower
379 $[NBO/T]^{melt}$ (Fig. 6a), although this parameter may not provide a comprehensive description of melt
380 structure at a level relevant to trace element partitioning (e.g., Bennett et al., 2004). On this basis,
381 Huang et al. (2006) found that D_0^{3+} is better correlated with the ratio of molar $[Ca^{2+}/(M^{+}+M^{2+})]^{melt}$,
382 where M^{+} and M^{2+} are, respectively, Na^{+} and K^{+}, and Fe^{2+}, Ca^{2+} and Mg^{2+} of the melt given as
383 percentages. Because of the similarity in ionic radius (and charge), REE^{3+} are more likely to
384 substitute for Ca^{2+} in the melt than Mg^{2+}, Fe^{2+}, or alkalis, so that the value of D_{REE} decreases
385 according to the following exchange reaction (Huang et al., 2006):

386

387 $[REE_{2/3}MgSi_2O_6]^{cpx} + [Ca\text{-}NBO]^{melt} \leftrightarrow [CaMgS_2O_6]^{cpx} + [REE_{2/3}\text{–}NBO]^{melt}$ (2)

388

389 Our data show that, for higher values of $[Ca^{2+}/(M^{+}+M^{2+})]^{melt}$, there is an effective increase in the
390 number of large structural sites critically important to accommodating large trace element cations in
391 the melt, serving to reduce the partition coefficient (Fig. 6b). However, due to simultaneous effects
392 of crystal and melt compositions on REE and Y partitioning, data in Fig. 6b do not align on a single
393 linear fit for the substitution reaction described by Eqn. (2). To eliminate such an effect, some
394 experiments should be designed for the comparison between clinopyroxenes with similar crystal-
395 chemical formulas and compositionally distinct host melts (cf. Huang et al. 2006).

396

397 Testing the model of Wood and Blundy (1997)

398

399 Most of the mathematical expressions used to model the evolutionary behaviour of magma assume
400 that the value of D_i remains constant throughout the entire differentiation process. This raises issues
401 for petrological and geochemical modelling to (i) adopt the best possible partition coefficients, (ii)
402 evaluate the extent to which these partition coefficients vary in the course of magma differentiation,
403 (iii) find the physicochemical parameters that closely describe the variance of D_i, and (iv) derive a
404 good predictive model that is easy and rapid to use (e.g., based on microprobe analyses). In order to
405 address all these issues, an increasing number of predictive equations for D_i have been derived in
406 the last decades on the basis of thermodynamic approaches (e.g., Wood and Blundy, 1997, 2011;
407 Hill et al., 2011), linear least squares regression analyses (e.g., Forsythe et al., 1994; Skulski et al.,
408 1994; Gaetani and Grove, 1995) and multivariable nonlinear least squares analyses (Yao et al.,
409 2012; Sun and Liang, 2012, 2013; Dygert et al., 2014). Among the number of equations found in
410 literature, we have primary used the whole dataset for partition coefficients of Campi Flegrei (i.e.,
411 D_{REE} from this study, Pappalardo et al., 2008, and Fedele et al., 2009) to test the early predictive

412 model of Wood and Blundy (1997). The authors modelled the clinopyroxene–melt REE partitioning
413 using the theoretical strain-free partition coefficient for 3+ cations in M2, which they then
414 parameterised as a function of *P* and *T*. By fitting experimental data to the temperature (*T* in Kelvin)
415 and pressure (*P* in GPa) derivatives of the bulk and shear moduli of diopside, Wood and Blundy
416 (1997) found a simple equation for calculating the Young's Modulus for the trace elements of +3
417 charge in the M2 site of clinopyroxene:
418
419 $$E_{M2}^{3+} = 318.6 + 6.9P - 0.036T \quad (3)$$
420
421 Given the expression (3) for E_{M2}^{3+}, the change of r_0 was also modelled through stepwise linear
422 regression of the values of r_0 derived from literature data against all major compositional
423 parameters, pressure and temperature. It emerged that only X_{Al}^{iv} and X_{Ca}^{M2} were important
424 controlling factors for r_0:
425
426 $$r_0 = 0.974 + 0.067 X_{Ca}^{M2} - 0.051 X_{Al}^{M1} \quad (4)$$
427
428 To calculate D_0^{3+}, a simple ionic equilibrium involving melt and clinopyroxene was considered:
429
430 $$REEMgAlSiO_6^{melt} = REEMgAlSiO_6^{cpx} \quad (5)$$
431
432 The equilibrium constant of the exchange reaction (5) is:
433
434 $$K_{ex}^{3+} = \frac{X_{REE}^{M2} X_{Mg}^{M1} X_{Al}^{T} X_{Si}^{T}}{X_{REE}^{melt} X_{Mg}^{melt} X_{Al}^{melt} X_{Si}^{melt}} \quad (6)$$
435

In a thermodynamic approach based on the lattice strain theory, X_{Mg}^{M1} and $Mg\#^{melt}$ are the expression of the activity compositions of clinopyroxene ($a_{REEMgAlSiO6}^{cpx} = X_{REE}^{M2} X_{Mg}^{M1}$) and melt ($a_{REEMgAlSiO6}^{melt} = X_{REE}^{melt} Mg\#^{melt}$), and D_0^{3+} is the ratio of X_{REE}^{M2} to X_{REE}^{melt}. Using these parameters, the equilibrium constant (6) was rearranged as:

$$K_{ex}^{3+} = \frac{D_0^{3+} X_{Mg}^{M1}}{Mg\#^{melt}} \quad (7)$$

If $\Delta H_T^0, \Delta S_T^0$, and ΔV refer to the differences in thermodynamic properties between pure melt and pure crystal, it was found that:

$$\Delta H_T^0 - T\Delta S_T^0 + P\Delta V - \frac{1}{2}\left(\frac{\partial \Delta V}{\partial P}\right)P^2 = RT \ln\left(\frac{D_0^{3+} X_{Mg}^{M1}}{Mg\#^{melt}}\right) \quad (8)$$

The regression analysis of REE data from literature provided the best fit of the thermodynamic parameters on the left side of the reaction (8):

$$RT \ln\left(\frac{D_0^{3+} X_{Mg}^{M1}}{Mg\#^{melt}}\right) - 7{,}050P + 770P^2 = 88{,}750 - 65.644T \quad (9)$$

When the dataset from the Campi Flegrei is used to test the equation (9), all the strain-free partition coefficients are successfully predicted (Fig. 7), and the regression analysis of measured vs. predicted values of D_0^{3+} yields a very high correlation coefficient (R^2 = 0.997) and low standard error of estimate (SEE = 0.048). To account for the dependence of D_i (Fig. 3) and D_0^{3+} (Fig. 5) on the amount of aluminium in the tetrahedral site of clinopyroxene, Wood and Trigila (2001) re-fitted

458 the original calibration dataset of D_0^{3+} by adding Al^{iv} as predictor to the *P* and *T* parameters
459 previously employed. It was found, however, that the tetrahedral aluminium is not statistically
460 significant for the predictive equation (9) and that D_0^{3+} is adequately described in terms of pressure
461 and temperature only. Moreover, when the value of D_0^{3+} is modelled after Wood and Blundy (2001)
462 assuming local charge balance between REE in the M2 site and adjacent Al^{iv} within clinopyroxene
463 (i.e., $[REE]^{cpx}/[X^{3+}]$, where $[X^{3+}]$ is the proportion of M2 sites charge-balanced by a 3+ cation), we
464 found that the ability prediction of equation (9) does not substantially change (R^2 = 0.997 and SEE
465 = 0.046; Fig. 7). On the other hand, Wood & Blundy (1997) assumed for simplicity that the activity
466 of REE in the melt is equal to its concentration, thus ignoring that the melt structure may potentially
467 control D_0^{3+}. Indeed, data plotted on Fig. 6a seems to suggest that X_{REE}^{melt} is better described by
468 $[REE]^{melt}/[Ca^{2+}/(M^{+}+M^{2+})]^{melt}$ rather than the simple concentrations of REE in the melt. Therefore,
469 we have incorporated the melt structure parameter into the predictive equation (9) but the regression
470 analysis of measured vs. predicted values did not provide any improvement for the prediction of
471 D_0^{3+} (R^2 = 0.994 and SEE = 0.063; Fig. 7). The same conclusion was reached in recent studies for
472 the partitioning of REE and Y between clinopyroxene/orthopyroxene and picritic/basaltic melts
473 (Yao et al., 2012; Sun and Liang, 2012, 2013). This finding is apparently in contrast with the effects
474 of $[NBO/T]^{melt}$ and $[Ca^{2+}/(M^{+}+M^{2+})]^{melt}$ on the lattice-free partition coefficient (Fig. 6). One
475 possible explanation is that, for moderately to highly depolymerized magmas, $[NBO/T]^{melt}$ is
476 constantly higher than the threshold value of 0.4 (cf. Sun and Liang, 2012), whereas its value is
477 persistently lower than 0.2 for polymerized magmas (Fig. 6a). On the other hand, due to the strong
478 rival effects of X_{Al}^{iv}, *P*, and *T*, no obvious correlations are found between $[Ca^{2+}/(M^{+}+M^{2+})]^{melt}$ and
479 D_0^{3+} when pressure, temperature, and clinopyroxene components change at the same time (cf.
480 Huang et al., 2006). As these parameters are to some extent interdependent, it is not easy to
481 differentiate between their relative influences over a broad range of crystallization conditions and
482 compositions (crystal and melt). It can be concluded that the role of melt chemistry is to reduce the
483 number of melt sites onto which REE can be accommodated. Thus, the melt structure can

potentially control the partitioning of trace elements over a wide spectrum of melt compositions (Fig. 6). However, for an isolated bulk melt composition, the final value of the REE partition coefficient is also determined by the relative (rival) effects of pressure, temperature and mineral chemistry.

Using a calibration dataset specific to basaltic compositions, Wood and Blundy (1997) found that *P* and *T* closely describe the variance of *E* according to the regression equation (3), whereas X_{Al}^{M1} and X_{Ca}^{M2} are the best predictors for r_0, as provided by the best fitting equation (4). Further nonlinear regression calculations performed by Sun and Liang, (2012) and Yao et al. (2012) on a more recent basaltic dataset provided that X_{Mg}^{M2} and X_{Al}^{M1} can also be suitable predictors for r_0. Due to the strong relationship between *E* and r_0, Wood and Blundy (1997) preferred to estimate the value of Young's modulus using only *P* and *T*. Conversely, an intrinsic trade-off between *E* and r_0 was also found by Sun and Liang, (2012) that favoured calculating *E* as a linear function of r_0. The authors demonstrated that the dependence of *E* and r_0 on the same clinopyroxene components does not weaken the predictive power of the lattice strain model. However, in multiple linear regression analyses some variables may closely describe the variance of the dataset, whereas some others may generate a set of predictions with low degrees of freedom that lead to strong data overfitting. Therefore, variables that do not improve the fit must be identified and removed from a model. Through an algorithm based on the Mallows' *Cp* statistic, we have performed systematic permutations of a number of independent variables to derive the best predictive models for r_0, and *E*. Mallows' *Cp* is expressed as (Hair et al., 1995):

$$Cp = \frac{RSS_k}{RSS_p} - n + 2p \tag{10}$$

RSS_k is the ratio of the residual sum of squares of all predictors *k*, RSS_p is the residual sum of squares of only *p* of the k predictors, and *n* is the number of observations. Mallows' *Cp* is a measure

of the bias in a model: if the type and number of selected predictors *p* (including the constant term in linear regression) are sufficient to provide a good description of the data, then *Cp* has values as close as possible to *p*. The independent variables used for permutations were X_{Al}^{iv}, X_{Al}^{M1}, X_{Ca}^{M2}, X_{Na}^{M2}, X_{Mg}^{M1}, X_{Mg}^{M2}, $[Ca^{2+}/(M^{+}+M^{2+})]^{melt}$, $[NBO/T]^{melt}$, *P* and *T*. Results are reported in Table 6S together with the mean squared error (*MSE*), R^2, *p*, and *Cp*. The Mallows' *Cp* statistic indicates that *E* and r_0 are both primary influenced by the same variables (i.e., X_{Ca}^{M2} and X_{Mg}^{M2}), corroborating the observation of Sun and Liang (2012) that *E* is indeed linearly correlated to r_0 (R^2 = 0.968). In contrast, the temperature, pressure and melt composition have minor effects on these parameters, as would be expected given (a) these are crystal-chemical parameters and (b) that the thermal expansivity of the M2 site is relatively small for the temperature range considered here (Nimis, 1999). Therefore, using X_{Ca}^{M2} and X_{Mg}^{M2} as independent variables, we have performed a multiple linear regression analysis of the data from the Campi Flegrei to derive an improved predictive model for *E* (Fig. 8a):

$$E = -82.35 + 636.56X_{Ca}^{M2} - 253.29X_{Mg}^{M2} \quad (11)$$

The statistics (R^2 = 0.967 and SEE = 4.72) of the equation (11) are much better than those observed for the original equation (3) when *T* and *P* of trachy-phonolitic magmas are used as input data (R^2 = 0.495 and SEE = 17.78). Through the same approach, we have also derived a predictive model for r_0 (Fig. 8b):

$$r_0 = 1.0231 + 0.0278X_{Ca}^{M2} - 0.0101X_{Mg}^{M2} \quad (12)$$

The equation (12) produces an improved fit to the data of the Campi Flegrei (R^2 = 0.954 and SEE = 0.002). Conversely, clinopyroxene compositions from trachytes and phonolites provide low

534 statistics for X_{Al}^{M1} and X_{Ca}^{M2} (R^2 = 0.552 and SEE = 0.007), as predictors of the original equation
535 (4).

536 It is apparent that the uncertainty measured for the recalibrated equations (11) and (12) is
537 reasonably low due to the restricted bounds of the calibration dataset that, in turn, closely describe
538 the crystallization conditions and compositions of magmas at Campi Flegrei (Fig. 1 and Table 1S).
539 On the other hand, the original equations (3) and (4) of Wood and Blundy (1997) were calibrated
540 using primitive compositions obtained prevalently at high-temperatures that, in turn, do not
541 reproduce the variability internal to the trachy-phonolitic dataset. For example, the percentage error
542 of *E* predicted by the equation (3) increases as the temperature decreases (Fig. 9a) due to the fact
543 that thermal conditions below 1,100 °C are not adequately represented into the calibration dataset of
544 Wood and Blundy (1997). Fig. 9a shows that this is valid either to natural alkaline differentiated
545 magmas from this study or to experimental basaltic compositions equilibrated at relatively low
546 temperatures (data from experiments of Green et al., 2000 and Adam and Green, 2006). Conversely,
547 Fig. 9b shows that the equation (11) has a very low percentage error of *E* at temperatures below
548 1,050 °C, but the error progressively increases with temperature, although T > 1,100 °C are rarely
549 recorded by alkaline differentiated products. This simple test clearly makes the recalibrated
550 equations (11) and (12) not suitable for high-temperature primitive magmas. We also observe that
551 values of *E* and r_0 from basaltic and more differentiated compositions are scattered through the
552 literature, consequently, the global regression analysis of these data did not provide statistically
553 significant parameters applicable over a wide range of temperatures, pressures, and compositions.

554 In the online supplementary material, we provide an Excel spreadsheet in which equations
555 (9), (11), and (12) are incorporated, and that can be used to predict D_{REE} and D_Y through major
556 element analyses of clinopyroxene in equilibrium with trachy-phonolitic magmas. In Fig. 10a we
557 have compared the standard error of estimate of each partition coefficient predicted by (i) the
558 original model of Wood and Blundy (1997), (ii) the Excel spreadsheet from this study, and (iii) the
559 parameterized model of Sun and Liang (2012). It is worth noting that this latter model was

560 calibrated specifically to basaltic systems. With respect to the original model of Wood and Blundy
561 (1997), our recalibrated model offers little improvements in the prediction of D_{LREE}, whereas its
562 accuracy is remarkably high for most of the D_{HREE} values. Conversely, the model of Sun and Liang
563 (2012) is affected by a systematic uncertainty in the prediction of D_{LREE}. This is not surprising if we
564 consider that the model was parameterized over crystallization conditions and compositions rather
565 different to those presented in this study. However, in the case of D_{Tm}, D_{Yb} and D_{Lu}, the standard
566 error of estimate is found to be lower than that of other models. This is due to the fact that the
567 model of Sun and Liang (2012) tends to overestimate the value of *E* that, in turn, reduces the width
568 of the partitioning parabola with minor effects on trace elements having low ionic radii. For
569 example, measured vs. predicted values for D_{Ce} (Fig. 10b) and D_{Yb} (Fig. 10c) show that partition
570 coefficients for larger LREE cations predicted by the model of Sun and Liang (2012) deviate
571 significantly from the one-to-one line, whereas partition coefficients for smaller HFSE cations
572 approach to the one-to-one line much better than those predicted by other models (see also Table 7S
573 for the whole dataset).
574
575 Applications to the Campanian Ignimbrite
576
577 As anticipated from the preceding discussion, the dependence of trace element partitioning on *P*, *T*,
578 and composition (crystal and melt) results in a variety of D_i values. However, most of the
579 petrological models from literature assume for simplicity that D_i is independent on the
580 physicochemical conditions of system, despite such an assumption is unlikely during crystallization
581 of natural magmas. In order to clearly demonstrate the importance of considering the change of D_i
582 for a better understanding of magmatic differentiation, we have selected four natural clinopyroxene-
583 melt pairs representative of the internal compositional variability of the Campanian Ignimbrite
584 eruption (data from Civetta et al., 1997 and Arienzo et al., 2009). These data yield ΔDiHd between
585 0.01 and 0.12 suggestive of near-equilibrium crystallization conditions (Mollo et al., 2013a), but are

586 also characterized by distinct features in terms of *P*, *T*, and composition (Table 8S). In particular,
587 thermometers and barometers of Masotta et al. (2013) suggest that the natural clinopyroxene-melt
588 pairs equilibrated at 100-300 MPa and 914-982 °C, in agreement with previous estimates from
589 petrological (e.g., Fulignati et al., 2004; Marianelli et al., 2006; Fowler et al., 2007) and geophysical
590 (e.g., Zollo et al., 2008) studies. As discussed above, the effect of pressure on trace element
591 partitioning between clinopyroxene and melt can be considered negligible at shallow crustal depths.
592 On the other hand, there is a well-documented inverse correlation between the concentration of
593 water dissolved in the melt and D_{REE} (cf. Blundy et al., 2002; Gaetani, 2004; Sun and Liang, 2012).
594 For trachytic and phonolitic compositions, it is not clear to what extent H_2O can influence D_0^{3+}
595 during magma differentiation. Undoubtedly, the macroscopic effect of increasing water is to depress
596 the liquidus temperature of the melt (Putirka, 2008). However, we have already tested that a water
597 change of ±2 wt.% in trachytic and phonolitic magmas corresponds to a negligible temperature
598 variation of ±12 °C. According to Mollo and Masotta (2014), low ΔDiHd values allow to (1)
599 minimize significantly the uncertainty of barometers and thermometers, and (2) find a good
600 correspondence between the crystallization temperature of magma and the geochemical evolution of
601 clinopyroxene. This latter point is better explained in Fig. 11a where $Mg\#^{cpx}$ correlates positively
602 with *T*, evidencing the relative effects of temperature and clinopyroxene composition on trace
603 element partitioning. Only when magnitudes of these two opposing effects are reciprocally
604 compensated, a set of nearly constant partition coefficients can be expected. Otherwise, temperature
605 and clinopyroxene composition dominate over the final value of D_i, hence controlling the
606 partitioning of trace elements during magma crystallization (e.g., Sun and Liang, 2012). Each
607 symbol plotted on Fig. 11a refers to the value of D_0^{3+} predicted using the Excel spreadsheet from
608 this study. D_0^{3+} increases from 0.67 to 0.91 with decreasing both *T* and $Mg\#^{cpx}$. In this view, the
609 whole range of values calculated for D_{REE} and D_Y has been used as input data for the Rayleigh
610 fractional crystallization equation (FC):
611

$$C_l^{FC} = C_0 F^{(Di-1)} \quad (13)$$

Where C_l^{FC} is the concentration of an element in remaining melt during fractional crystallization, C_0 is the concentration of the trace element in parental liquid (starting composition), D_i is the partition coefficient of the trace element of interest whose value changes as a function of the physicochemical conditions of the system (see below), F is the fraction of melt remaining during crystallization. At the beginning of the modelling, low degrees of clinopyroxene fractionation (i.e., 3%, 5%, 7%, and 9%) have been considered to constrain its early effect as liquidus phase on the geochemical signature of magma. Stepwise calculations were performed changing the clinopyroxene composition and temperature at each step of fractionation (Fig. 11a), in order to derive a set of four different partition coefficients rather than one single value. In Fig. 11b, modelled Ce and Y concentrations are compared with those of rock samples from the Campanian Ignimbrite. Notably, the ratio of Ce/Y for the Campanian Ignimbrite eruption changes significantly from 0.21 to 0.33, in contrast to what would be expected for igneous products sharing a common parental magma. This discrepancy is reconciled by the nonlinear trajectory of the ^{cpx}FC vector that is controlled by the variation of the partition coefficient. Thus, at the early stage of clinopyroxene crystallization, the incorporation of variable proportions of Ce and Y into the crystal lattice provides explanation for the strong variability of the natural dataset. According to Civetta et al. (1997), the internal differentiation of the Campanian Ignimbrite can be addressed to the fractionation of <10% and ~50% of clinopyroxene and feldspar, respectively. Considering that Ce and Y are highly incompatible in feldspar (D_{Ce} = 0.039 and D_Y = 0.017; Larsen, 1979), further fractional crystallization steps have been developed accounting for the segregation of 50% of feldspars from the solidifying magma. Notably, due to the highly incompatible behaviour of Ce and Y, feldspar fractionation may only increase the REE content in magma but cannot control the internal REE variability of the Campanian Ignimbrite eruption. Modelling results are aligned along four different FC trajectories (i.e., from ^{kfs}FC1 to ^{kfs}FC4) that faithfully reproduce the entire differentiation path of

638 the Campanian Ignimbrite, from lowest to highest Ce/Y ratios (Fig. 11a). Clearly, the constancy of
639 the clinopyroxene-melt partition coefficient would yield only one single FC trend that, in turn, is
640 inadequate to reproduce in full the complex trace element pattern of natural products. Therefore, the
641 process responsible for the heterogeneous REE concentrations of the Campanian Ignimbrite
642 products is twofold: (1) the early fractionation of clinopyroxene at relative high temperature and (2)
643 the subsequent fractionation of feldspars during the final stage of magma cooling (cf. Fowler et al.,
644 2007). Additional complexities, including crystallization of other phases (oxides, biotite, apatite)
645 and partial cumulate mush remelting (e.g., Wolff et al., 2015) can further explain some of the trace
646 element variations observed in the Campanian Ignimbrite .
647
648 **Conclusions**
649
650 Coherently with previous natural and experimental studies, we documented that the partitioning of
651 trace elements between clinopyroxene and trachy-phonolitic melts can be addressed to (1) the entry
652 of REE+Y and HFSE in the M2 and M1 sites, respectively, due to substitution of Si^{4+} with Al^{iv}, (2)
653 the increased net charge on the M1 site that causes divalent TE to become less compatible within
654 clinopyroxene crystal lattice, (3) a charge-balanced cation substitution reaction reflecting an
655 increased ease of locally balancing the excess charge as the number of surrounding tetrahedrally-
656 coordinated aluminium atoms increases, and (4) the effect of changes in melt structure that increase
657 the number of large sites critically important to accommodating large REE cations. On the other
658 hand, we tested that the incorporation of additional crystallochemical parameters (assuming local
659 charge balance between REE in the M2 site and adjacent Al^{iv}) and melt structure parameters (given
660 as the ratio of non-bridging oxygens to tetrahedral cations and/or the ratio of molar calcium to the
661 sum of monovalent and divalent cations) into the lattice strain model of Wood & Blundy (1997) did
662 not provide any improvement for its ability prediction. This is due to the strong rival effects of
663 pressure, temperature, and crystal/melt parameters. Therefore, over a broad range of crystallization

conditions and crystal/melt compositions, it is not possible to differentiate between the relative influence of each single parameter on REE+Y partitioning. As a consequence, no obvious correlations are found when the physicochemical conditions of the system change at the same time. According to the lattice strain theory, we observe that, D_0^{3+}, r_0 and E can be successfully predicted once T, P, X_{Ca}^{M2} and X_{Mg}^{M2} are knows for trachy-phonolitic compositions. On this basis, we updated the existing partitioning equations to derive a self-consistent model for trachy-phonolitic magmas. The application of this model to natural products from the Campanian Ignimbrite, the largest caldera-forming eruption at the Campi Flegrei, reveals that the complex REE pattern of magma can be successfully described by the stepwise fractional crystallization of clinopyroxene and feldspar where the clinopyroxene-melt partition coefficient changes progressively as a function of the physicochemical conditions of the system.

Acknowledgments

We are grateful to Yan Liang and an anonymous reviewer for their useful and constructive comments that helped to improve significantly the quality of the paper. We are also indebted to Andrew C. Kerr as Editor-in-Chief of Lithos for his instructive editorial guidance. A. Cavallo is acknowledged for assistance during electron microprobe analysis. Parts of this research were supported by Swiss NSF fund # 200021-146268.S, ERC Advanced Grant (247162-CRITMAG), Wolfson Research Merit Award, and MIUR, Premiale project – NoRth: New hORizons of the Technology applied to experimental researches and geophysical and volcanological monitoring.

References

688 Arienzo I, Civetta L, Heumann A, Worner G and Orsi G (2009) Isotopic evidence for open system
689 processes within the Campanian Ignimbrite (Campi Flegrei, Italy) magma chamber. B. Volcanol.
690 71(3):285–300.
691 Armienti, P, Tonarini, S, Innocenti, F, D'Orazio, M, 2007. Mount Etna pyroxene as tracer of
692 petrogenetic processes and dynamics of the feeding system, in: Beccaluva, L. Bianchini, G., Wilson,
693 M. (Eds.), Cenozoic Volcanism in the Mediterranean, Geological Society of America Special
694 Papers, pp. 265-276.
695 Bennett SL, Blundy J, Elliott T (2004) The effect of sodium and titanium on crystal-melt
696 partitioning of trace elements. Geochim Cosmochim Ac 68(10):2335-2347 doi:Doi
697 10.1016/J.Gca.2003.11.006
698 Blundy J, Wood B (1994) Prediction of Crystal-Melt Partition-Coefficients from Elastic-Moduli.
699 Nature 372(6505):452-454 doi:Doi 10.1038/372452a0
700 Blundy J D, Falloon T J, Wood B J, Dalton J A (1995) Sodium partitioning between clinopyroxene
701 and silicate melts. J Geophys Res 100: 15501-15516.
702 Blundy J, Wood B (2003) Partitioning of trace elements between crystals and melts. Earth Planet Sc
703 Lett 210(3-4):383-397 doi:Doi 10.1016/S0012-821x(03)00129-8
704 Blundy JD, Robinson JAC, Wood BJ (1998) Heavy REE are compatible in clinopyroxene on the
705 spinel lherzolite solidus. Earth Planet Sc Lett 160(3-4):493-504 doi:Doi 10.1016/S0012-
706 821x(98)00106-X
707 Civetta L, Orsi G, Pappalardo L, Fisher RV, Heiken G, Ort M (1997) Geochemical zoning,
708 mingling, eruptive dynamics and depositional processes - The Campanian Ignimbrite, Campi
709 Flegrei caldera, Italy. J Volcanol Geoth Res 75(3-4):183-219 doi:Doi 10.1016/S0377-
710 0273(96)00027-3
711 D'Antonio M (2011) Lithology of the basement underlying the Campi Flegrei caldera:
712 Volcanological and petrological constraints. J Volcanol Geoth Res 200(1-2):91-98 doi:Doi
713 10.1016/J.Jvolgeores.2010.12.006

714 Deino A L, Orsi G, Piochi M, de Vita S (2004) The age of the Neapolitan Yellow Tuff caldera-
715 forming eruption (Campi Flegrei caldera—Italy) assessed by $^{40}Ar/^{39}Ar$ dating method. J Volcanol
716 Geotherm Res 133:157–170 doi:10.1016/S0377-0273(03)00396-2
717 De Vivo B, Rolandi G, Gans PB, Calvert A, Bohrson WA, Spera FJ, Belkin HE (2001) New
718 constraints on the pyroclastic eruptive history of the Campanian volcanic Plain (Italy). Miner Petrol
719 73(1-3):47-65 doi:Doi 10.1007/S007100170010
720 Del Bello E, Mollo S, Scarlato P, von Quadt A, Forni F, Bachmann O (2014) New petrological
721 constraints on the last eruptive phase of the Sabatini Volcanic District (central Italy): Clues from
722 mineralogy, geochemistry, and Sr–Nd isotopes. Lithos 205(0):28-38
723 doi:http://dx.doi.org/10.1016/j.lithos.2014.06.015
724 Dygert N, Liang Y, Sun C, Hess P (2014) An experimental study of trace element partitioning
725 between augite and Fe-rich basalts. Geochim Cosmochim Ac 132:170-186 doi:
726 10.1016/j.gca.2014.01.042
727 Fabbrizio A, Carroll MR (2008) Experimental constraints on the differentiation process and pre-
728 emptive conditions in the magmatic system of Phlegraean Fields (Naples, Italy). J Volcanol Geoth
729 Res 171(1-2):88-102 doi:Doi 10.1016/J.Jvolgeores.2007.11.002
730 Fedele L, Zanetti A, Morra V, Lustrino M, Melluso L, Vannucci R (2009) Clinopyroxene/liquid
731 trace element partitioning in natural trachyte-trachyphonolite systems: insights from Campi Flegrei
732 (southern Italy). Contrib Mineral Petr 158(3):337-356 doi:Doi 10.1007/S00410-009-0386-5
733 Forsythe LM, Nielsen RL, Fisk MR (1994) High-Field-Strength Element Partitioning between
734 Pyroxene and Basaltic to Dacitic Magmas. Chem Geol 117(1-4):107-125 doi:Doi 10.1016/0009-
735 2541(94)90124-4
736 Fowler SJ, Spera F, Bohrson W, Belkin HE, De Vivo B (2007) Phase equilibria constraints on the
737 chemical and physical evolution of the campanian ignimbrite. J Petrol 48(3):459-493 doi:Doi
738 10.1093/Petrology/Egl068

739 Francis D, Minarik W (2008) Aluminum-dependent trace element partitioning in clinopyroxene.
740 Contrib Mineral Petr 156(4):439-451 doi:Doi 10.1007/S00410-008-0295-Z
741 Freda C, Gaeta M, Misiti V, Mollo S, Dolfi D, Scarlato P (2008) Magma–carbonate interaction: an
742 experimental study on ultrapotassic rocks from Alban Hills (Central Italy). Lithos 101(3):397-415
743 Fulignati P, Marianelli P, Proto M, Sbrana A (2004) Evidences for disruption of a crystallizing front
744 in a magma chamber during caldera collapse: an example from the Breccia Museo unit (Campanian
745 Ignimbrite eruption, Italy). J Volcanol Geoth Res 133:141-155
746 Gaetani GA (2004) The influence of melt structure on trace element partitioning near the peridotite
747 solidus. Contrib Mineral Petr 147(5):511-527 doi:Doi 10.1007/S00410-004-0575-1
748 Gaetani GA, Grove TL (1995) Partitioning of Rare-Earth Elements between Clinopyroxene and
749 Silicate Melt - Crystal-Chemical Controls. Geochim Cosmochim Ac 59(10):1951-1962 doi:Doi
750 10.1016/0016-7037(95)00119-0
751 Gaetani GA, Kent AJR, Grove TL, Hutcheon ID, Stolper EM (2003) Mineral/melt partitioning of
752 trace elements during hydrous peridotite partial melting. Contrib Mineral Petr 145(4):391-405
753 doi:Doi 10.1007/S00410-003-0447-0
754 Hair Jr J F, Anderson R E, Tatham R L, Black W C (1995) Multivariate data analysis. 3rd ed, New
755 York, Macmillan, 742p.
756 Hart SR, Dunn T (1993) Experimental Cpx Melt Partitioning of 24 Trace-Elements. Contrib
757 Mineral Petr 113(1):1-8 doi:Doi 10.1007/Bf00320827
758 Hill E, Wood BJ, Blundy JD (2000) The effect of Ca-Tschermaks component on trace element
759 partitioning between clinopyroxene and silicate melt. Lithos 53(3-4):203-215 doi:Doi
760 10.1016/S0024-4937(00)00025-6
761 Huang F, Lundstrom CC, McDonough WF (2006) Effect of melt structure on trace-element
762 partitioning between clinopyroxene and silicic, alkaline, aluminous melts. Am Mineral 91(8-
763 9):1385-1400 doi:Doi 10.2138/Am.2006.1909

764 Kennedy AK, Lofgren GE, Wasserburg GJ (1993) An experimental study of trace element
765 partitioning between olivine, orthopyroxene and melt in chondrules: equilibrium values and kinetic
766 effects. Earth Planet Sc Lett 115(1–4):177-195 doi:http://dx.doi.org/10.1016/0012-821X(93)90221-
767 T
768 Klemme S, Blundy JD, Wood BJ (2002) Experimental constraints on major and trace element
769 partitioning during partial melting of eclogite. Geochim Cosmochim Ac 66(17):3109-3123 doi:Doi
770 10.1016/S0016-7037(02)00859-1
771 Lanzafame G, Mollo S, Iezzi G, Ferlito C, Ventura G (2013) Unraveling the solidification path of a
772 pahoehoe "cicirara" lava from Mount Etna volcano. B Volcanol 75(4) doi:Doi 10.1007/S00445-
773 013-0703-8
774 Larsen, LM (1979) Distribution of REE and Other Trace-Elements between Phenocrysts and
775 Peralkaline Undersaturated Magmas, Exemplified by Rocks from the Gardar Igneous Province,
776 South Greenland. Lithos 12(4): 303-315 doi: 10.1016/0024-4937(79)90022-7.
777 Le Bas MJ, Le Maitre RW, Streckeisen A, Zanettin B, Rocks ISotSoI (1986) A Chemical
778 Classification of Volcanic Rocks Based on the Total Alkali-Silica Diagram. J Petrol 27(3):745-750
779 doi:10.1093/petrology/27.3.745
780 Lemarchand F, Villemant B, Calas G (1987) Trace-Element Distribution Coefficients in Alkaline
781 Series. Geochim Cosmochim Ac 51(5):1071-1081 doi:Doi 10.1016/0016-7037(87)90201-8
782 Liang Y, Sun CG, Yao LJ (2013) A REE-in-two-pyroxene thermometer for mafic and ultramafic
783 rocks. Geochim Cosmochim Ac 102:246-260 doi:Doi 10.1016/J.Gca.2012.10.035
784 Lindstrom DJ (1976) Partitioning of Ferric Iron between Diopside and Silicate Liquid. Eos T Am
785 Geophys Un 57(4):339-339
786 Lofgren GE, Huss GR, Wasserburg GJ (2006) An experimental study of trace-element partitioning
787 between Ti-Al-clinopyroxene and melt: Equilibrium and kinetic effects including sector zoning. Am
788 Mineral 91(10):1596-1606 doi:10.2138/am.2006.2108

789 Lundstrom CC, Shaw HF, Ryerson FJ, Phinney DL, Gill JB, Williams Q (1994) Compositional
790 Controls on the Partitioning of U, Th, Ba, Pb, Sr and Zr between Clinopyroxene and Haplobasaltic
791 Melts - Implications for Uranium Series Disequilibria in Basalts. Earth Planet Sc Lett 128(3-4):407-
792 423 doi:Doi 10.1016/0012-821x(94)90159-7
793 Lundstrom CC, Shaw HF, Ryerson FJ, Williams Q, Gill J (1998) Crystal chemical control of
794 clinopyroxene-melt partitioning in the Di-Ab-An system: Implications for elemental fractionations
795 in the depleted mantle. Geochim Cosmochim Ac 62(16):2849-2862 doi:Doi 10.1016/S0016-
796 7037(98)00197-5
797 Mahood G, Hildreth W (1983) Large Partition-Coefficients for Trace-Elements in High-Silica
798 Rhyolites. Geochim Cosmochim Ac 47(1):11-30 doi:Doi 10.1016/0016-7037(83)90087-X
799 Marianelli P, Sbrana A, Proto M (2006) Magma chamber of the Campi Flegrei supervolcano at the
800 time of eruption of the Campanian Ignimbrite. Geology 34(11):937-940 doi:Doi
801 10.1130/G22807a.1
802 Marks M, Halama R, Wenzel T, Markl G (2004) Trace element variations in clinopyroxene and
803 amphibole from alkaline to peralkaline syenites and granites: implications for mineral-melt trace-
804 element partitioning. Chem Geol 211(3-4):185-215 doi:Doi 10.1016/J.Chemgeo.2004.06.032
805 Masotta M, Gaeta M, Gozzi F, Marra F, Palladino DM, Sottili G (2010) H2O- and temperature-
806 zoning in magma chambers: The example of the Tufo Giallo della Via Tiberina eruptions (Sabatini
807 Volcanic District, central Italy). Lithos 118(1-2):119-130 doi:Doi 10.1016/J.Lithos.2010.04.004
808 Masotta M, Mollo S, Freda C, Gaeta M, Moore G (2013) Clinopyroxene-liquid thermometers and
809 barometers specific to alkaline differentiated magmas. Contrib Mineral Petr 166(6):1545-1561
810 doi:Doi 10.1007/S00410-013-0927-9
811 Matsui Y, Onuma N, Nagasawa H, Higuchi H, Banno S (1977) Crystal-Structure Control in Trace-
812 Element Partition between Crystal and Magma. B Soc Fr Mineral Cr 100(6):315-324
813 McDade P, Blundy JD, Wood BJ (2003) Trace element partitioning between mantle wedge
814 peridotite and hydrous MgO-rich melt. Am Mineral 88(11-12):1825-1831

Mollo S, Giacomoni PP, Andronico D, Scarlato P (2015a) Clinopyroxene and titanomagnetite cation redistributions at Mt. Etna volcano (Sicily, Italy): Footprints of the final solidification history of lava fountains and lava flows. Chemical Geology, 406:45-54 doi:http://dx.doi.org/10.1016/j.chemgeo.2015.04.017.

Mollo S, Masotta M, Forni F, Bachmann O, De Astis G., Moore G, Scarlato P (2015b) A K-feldspar-liquid hygrometer specific to alkaline differentiated magmas. Chemical Geology, 392:1-8, doi:10.1016/j.chemgeo.2014.11.010.

Mollo S, Masotta M, Forni F, Bachmann O, De Astis G, Moore G, Scarlato P (2014) A K-feldspar–liquid hygrometer specific to alkaline differentiated magmas. Chemical Geology, in press.

Mollo S, Blundy JD, Iezzi G, Scarlato P, Langone A (2013a) The partitioning of trace elements between clinopyroxene and trachybasaltic melt during rapid cooling and crystal growth. Contrib Mineral Petr 166(6):1633-1654

Mollo S, Putirka K, Misiti V, Soligo M, Scarlato P (2013b) A new test for equilibrium based on clinopyroxene-melt pairs: Clues on the solidification temperatures of Etnean alkaline melts at post-eruptive conditions. Chem Geol 352:92-100

Mollo S, Iezzi G, Ventura G, Cavallo A, Scarlato P (2012) Heterogeneous nucleation mechanisms and formation of metastable phase assemblages induced by different crystalline seeds in a rapidly cooled andesitic melt. Journal of Non-Crystalline Solids 358(12-13):1624-1628

Mollo S, Lanzafame G, Masotta M, Iezzi G, Ferlito C, Scarlato P (2011a) Cooling history of a dike as revealed by mineral chemistry: A case study from Mt. Etna volcano. Chem Geol 288(1-2):39-52

Mollo S, Masotta M (2014) Optimizing pre-eruptive temperature estimates in thermally and chemically zoned magma chambers. Chem Geol 368:97-103

Mollo S, Putirka K, Iezzi G, Del Gaudio P, Scarlato P (2011b) Plagioclase-melt (dis)equilibrium due to cooling dynamics: Implications for thermometry, barometry and hygrometry. Lithos 125(1-2):221-235

840 Morimoto N (1988) Nomenclature of Pyroxenes. Miner Petrol 39(1):55-76
841 doi:10.1007/BF01226262
842 Muñoz M, Sagredo J (1974) Clinopyroxenes as geobarometric indicators in mafic and ultramafic
843 rocks from Canary Islands. Contrib Mineral Petr 44(2):139-147 doi:10.1007/BF00385786
844 Nagasawa H (1973) Rare-Earth Distribution in Alkali Rocks from Oki-Dogo-Island, Japan. Contrib
845 Mineral Petr 39(4):301-308 doi:Doi 10.1007/Bf00376470
846 Nagasawa H, Schnetzler CC (1971) Partitioning of Rare Earth,Alkali and Alkaline Earth Elements
847 between Phenocrysts and Acidic Igneous Magma. Geochim Cosmochim Ac 35(9):953-& doi:Doi
848 10.1016/0016-7037(71)90008-1
849 Nimis P (1999) Clinopyroxene geobarometry of magmatic rocks. Part 2. Structural geobarometers
850 for basic to acid, tholeiitic and midly alkaline magmatic systems. Contrib Mineral Petrol 135:62–74
851 doi:10.1007/s004100050498
852 Onuma N, Higuchi H, Wakita H, Nagasawa H (1968) Trace Element Partition between 2 Pyroxenes
853 and Host Lava. Earth Planet Sc Lett 5(1):47-& doi:Doi 10.1016/S0012-821x(68)80010-X
854 Orsi G, Dantonio M, Devita S, Gallo G (1992) The Neapolitan Yellow Tuff, a Large-Magnitude
855 Trachytic Phreatoplinian Eruption - Eruptive Dynamics, Magma Withdrawal and Caldera Collapse.
856 J Volcanol Geoth Res 53(1-4):275-287 doi:Doi 10.1016/0377-0273(92)90086-S
857 Orsi G, Di Vito MA, Selva J, Marzocchi W (2009) Long-term forecast of eruption style and size at
858 Campi Flegrei caldera (Italy). Earth Planet Sc Lett 287(1-2):265-276 doi:Doi
859 10.1016/J.Epsl.2009.08.013
860 Pabst S, Worner G, Civetta L, Tesoro R (2008) Magma chamber evolution prior to the Campanian
861 Ignimbrite and Neapolitan Yellow Tuff eruptions (Campi Flegrei, Italy). B Volcanol 70(8):961-976
862 doi:Doi 10.1007/S00445-007-0180-Z
863 Pappalardo L, Mastrolorenzo G (2012) Rapid differentiation in a sill-like magma reservoir: a case
864 study from the campi flegrei caldera. Sci Rep-Uk 2 doi:Artn 712. Doi 10.1038/Srep00712

865 Pappalardo L, Ottolini L, Mastrolorenzo G (2008) The Campanian Ignimbrite (southern Italy)
866 geochemical zoning: insight on the generation of a super-eruption from catastrophic differentiation
867 and fast withdrawal. Contrib Mineral Petr 156(1):1-26 doi:Doi 10.1007/S00410-007-0270-0
868 Pappalardo L, Piochi M, D'Antonio M, Civetta L, Petrini R, (2002) Evidence for multi-stage
869 magmatic evolution during the past 60 ka at Campi Flegrei (Italy) deduced from Sr, Nd and Pb
870 isotope data. J Petrol 43:1415–1434
871 Putirka K, Johnson M, Kinzler R, Longhi J, Walker D (1996) Thermobarometry of mafic igneous
872 rocks based on clinopyroxene-liquid equilibria, 0-30 kbar. Contrib Mineral Petr 123(1):92-108
873 doi:Doi 10.1007/S004100050145
874 Ray GL, Shimizu N, Hart SR (1983) An Ion Microprobe Study of the Partitioning of Trace-
875 Elements between Clinopyroxene and Liquid in the System Diopside-Albite-Anorthite. Geochim
876 Cosmochim Ac 47(12):2131-2140 doi:Doi 10.1016/0016-7037(83)90038-8
877 Scarlato P, Mollo S, Blundy JD, Iezzi G, Tiepolo M (2014) The role of natural solidification paths
878 on REE partitioning between clinopyroxene and melt. B Volcanol 76(3) doi:Artn 810. Doi
879 10.1007/S00445-014-0810-1
880 Schnetzler CC, Philpotts JA (1970) Li, K, Rb, Sr, Ba and Rare-Earth Concentrations to Apollo-12
881 Lunar Soil. Eos T Am Geophys Un 51(7):583-&
882 Shannon RD (1976) Revised Effective Ionic-Radii and Systematic Studies of Interatomic Distances
883 in Halides and Chalcogenides. Acta Crystallogr A 32(Sep1):751-767 doi:Doi
884 10.1107/S0567739476001551
885 Signorelli S, Vaggelli G, Romano C, Carroll MR (2001) Volatile element zonation in Campanian
886 Ignimbrite magmas (Phlegrean Fields, Italy): evidence from the study of glass inclusions and matrix
887 glasses. Contrib Mineral Petr 140(5):543-553
888 Skulski T, Minarik W, Watson EB (1994) High-Pressure Experimental Trace-Element Partitioning
889 between Clinopyroxene and Basaltic Melts. Chem Geol 117(1-4):127-147 doi:Doi 10.1016/0009-
890 2541(94)90125-2

Sun CG, Liang Y (2012) Distribution of REE between clinopyroxene and basaltic melt along a mantle adiabat: effects of major element composition, water, and temperature. Contrib Mineral Petr 163(5):807-823 doi:Doi 10.1007/S00410-011-0700-X

Sun CG, Liang Y (2013) The importance of crystal chemistry on REE partitioning between mantle minerals (garnet, clinopyroxene, orthopyroxene, and olivine) and basaltic melts. Chem Geol 358:23-36 doi:Doi 10.1016/J.Chemgeo.2013.08.045

Tuff J, Gibson SA (2007) Trace-element partitioning between garnet, clinopyroxene and Fe-rich picritic melts at 3 to 7 GPa. Contrib Mineral Petr 153(4):369-387 doi:Doi 10.1007/S00410-006-0152-X

Villemant B (1988) Trace-Element Evolution in the Phlegrean Fields (Central-Italy) - Fractional Crystallization and Selective Enrichment. Contrib Mineral Petr 98(2):169-183 doi:Doi 10.1007/Bf00402110

Watson EB, Muller T (2009) Non-equilibrium isotopic and elemental fractionation during diffusion-controlled crystal growth under static and dynamic conditions. Chem Geol 267(3-4):111-124 doi:Doi 10.1016/J.Chemgeo.2008.10.036

Webster JD, Raia F, Tappen C, De Vivo B (2003) Pre-eruptive geochemistry of the ignimbrite-forming magmas of the Campanian Volcanic Zone, Southern Italy, determined from silicate melt inclusions. Miner Petrol 79(1-2):99-125 doi:Doi 10.1007/S00710-003-0004-6

Wolff JA, Ellis BS, Ramos FC, Starkel WA, Boroughs S, Olin PH, Bachmann, O (2015) Remelting of cumulates as a process for producing chemical zoning in silicic tuffs: A comparison of cool, wet and hot, dry rhyolitic magma systems. Lithos 236-237, 275-286.

Wood BJ, Blundy JD (1997) A predictive model for rare earth element partitioning between clinopyroxene and anhydrous silicate melt. Contrib Mineral Petr 129(2-3):166-181 doi:Doi 10.1007/S004100050330

Wood BJ, Blundy JD (2001) The effect of cation charge on crystal-melt partitioning of trace elements. Earth Planet Sc Lett 188(1-2):59-71 doi:Doi 10.1016/S0012-821x(01)00294-1

Wood BJ, Blundy JD (2002) Trace element partitioning - new developments building on the lattice strain model. Geochim Cosmochim Ac 66(15A):A846-A846

Wood BJ, Trigila R (2001) Experimental determination of aluminous clinopyroxene-melt partition coefficients for potassic liquids, with application to the evolution of the Roman province potassic magmas. Chem Geol 172(3-4):213-223 doi:Doi 10.1016/S0009-2541(00)00259-X

Yao LJ, Sun CG, Liang Y (2012) A parameterized model for REE distribution between low-Ca pyroxene and basaltic melts with applications to REE partitioning in low-Ca pyroxene along a mantle adiabat and during pyroxenite-derived melt and peridotite interaction. Contrib Mineral Petr 164(2):261-280 doi:Doi 10.1007/S00410-012-0737-5

Zollo A, Maercklin N, Vassallo M, Dello Iacono D, Virieux J, Gasparini P (2008) Seismic reflections reveal a massive melt layer feeding Campi Flegrei caldera. Geophysical Research Letters 35(12) doi:Doi 10.1029/2008gl034242

Figure captions

Fig. 1. The compositions of host melts and clinopyroxene phenocryst cores from this study are compared with those of natural products at Campi Flegrei in terms of total alkali vs. silica of the melt (a), ΣHREE vs. ΣLREE of the melt (b), Di vs. Hd of clinopyroxene, and (c) ΣHREE vs. ΣLREE of clinopyroxene. Natural data from Villemant (1988), Civetta et al. (1997), Fulignati et al. (2004), Marianelli et al. (2006), Fedele et al. (2007), Pappalardo et al. (2002; 2008), and Arienzo et al. (2009).

Fig. 2. Example of the textural features of clinopyroxene phenocrysts from this study. (a) Backscattered electron images show that crystals are euhedral and complex zoning patters are absent. Microprobe compositional profiles reveal the occurrence of some chemical heterogeneities

942 at the crystal-melt interface. (b) Diffusive boundary layer occurs into the glass next to
943 clinopyroxene rims showing Al and Na enrichments (see also data in Table 5S).
944
945 Fig. 3. Plots of partition coefficients for HFSE (Ti, Zr, Nb, Ta), REE (La) and TE (Co) vs. Al^{iv}.
946 Data from this study have been compared with those from literature to highlight the dependence of
947 D_i on Al^{iv}.
948
949 Fig. 4. Plots of partition coefficients for REE and Y vs. ionic radii (data from Shannon 1976) for the
950 samples object of this study. The near parabolic dependence found by Onuma et al. (1968) dictates
951 the distribution of the data. The lines show fits to the lattice strain model of Blundy and Wood
952 (1994). Fit parameters are listed in Table 4S. The agreement of our data with the model emphasizes
953 the importance of lattice strain in controlling REE and Y partitioning at equilibrium crystallization
954 conditions.
955
956 Fig. 5. Plots of D_0^{3+} for clinopyroxene-melt partitioning of REE vs. Al^{iv} content in clinopyroxenes
957 from this study and previous works. D_0^{3+} is calculated through the lattice strain model of Blundy
958 and Wood (1994).
959
960 Fig. 6. Plot of D_0^{3+} for clinopyroxene-melt partitioning of REE vs. *NBO/T* of the melt. (a) Our data
961 for trachy-phonolitic melts are compared with those from literature obtained for highly polymerized
962 silicic melts, and moderately-to-poorly polymerized silicic melts. According to Gaetani (2004) and
963 Huang et al. (2006) the melt structure have a significant influence on partition coefficients for
964 $[NBO/T]^{melt}$ values higher than 0.4. (b) Plot of D_0^{3+} for clinopyroxene–melt partitioning of REE vs.
965 $[Ca^{2+}/(M^{+}+M^{2+})]^{melt}$, where M^{+} and M^{2+} are $Na^{+}+K^{+}$ and $Fe^{2+}+Ca^{2+}+Mg^{2+}$, respectively . The
966 negative correlation between D_0^{3+} and $[Ca^{2+}/(M^{+}+M^{2+})]^{melt}$ confirms the reliability of Eqn. (2)

967 favouring large structural sites critically important to accommodating large trace element cations in
968 the melt.
969
970 Fig. 7. Clinopyroxene-melt pairs from this study, Pappalardo et al. (2008) and Fedele et al. (2009)
971 have been used as input data for the original equation for D_0^{3+} derived by Wood and Blundy (1997).
972 New predictors have been also introduced in this equation, i.e., $[REE]^{cpx}/[X^{3+}]$ (after Wood and
973 Blundy, 2001) and $[REE]^{melt}/[Ca^{2+}/(M^{+}+M^{2+})]^{melt}$. The analysis of predicted vs. measured values
974 indicates that these new predictors do not offer improvements for the ability prediction of the
975 original equation of Wood and Blundy (1997).
976
977 Fig. 8. Clinopyroxene-melt pairs from this study, Pappalardo et al. (2008) and Fedele et al. (2009)
978 have been used as input data for the original equations for (a) E and (b) r_0 derived by Wood and
979 Blundy (1997). The analysis of predicted vs. measured values indicates that these equations are
980 affected by a high uncertainty. The best fitting equations have been derived through the regression
981 analysis of trachy-phonolitic data using X_{Ca}^{M2} and X_{Mg}^{M2} as predictors.
982
983 Fig. 9. The predictive equations for E from (a) Wood and Blundy (1997) and (b) this study have
984 been tested using trachy-phonolitic (this study, Pappalardo et al., 2008 and Fedele et al., 2009) and
985 basaltic (Green et al., 2000 and Adam and Green, 2006) data. For the original equation of Wood
986 and Blundy (1997), the percentage error of E increases with decreasing temperature. The opposite
987 occurs for the equation from this study showing low ability prediction for high-temperature basaltic
988 magmas.
989
990 Fig. 10. D_{REE} and D_Y "measured" in this study are compared with those "predicted" by the original
991 model of Wood and Blundy (1997), the parameterized model of Sun and Liang (2012) for basaltic
992 compositions, and the recalibrated model from this study for trachy-phonolitic compositions. (a)

993 Comparison of the standard error of estimate. (b) Comparison of D_{Ce} values as representative of
994 partitioning of larger LREE cations. (c) Comparison of D_{Yb} values as representative of partitioning
995 of smaller LREE cations.
996
997 Fig. 11. Natural clinopyroxene-melt pairs from the Campanian Ignimbrite have been used as input
998 data for the thermobarometer of Masotta et al. (2013) and the trace element model presented in this
999 study. (a) Temperature vs. $Mg\#^{cpx}$ diagram shows that the geochemical evolution of clinopyroxene
1000 parallels the decreasing temperature of magma. Each symbol plotted on the diagram refers to the
1001 value of D_0^{3+} predicted using the Excel spreadsheet from this study. D_0^{3+} is found to increase from
1002 0.60 to 0.85 with decreasing both T and $Mg\#^{cpx}$. (b) Ce vs. Y diagram showing the geochemical
1003 evolution of the Campanian Ignimbrite modelled through the Rayleigh fractional crystallization
1004 equation. At the beginning of the modelling, low degrees of clinopyroxene fractionation (i.e., 3%,
1005 5%, 7%, and 9%) have been considered. Stepwise calculations were performed changing the
1006 clinopyroxene composition and temperature at each step of fractionation. Modelled Ce and Y
1007 concentrations were used to draw the ^{cpx}FC vector. Fractional crystallization calculations were
1008 further developed accounting for the segregation of ~50% of K-feldspar from the solidifying
1009 magma. Modelling results are aligned along four different FC trajectories (i.e., from ^{kfs}FC1 to
1010 ^{kfs}FC4).

Trace element partitioning between clinopyroxene and trachy-phonolitic melts: A case study from the Campanian Ignimbrite (Campi Flegrei, Italy)

S. Mollo[1,2], F. Forni[3], O. Bachmann[3], J. D. Blundy[4], G. De Astis[2], P. Scarlato[2]

[1]Dipartimento di Scienze della Terra, Sapienza-Università di Roma, P.le Aldo Moro 5, 00185 Roma, Italy

[2] Istituto Nazionale di Geofisica e Vulcanologia, Roma, Italy

[3] Department of Earth Sciences, Institute of Geochemistry and Petrology, ETH, Zurich, Switzerland

[4] School of Earth Sciences, University of Bristol, Bristol, United Kingdom

Corresponding author:
Silvio Mollo
Sapienza-Università di Roma
Dipartimento di Scienze della Terra
P.le Aldo Moro 5
00185 Roma, Italy
e-mail silvio.mollo@uniroma1.it

Abstract

The partitioning of trace elements between crystals and melts provides an important petrogenetic tool for understanding magmatic processes. We present trace element partition coefficients measured between clinopyroxene phenocrysts and trachy-phonolitic magmas at the Campi Flegrei (Italy), whose late Quaternary volcanism has been characterized by two major caldera-forming events (Campanian Ignimbrite at ~39 ka, and the Neapolitan Yellow Tuff at ~15 ka). Our data indicate that the increase of trivalent rare earth elements and yttrium into the crystal lattice M2 site is facilitated by the charge-balancing substitution of Si^{4+} with Al^{3+} on the tetrahedral site. Higher concentrations of tetravalent and pentavalent high field strength elements on the M1 site are also measured when the average charge on this site is increased by the substitution of divalent cations by Al^{vi}. In contrast, due to these charge balance requirements, divalent transitional elements become less compatible within the crystal lattice. On the basis of the lattice strain theory, we document that the incorporation of rare earth elements and yttrium in clinopyroxene is influenced by both compositional and physical parameters. Data from this study allow to update existing partitioning equations for rare earth elements in order to construct a self-consistent model for trachy-phonolitic magmas based on the lattice strain theory. The application of this model to natural products from the Campanian Ignimbrite, the largest caldera-forming eruption at the Campi Flegrei, reveals that the complex rare earth element pattern recorded by the eruptive products can be successfully described by the stepwise fractional crystallization of clinopyroxene and feldspar where the clinopyroxene-melt partition coefficient changes progressively as a function of the physicochemical conditions of the system.

Keywords: clinopyroxene-melt trace element partitioning; lattice strain theory; trachy-phonolitic magmas; Campi Flegrei.

Introduction

Clinopyroxene is one of the most important constituents of igneous rocks and its crystallization behaviour impacts significantly the composition of magmas. The partitioning of trace elements between clinopyroxene and melt is frequently used in petrological and geochemical studies to better understand magma differentiation processes, such as fractional or equilibrium crystallization, assimilation, and partial melting. For simplicity, the clinopyroxene-melt partition coefficient [$D_i = {}^{xls}(I)/{}^{melt}(I)$ on a weight basis] is generally assumed to be constant for magma modelling. However, this simple approximation does not take into account for the effects of crystal and melt compositions, as well as the physical conditions of the system on trace element partitioning. Wood and Blundy (1997) showed for the first time that partition coefficients of rare earth elements (REE) can be modelled as a function of composition of the crystal (X_{Mg}^{M1}), *Mg*-number of the melt [$Mg\#^{melt} = X_{Mg}^{melt} / (X_{Fe}^{melt} + X_{Mg}^{melt})$], pressure ($P$) and temperature ($T$). Crystal chemistry influences both the dimensions of the M2 site, into which REE partition, and the molar fraction of the hypothetical REE end-member, such as $REEMgAlSiO_6$. Blundy et al. (1998) and Bennett et al. (2004) also argued that D_{REE} is dependent on X_{Na}^{M2} due to the higher incorporation of Na^+ in M2 with increasing P, for example via the hypothetic end-member $Na_{0.5}REE_{0.5}MgSi_2O_6$. Furthermore, Hill et al. (2000), Wood and Trigila (2001) and Wood and Blundy (2001) documented a close relationship between REE partitioning and the concentration of tetrahedrally-coordinated aluminum in clinopyroxene, as required for charge balance. Sun and Liang (2012) derived a predictive model in which D_{REE} is positively correlated with X_{Al}^{iv} and X_{Mg}^{M2} , and negatively correlated with T and H_2O dissolved in the melt. Gaetani et al. (2003) attributed the decrease of D_{REE} with increasing H_2O to the depolymerizing effect of water on the melt structure. Moreover, complementary studies of Gaetani (2004) and Huang et al. (2006) pointed out that the melt structure becomes dominantly important

below a threshold value of the number of non-bridging oxygens per tetrahedral cations *(NBO/T*) corresponding to 0.4. As a whole, results from previous works highlight that the partitioning of trace elements between clinopyroxene and melt is governed by complex mechanisms whose effects and magnitudes on D_i depend on specific compositional and physical parameters that are still poorly understood for a significant number of natural cases.

In this study, we present a new set of apparent partition coefficients calculated for clinopyroxene phenocrysts in equilibrium with trachytic and phonolitic compositions from the Campi Flegrei (Italy). Despite the highly explosive nature of these magmas and their common involvement in hazardous volcanic settings, little attention has been given to the most important parameters that influence the partitioning of trace elements (however, see Pappalardo et al., 2008; Fedele et al., 2009). On the basis of the lattice strain theory derived by Blundy and Wood (1994), it has been determined to what extent the physicochemical conditions of the system may influence the partitioning of trace elements. Through an improved version of the predictive equations of Wood and Blundy (1997), we have also modelled the complex trace element compositions of several rock samples from the Campanian Ignimbrite, one of the largest late Quaternary volcanic eruptions in Europe.

Geological background

The Campi Flegrei, located within the Campanian Plain, belong to the potassic alkaline volcanic province of central Italy. Volcanism is still active, as demonstrated by fumarolic and seismic activity, and by recurrent episodes of unrest in the past 30 years (Orsi et al., 1999 and references therein). The highly explosive behaviour of magmas represents a continuous threat to more than one million people living in the city of Naples and its densely inhabited suburbs. This makes the Campi Flegrei one of the most dangerous volcanic systems in the world.

The caldera is a resurgent nested structure formed during two major collapses related to the eruptions of the Campanian Ignimbrite (CI) and the Neapolitan Yellow Tuff (NYT). Seismic reflections indicate the presence of a discontinuity at 7.5 km depth, where seismic velocities are consistent with values expected for a magma body set in a densely fractured volume of rock (Zollo et al., 2008). Petrological and melt inclusion studies suggest that differentiated alkaline melts formed dominantly through fractional crystallization from a more mafic parental magma, likely emplaced at depths between 4 and 8 km, with little assimilation of surrounding crust (Signorelli et al., 2001; Webster et al., 2003; Marianelli et al., 2006; Pabst et al., 2008; D'Antonio, 2011).

The Campanian Ignimbrite eruption (~39 ka; De Vivo et al., 2001) is regarded as the dominant event in the history of the Campi Flegrei with an initial areal distribution of ~30,000 km^2 (Rolandi et al., 2003). It consists of ~200 km^3 of pyroclastic-fall and pyroclastic-flow deposits (Civetta et al., 1997). The composition of the erupted products changed from trachyte to phonolite during the eruption. Phase equilibria data, geothermometry, and fluid inclusion analysis, suggest an overall thermal path of the magma from 840 to 1,080 °C (Fulignati et al., 2004; Marianelli et al., 2006; Fowler et al., 2007; Fedele et al., 2009; Masotta et al., 2013). Melt inclusion measurements and hygrometric predictions indicate a melt-water concentration ranging from 3 to 6 wt.% (Signorelli et al., 2001; Webster et al., 2003; Marianelli et al., 2006; Mollo et al., 2014). On the basis of these heterogeneous petrological information, it has been proposed that the CI magma evolved in a thermally and chemically zoned magmatic reservoir (Pappalardo et al., 2008; Pappalardo and Mastrolorenzo, 2012).

The Neapolitan Yellow Tuff eruption (~15 ka ; Deino et al., 2004) was the second more recent phreatoplinian event in the history of the Campi Flegrei. It erupted ~40 km^3 of pyroclastic-fall and pyroclastic-flow deposits dispersed over an area of more than ~1,000 km^2 (Orsi et al. 1992). The erupted products are characterized by latitic to trachytic compositions. The vent for the NYT eruption was located inside the caldera formed during collapse of the CI eruption, resulting in a final caldera that covered an area of ~90 km^2 (Orsi et al., 2009).

Analytical methods

Field emission gun scanning electron microscope (FE-SEM) images and electron probe micro analyses (EPMA) of twelve clinopyroxenes were collected at the HPHT Laboratory of Experimental Volcanology and Geophysics of the Istituto Nazionale di Geofisica e Vulcanologia (INGV) in Rome, Italy. Images were obtained through the backscattered electron (BSE) mode of a JEOL 6500F FE-SEM equipped with an energy-dispersive spectrometer (EDS) detector. Microprobe analyses were performed with a JEOL-JXA8200 EPMA equipped with five spectrometers. The beam diameter was ~1 μm with a counting time of 20 and 10 s on peaks and background respectively. The following standards were used: jadeite (Si and Na), corundum (Al), forsterite (Mg), andradite (Fe), rutile (Ti), orthoclase (K), barite (Ba), apatite (P), spessartine (Mn) and chromite (Cr). Sodium and potassium were analyzed first to prevent alkali migration effects. The precision of the microprobe was measured through the analysis of well-characterized synthetic oxides and minerals. Data quality was ensured by analyzing standard materials as unknowns. Based on counting statistics, analytical precision was better than 5% for all cations.

Major and trace elements of whole-rocks, and trace elements of clinopyroxene phenocrysts were measured at the Institute of Geochemistry and Petrology of the ETH Zürich, Switzerland. For the whole-rock analyses 1.5 g of powdered sample was heated to 950 °C for 2 h in a chamber furnace and then weighed to determine the loss on ignition (LOI). The ignited material was charged in a Pt-Au crucible and fused with a 1:5 Lithium-Tetraborate mixture using a Claisse M4® fluxer. The fused disk was analysed for major elements using a wave-length dispersive X-ray fluorescence spectrometer (WD-XRF; Axios PANanalytical) equipped with five diffraction crystals. Calibration was based on thirty certified international standards of predominantly igneous and metamorphic rocks. Trace element analyses of both whole-rock disks and clinopyroxene phenocrysts were performed through a 193 nm excimer laser coupled with a second generation two-volume constant

geometry ablation cell (Resonetics:S-155LR) and a high-sensitivity, sector-field inductively-coupled plasma mass spectrometer (ICP-MS; Thermo:Element XR). Points with a spot size of 45 μm were set on chemically homogeneous portions of the material (i.e., clinopyroxene cores) previously analyzed by EPMA, and ablated with a pulse rate of 10 Hz and an energy density of 3.5 J/cm^3 for 40 sec. The isotopes were analyzed relative to an internal standard of known composition (i.e., NIST612). A second standard (i.e., GSD-1G) was used as an unknown to check the quality of data during each analytical run. ^{43}Ca or ^{29}Si were used as internal standards for clinopyroxene and whole-rock analyses, respectively, in order to recover the concentrations of light and heavy rare earth elements (REE divided in LREE and HREE), high field strength elements (HFSE), large ion lithophile elements (LILE) and transition elements (TE). The precision of individual analyses varied depending upon a number of factors, e.g., the element and isotope analyzed as well as the homogeneity of the ablated material. However, the 1 sigma errors calculated from variations in replicate analyses of crystals and whole-rock disks were invariably several times larger than the fully integrated 1 sigma errors determined from counting statistics alone.

Sample description

Sampled rocks belong to twelve pyroclastic deposits at the Campi Flegrei characterized by variable proportions of juvenile material (i.e., pumices, scoriae, spatter clasts, fiamme and obsidians), variably porphyritic textures (10-25 vol.% of phenocrysts), and the ubiquitous occurrence of clinopyroxene, biotite, K-feldspar, plagioclase, opaques, and rare apatite. Samples were collected from different outcrops in order to fully characterize the compositions of clinopyroxene phenocrysts and host magmas of pre-CI, CI, post-CI, NYT, and post-NYT eruptions (see Table 1S for the locations). Major and trace element concentrations measured for crystals and melts are reported in Tables 1S and 2S, respectively. We present our data in comparison with those of Pappalardo et al. (2008) and Fedele et al. (2009) that provided a complete dataset comprising whole-rock analyses,

clinopyroxene chemistries, apparent partition coefficients for REE, and lattice strain parameters (see below) of four additional rock samples from the Campanian Ignimbrite eruption.

Whole-rock analyses show increasing SiO_2 contents (57-62 wt.%) with decreasing CaO (1.8-5.3 wt.%) and $Mg\#^{melt}$ (16-40). All compositions are also rich in alkali (Na_2O+K_2O = 11-14 wt.%). In the TAS (total alkali vs. silica; Le Bas et al., 1986) diagram, samples are classified as trachytes and phonolites, in agreement with most of the differentiated alkaline products at Campi Flegrei (Fig. 1a). Whole-rocks exhibit a variable degree of differentiation that, in terms of trace element concentrations, reproduces well the evolutionary behaviour of magmas (Fig. 1b). The increase of REE is commonly associated with a significant increase in Th, U, Nb, Ta, Zr and Hf, and decrease in Sr testifying to an increased plagioclase fractionation (Table 2S).

Clinopyroxenes occur as euhedral phenocrysts (longest size dimensions > 0.3 mm) with diopsidic compositions (Morimoto, 1988). Al^{iv} (0.05-0.13 apfu) is positively correlated with Ti^{+4} (0.01-0.04 apfu) and negatively correlated with $Mg\#^{cpx}$ (0.73-0.84). The ratio of octahedrally-coordinated to tetrahedrally-coordinated aluminium cations is less than 1 in all phenocrysts, indicating preferential incorporation of Al^{iv} at low pressure crystallization conditions (Muñoz and Sagredo, 1974; Putirka, 1996; Mollo et al., 2011b). The ratio of Fe^{3+}/Fe^{2+} in clinopyroxenes, as calculated from stoichiometry, ranges between 0 and 0.5 with values identical to those experimentally-derived for magmas at Campi Flegrei equilibrated at NNO+1 and NNO+2 oxygen fugacity (Fabbrizio and Carroll, 2008; Masotta et al., 2013). Diopside vs. hedenbergite (Fig. 1c) and Ce vs. Y (Fig. 1d) diagrams suggest that major and trace elements of our clinopyroxenes capture most of the geochemical evolution of phenocrysts at Campi Flegrei.

Apparent trace element partition coefficients were measured for pre-CI, CI, post-CI, NYT, and post-NYT samples using clinopyroxene core and whole-rock analyses that were found to be in equilibrium (see below) and are reported in Table 3S. The most important changes of D_i can be summarized as follows: (i) LREE (e.g., $D_{La} \leq 0.27$) are more incompatible than HREE (e.g., $D_{Dy} \leq 1.67$); (ii) TE are always compatible within clinopyroxene (e.g., $D_{Co} \leq 10.07$); (iii) pentavalent

HFSE cations are more incompatible (D_{Nb} and $D_{Ta} \leq 0.05$) that tetravalent HFSE cations (D_{Zr} and $D_{Hf} \leq 0.87$) and; (iv) LILE are generally incompatible (e.g., $D_{Sr} \leq 0.8$) with the exception of one sample ($D_{Sr} = 1.39$ for PM2).

Assessment of equilibrium crystallization conditions

Laboratory investigations of clinopyroxene-melt partition coefficients are generally designed to guarantee the achievement of equilibrium between crystals and melts. The initial rate of cooling and the time duration of experiments are set to ensure that the melt supplies nutrients at equilibrium proportions to the growing crystals. The experimental charges are then quenched at very fast cooling rates and the system is almost instantaneously "frozen-in" (e.g., quenching rate of 2,000 °C/min; Freda et al., 2008). Due to the use of rapid quenching conditions, disequilibrium processes may only operate at the nanometre scale, leading to the formation of a diffusive boundary layer with thickness orders of magnitude lower that the analytical spot size used for major and trace element measurements (e.g., Mollo et al., 2012). On the other hand, apparent partition coefficients obtained from natural samples measuring the compositional ratios between bulk phenocrysts and host lavas (i.e., whole-rock analyses) are potentially biased by contamination or disequilibrium processes. Even when single point analyses are carried out at the crystal-melt interface, the compositional zoning of minerals and surrounding glasses can make the accurate determination of D_i extremely difficult. The entrapment of melt in rapidly growing crystals may increase the value of D_i by up to 3 orders of magnitude (Kennedy et al., 1993). Additionally, rapid crystal growth conditions are not necessary accompanied by detectable melt entrapments or crystal discontinuities and, under such circumstances, disequilibrium values of D_i can exhibit variations in the same order of magnitude of equilibrium data (Mollo et al., 2013a).

For the purpose of this study, we have accurately inspected each phenocryst and coexisting glass using SEM and EPMA, in order to make sure that the occurrence of melt inclusions, crystal

zoning and/or melt diffusion phenomena were kept to a minimum. Clinopyroxenes are generally euhedral with well-defined edges and without evident zoning patters (Fig. 2a). However, microprobe compositional profiles reveal the occurrence of chemical heterogeneities at the crystal-melt interface (Fig. 2b and Table 5S). A diffusive boundary layer occurs into the glass next to clinopyroxene surface. This thin diffusive boundary layer is enriched in chemical species less compatible in clinopyroxene crystal lattice (e.g., Al and Na). Concentration–dependent partitioning produces crystal growth layers that respond to the chemical gradients in the melt, producing Al and Na enrichments in clinopyroxene that are identical to those experimentally documented by cooling rate studies (Lofgren et al., 2006; Mollo et al., 2013b). Compositional perturbations at the crystal rim also suggest that, at the closure temperature of the crystal growth (i.e., $T_{final} << T_{liquidus}$), the free energy difference between the crystal surface and the liquid was large enough that diffusion became the rate-controlling process (Watson and Muller, 2009). Due to the high explosivity of eruptions at Campi Flegrei, phenocrysts underwent typically high degrees of undercooling during magma ascent in the volcanic conduit and eruption to the surface (Pappalardo and Mastrolorenzo, 2012 and references therein). Mollo et al. (2013b) proposed an equilibrium model based on the difference (Δ) between diopside+hedenbergite (DiHd) components predicted for clinopyroxene via regression analyses of clinopyroxene-liquid pairs in equilibrium conditions, with those measured in the analyzed phenocrysts. Mollo and Masotta (2014) successfully tested this model on trachytic and phonolitic compositions obtained at both equilibrium and disequilibrium conditions. Calculations performed using clinopyroxene rim and coexisting melt compositions yield values of 0.11-0.16 (Fig. 2b) that are considerably higher than those measured at near-equilibrium conditions (ΔDiHd $\leq$ 0.02). This suggests that D_i values measured at the crystal-melt interface results from disequilibrium partitioning due to the effect of rapid magma decompression and degassing at the time of eruption (e.g., Lanzafame et al., 2013; Mollo et al., 2015a). On the other hand, it is reasonable to infer that, over the timescale of magma chamber evolution and in absence of perturbation phenomena (e.g., magma mixing), early-formed clinopyroxene phenocrysts may have crystallized in equilibrium with

259 the host magma, despite the occasional occurrence of chemical heterogeneities or melt inclusions in
260 crystal that tend to reduce the accuracy of D_i calculations. In light of this, apparent trace element
261 partition coefficients have been calculated by the analyses of bulk phenocrysts and whole-rock
262 compositions (e.g., Schnetzler and Philpotts 1970; Nagasawa and Schnetzler 1971; Nagasawa 1973;
263 Mahood and Hildreth 1983; Lemarchand et al. 1987; Villemant 1988).

264 Experiments and thermodynamic studies have clearly documented that clinopyroxene is the
265 liquidus phase of trachytic and phonolitic melts (Fowler et al., 2007; Fabbrizio and Carroll, 2008;
266 Masotta et al., 2013, Del Bello et al., 2014). Under such circumstances, near-liquidus crystals are
267 represented by early-formed cores of large phenocrysts that likely equilibrated with the host magma
268 (i.e., whole-rock analysis) in terms of major and trace element concentrations (see for example the
269 studies of Armienti et al., 2007; Masotta et al., 2010; Mollo et al., 2011a; Lanzafame et al., 2013;
270 Scarlato et al., 2014). In this respect, Fig. 2b shows the development of an almost homogeneous
271 plateau composition at the clinopyroxene core that suggests near-equilibrium crystallization and
272 excludes chemical perturbations in the original magma. Tests conducted with the model of Mollo et
273 al. (2013b) yield ΔDiHd values between 0 and 0.02 testifying to equilibrium or near-equilibrium
274 conditions between phenocryst core and whole-rock data that were therefore used for our D_i
275 calculations (see also ΔDiHd values reported in Table 1S).

276 As stated above, the differentiation of magmas mostly occurs at shallow crustal levels (100-
277 300 MPa) where the effect of pressure on near-liquidus clinopyroxene-melt partition coefficients is
278 expected to be minimal. Thermodynamic data derived by the lattice strain model indicate that the
279 influence of P on D_i can be considered negligible at pressures lower than 500 MPa (Blundy and
280 Wood, 2003). It could be argued that REE partitioning is also sensitive to sodium in clinopyroxene,
281 which in turn varies with pressure (Blundy et al., 1995; Bennett et al., 2004). However, the control
282 of Na^+ on D_{REE} is dominant only at mantle pressures (≥ 3 GPa) where sodium concentration (Na_2O
283 = 2.2-13.5 wt.%; data from Klemme et al., 2002; Bennett et al., 2004; Marks et al., 2004) is one to
284 two order of magnitude higher than that measured in our phenocrysts (Na_2O = 0.15-0.56 wt.%;

Table 1S). Therefore, in terms of physical parameters, temperature is likely the most important variable that can influence D_i at the crystallization conditions of magmas. To estimate the equilibration temperatures and pressures of clinopyroxene-melt pairs from this study (Table 1S), we have used the thermometers and barometers of Masotta et al. (2013) specifically calibrated for trachytic and phonolitic compositions. A melt-water content of 3 wt.% has been set in the model, in agreement with most of the water concentrations measured by melt inclusion studies on Campi Flegrei (Signorelli et al., 2001; Webster et al., 2003; Marianelli et al., 2006). We have established that a water change of ±2 wt.% produces temperature and pressures variations of only ±12 °C and ±15 MPa, which are well below the errors of estimate of the thermometer (±24 °C) and barometer (±114 MPa). Results from calculations indicate that our clinopyroxenes crystallized at temperatures and pressures of 840-1,020 °C and 85-309 MPa (Table 1S), in close correspondence with those (840-1,080 °C and 20-300 MPa) derived for trachy-phonolitic products belonging to the Campanian Ignimbrite eruption (Fedele et al., 2009; Masotta et al., 2013).

Discussion

Trace element partition coefficients

The dependence of trace element partition coefficient on tetrahedrally-coordinated aluminium has been the focus of many studies on clinopyroxene (Lindstrom 1976; Ray et al. 1983; Hart and Dunn 1993; Forsythe et al. 1994; Lundstrom et al. 1994, 1998; Skulski et al. 1994; Blundy et al. 1998; Hill et al. 2000; Wood and Trigila 2001; Sun and Liang, 2012; 2013; Mollo et al., 2013a; Yao et al., 2013; Scarlato et al., 2014). In Fig. 3, the close correspondence between D_i and Al^{iv} for representative HFSE, REE and TE, is confirmed and extended to trachytic and phonolitic magmas. Note that the gray fields in Fig. 3 indicate that our D_i values are consistent with those previously calculated for magmas at Campi Flegrei (data from Pappalardo et al., 2008 and Fedele et al., 2009).

From a crystallochemical point of view, HFSE enter the smaller M1 octahedral site, and the correlation between D_{HFSE} and Al reflects the increasing charge on this site with increasing $CaAl_2SiO_6$ and $CaFeAlSiO_6$ substitution, i.e., with increasing replacement of Mg^{2+} by Fe^{3+} and Al^{3+} (Wood and Trigila, 2001). Thus, entry of +4 and +5 ions into M1 is enabled by the substitution of Al^{+3} for Si^{+4} in the tetrahedral site (Hill et al., 2000; Mollo et al., 2013a). In the case of trivalent trace elements, REE and Y enter the large M2 site that, apart from minor amounts of Na^{+}, is almost exclusively occupied by Ca^{2+}, Mg^{2+}, and Fe^{2+}. Data plotted in Fig. 3 show a clear positive correlation between D_{La} and Al^{iv} that has been extensively documented under both equilibrium and disequilibrium crystal growth conditions (Gaetani and Grove, 1995; Blundy et al., 1998; Mollo et al., 2013a; Scarlato et al., 2014). The dependence of REE partitioning on tetrahedral aluminium reflects an increased ease of locally balancing the excess charge at M2 as the number of surrounding Al^{iv} atoms increases. For example, the concentration of La in our clinopyroxenes progressively increases from 8 to 46 ppm as the molar Al/Si ratio decreases from 0.11 to 0.05 (Tables 1S and 2S). This matches with the consideration that clinopyroxenes can accommodate REE simply by adjusting their Al/Si ratios, without producing an energetically unfavourable vacancy (Hill et al., 2000; Wood and Trigila, 2001). The importance of site charge for achieving local charge balance is provided by the different behaviour of Sr and Co as divalent cations entering M2 and M1 sites, respectively. Since charge on the M2 site is the same in both $CaMgSiO_2$ and $CaAl_2SiO_6$, no correlation is found between D_{Sr} and tetrahedrally-coordinated aluminum (cf. Hill et al., 2000). In contrast, the M1 site requires an increased net charge (2+ to 3+) to balance the increase in Al substitution for Si (cf. Mollo et al., 2013a), such that Co becomes less compatible as $CaAl_2SiO_6$ content increases (Fig. 3).

The lattice strain model

Fig. 4 shows that our apparent partition coefficients for REE and Y lie on parabola-like curves of Onuma diagrams (Onuma et al., 1968), resembling the regular trajectories found by Pappalardo et al. (2008) and Fedele et al. (2009) for magmas at Campi Flegrei. The height of the parabola depends on the crystal composition (Matsui et al., 1977; Blundy and Wood, 1994; 2003) and the physical conditions of the system (Blundy and Wood, 2001; Sun and Liang, 2012). Blundy and Wood (1994) provided a quantitative model for the parabolic trend of an isovalent series of cations with radius, r_i, entering crystal lattice site M, where the partition coefficient, D_i, can be described in terms of (i) the radius of the site, r_0, (ii) the elastic response of that site, E (as measured by Young's Modulus), to lattice strain caused by cations that are larger or smaller than r_0, and (iii) the strain-free partition coefficient, D_0, for a (fictive) cation with radius r_0:

$$D_i = D_0 \exp\left(\frac{-4\pi E N_A\left(\frac{r_0}{2}(r_i - r_0)^2 + \frac{1}{3}(r_i - r_0)^3\right)}{RT}\right) \quad (1)$$

In Eqn. (1), N_A is Avogadro's number (6.022×10^{23} mol^{-1}), R is the universal gas constant (8.3145 J mol^{-1} K^{-1}), and T is the temperature (in Kelvin). The effective use of the lattice strain model requires partition coefficients for a large range of isovalent cations of appropriate ionic radii for substitution into the M site. Therefore, to obtain reliable estimates and minimize the standard error, we focused on r_0, D_0, and E for the partitioning of trivalent REE and Y cations (Table 3S), as they form the largest group of isovalent elements in our analytical dataset. Except for one sample with $D_0^{3+} \approx 1$, we observe that, as a general rule, the peak position of our partitioning parabolas corresponds to $D_0^{3+} \geq 1$ when $Al^{iv} \geq 0.09$ apfu and $T \leq 950$ °C (Tables 1S and 3S and Fig. 4). Otherwise, the peak position can be alternatively higher or lower than 1 as a function of Al^{iv} and T, in agreement with the observation that these parameters have opposing effects on trace element partitioning (cf. Sun and Liang, 2012). Fitting of the parabolic trends indicates a good agreement between modelled and

360 measured values of D_0^{3+} (Table 4S and Fig. 4), suggesting the attainment of a thermodynamic
361 equilibrium between phenocrysts and host magmas.

362 At first, D_0^{3+} and D_{REE} were taken to be independent of the Al^{iv} content in clinopyroxene
363 due to assumed complete short-range order between REE on M2 site and Al in T site in the
364 molecule $REEMgAlSiO_6$ (e.g., Wood and Blundy, 1997). Subsequently, this assumption has since
365 been found to be an oversimplification (Wood and Trigila, 2001; Hill et al., 2000; Tuff and Gibson,
366 2007, Mollo et al., 2013a; Scarlato et al., 2014), probably due to more complex charge-balance
367 mechanisms than simple short-range order (Wood & Blundy, 2001). In Fig. 5, lattice strain-free
368 partition coefficients for clinopyroxenes in trachy-phonolitic melts are compared with those
369 obtained by previous studies on ultramafic, mafic and silicic compositions. D_0^{3+} increases
370 significantly with increasing tetrahedral aluminium, providing clear evidence of the effect of crystal
371 composition on REE and Y partitioning. Importantly, three different trends are depicted in Fig. 5 for
372 different bulk melt chemistries. The value of D_0^{3+} and the slope of each single trend increase as a
373 function of the melt composition (i.e., SiO_2), suggesting that the control of Al^{iv} on D_0^{3+} is mediated
374 by the increasing silicic character of the bulk melt (Fig. 5). Gaetani (2004) observed that the
375 magnitude of the partition coefficient correlates with the degree of melt polymerization due to a
376 melt structural influence on trace element partitioning. The complementary results from Gaetani
377 (2004) and Huang et al. (2006) noted that melt structure affects the trace element compatibility only
378 if $[NBO/T]^{melt} < 0.4$. This is confirmed by our data showing a somewhat higher D_0^{3+} for a lower
379 $[NBO/T]^{melt}$ (Fig. 6a), although this parameter may not provide a comprehensive description of melt
380 structure at a level relevant to trace element partitioning (e.g., Bennett et al., 2004). On this basis,
381 Huang et al. (2006) found that D_0^{3+} is better correlated with the ratio of molar $[Ca^{2+}/(M^{+}+M^{2+})]^{melt}$,
382 where M^{+} and M^{2+} are, respectively, Na^{+} and K^{+}, and Fe^{2+}, Ca^{2+} and Mg^{2+} of the melt given as
383 percentages. Because of the similarity in ionic radius (and charge), REE^{3+} are more likely to
384 substitute for Ca^{2+} in the melt than Mg^{2+}, Fe^{2+}, or alkalis, so that the value of D_{REE} decreases
385 according to the following exchange reaction (Huang et al., 2006):

386

387 $[REE_{2/3}MgSi_2O_6]^{cpx} + [Ca\text{-}NBO]^{melt} \leftrightarrow [CaMgS_2O_6]^{cpx} + [REE_{2/3}\text{–}NBO]^{melt}$ (2)

388

389 Our data show that, for higher values of $[Ca^{2+}/(M^{+}+M^{2+})]^{melt}$, there is an effective increase in the
390 number of large structural sites critically important to accommodating large trace element cations in
391 the melt, serving to reduce the partition coefficient (Fig. 6b). However, due to simultaneous effects
392 of crystal and melt compositions on REE and Y partitioning, data in Fig. 6b do not align on a single
393 linear fit for the substitution reaction described by Eqn. (2). To eliminate such an effect, some
394 experiments should be designed for the comparison between clinopyroxenes with similar crystal-
395 chemical formulas and compositionally distinct host melts (cf. Huang et al. 2006).

396

397 Testing the model of Wood and Blundy (1997)

398

399 Most of the mathematical expressions used to model the evolutionary behaviour of magma assume
400 that the value of D_i remains constant throughout the entire differentiation process. This raises issues
401 for petrological and geochemical modelling to (i) adopt the best possible partition coefficients, (ii)
402 evaluate the extent to which these partition coefficients vary in the course of magma differentiation,
403 (iii) find the physicochemical parameters that closely describe the variance of D_i, and (iv) derive a
404 good predictive model that is easy and rapid to use (e.g., based on microprobe analyses). In order to
405 address all these issues, an increasing number of predictive equations for D_i have been derived in
406 the last decades on the basis of thermodynamic approaches (e.g., Wood and Blundy, 1997, 2011;
407 Hill et al., 2011), linear least squares regression analyses (e.g., Forsythe et al., 1994; Skulski et al.,
408 1994; Gaetani and Grove, 1995) and multivariable nonlinear least squares analyses (Yao et al.,
409 2012; Sun and Liang, 2012, 2013; Dygert et al., 2014). Among the number of equations found in
410 literature, we have primary used the whole dataset for partition coefficients of Campi Flegrei (i.e.,
411 D_{REE} from this study, Pappalardo et al., 2008, and Fedele et al., 2009) to test the early predictive

412 model of Wood and Blundy (1997). The authors modelled the clinopyroxene–melt REE partitioning
413 using the theoretical strain-free partition coefficient for 3+ cations in M2, which they then
414 parameterised as a function of *P* and *T*. By fitting experimental data to the temperature (*T* in Kelvin)
415 and pressure (*P* in GPa) derivatives of the bulk and shear moduli of diopside, Wood and Blundy
416 (1997) found a simple equation for calculating the Young's Modulus for the trace elements of +3
417 charge in the M2 site of clinopyroxene:
418
419 $$E_{M2}^{3+} = 318.6 + 6.9P - 0.036T \quad (3)$$
420
421 Given the expression (3) for E_{M2}^{3+}, the change of r_0 was also modelled through stepwise linear
422 regression of the values of r_0 derived from literature data against all major compositional
423 parameters, pressure and temperature. It emerged that only X_{Al}^{iv} and X_{Ca}^{M2} were important
424 controlling factors for r_0:
425
426 $$r_0 = 0.974 + 0.067 X_{Ca}^{M2} - 0.051 X_{Al}^{M1} \quad (4)$$
427
428 To calculate D_0^{3+}, a simple ionic equilibrium involving melt and clinopyroxene was considered:
429
430 $$REEMgAlSiO_6^{melt} = REEMgAlSiO_6^{cpx} \quad (5)$$
431
432 The equilibrium constant of the exchange reaction (5) is:
433
434 $$K_{ex}^{3+} = \frac{X_{REE}^{M2} X_{Mg}^{M1} X_{Al}^{T} X_{Si}^{T}}{X_{REE}^{melt} X_{Mg}^{melt} X_{Al}^{melt} X_{Si}^{melt}} \quad (6)$$
435

In a thermodynamic approach based on the lattice strain theory, X_{Mg}^{M1} and $Mg\#^{melt}$ are the expression of the activity compositions of clinopyroxene ($a_{REEMgAlSiO6}^{cpx} = X_{REE}^{M2} X_{Mg}^{M1}$) and melt ($a_{REEMgAlSiO6}^{melt} = X_{REE}^{melt} Mg\#^{melt}$), and D_0^{3+} is the ratio of X_{REE}^{M2} to X_{REE}^{melt}. Using these parameters, the equilibrium constant (6) was rearranged as:

$$K_{ex}^{3+} = \frac{D_0^{3+} X_{Mg}^{M1}}{Mg\#^{melt}} \quad (7)$$

If $\Delta H_T^0, \Delta S_T^0$, and ΔV refer to the differences in thermodynamic properties between pure melt and pure crystal, it was found that:

$$\Delta H_T^0 - T\Delta S_T^0 + P\Delta V - \frac{1}{2}\left(\frac{\partial \Delta V}{\partial P}\right)P^2 = RT \ln\left(\frac{D_0^{3+} X_{Mg}^{M1}}{Mg\#^{melt}}\right) \quad (8)$$

The regression analysis of REE data from literature provided the best fit of the thermodynamic parameters on the left side of the reaction (8):

$$RT \ln\left(\frac{D_0^{3+} X_{Mg}^{M1}}{Mg\#^{melt}}\right) - 7{,}050P + 770P^2 = 88{,}750 - 65.644T \quad (9)$$

When the dataset from the Campi Flegrei is used to test the equation (9), all the strain-free partition coefficients are successfully predicted (Fig. 7), and the regression analysis of measured vs. predicted values of D_0^{3+} yields a very high correlation coefficient (R^2 = 0.997) and low standard error of estimate (SEE = 0.048). To account for the dependence of D_i (Fig. 3) and D_0^{3+} (Fig. 5) on the amount of aluminium in the tetrahedral site of clinopyroxene, Wood and Trigila (2001) re-fitted

458 the original calibration dataset of D_0^{3+} by adding Al^{iv} as predictor to the *P* and *T* parameters
459 previously employed. It was found, however, that the tetrahedral aluminium is not statistically
460 significant for the predictive equation (9) and that D_0^{3+} is adequately described in terms of pressure
461 and temperature only. Moreover, when the value of D_0^{3+} is modelled after Wood and Blundy (2001)
462 assuming local charge balance between REE in the M2 site and adjacent Al^{iv} within clinopyroxene
463 (i.e., $[REE]^{cpx}/[X^{3+}]$, where $[X^{3+}]$ is the proportion of M2 sites charge-balanced by a 3+ cation), we
464 found that the ability prediction of equation (9) does not substantially change (R^2 = 0.997 and SEE
465 = 0.046; Fig. 7). On the other hand, Wood & Blundy (1997) assumed for simplicity that the activity
466 of REE in the melt is equal to its concentration, thus ignoring that the melt structure may potentially
467 control D_0^{3+}. Indeed, data plotted on Fig. 6a seems to suggest that X_{REE}^{melt} is better described by
468 $[REE]^{melt}/[Ca^{2+}/(M^{+}+M^{2+})]^{melt}$ rather than the simple concentrations of REE in the melt. Therefore,
469 we have incorporated the melt structure parameter into the predictive equation (9) but the regression
470 analysis of measured vs. predicted values did not provide any improvement for the prediction of
471 D_0^{3+} (R^2 = 0.994 and SEE = 0.063; Fig. 7). The same conclusion was reached in recent studies for
472 the partitioning of REE and Y between clinopyroxene/orthopyroxene and picritic/basaltic melts
473 (Yao et al., 2012; Sun and Liang, 2012, 2013). This finding is apparently in contrast with the effects
474 of $[NBO/T]^{melt}$ and $[Ca^{2+}/(M^{+}+M^{2+})]^{melt}$ on the lattice-free partition coefficient (Fig. 6). One
475 possible explanation is that, for moderately to highly depolymerized magmas, $[NBO/T]^{melt}$ is
476 constantly higher than the threshold value of 0.4 (cf. Sun and Liang, 2012), whereas its value is
477 persistently lower than 0.2 for polymerized magmas (Fig. 6a). On the other hand, due to the strong
478 rival effects of X_{Al}^{iv}, *P*, and *T*, no obvious correlations are found between $[Ca^{2+}/(M^{+}+M^{2+})]^{melt}$ and
479 D_0^{3+} when pressure, temperature, and clinopyroxene components change at the same time (cf.
480 Huang et al., 2006). As these parameters are to some extent interdependent, it is not easy to
481 differentiate between their relative influences over a broad range of crystallization conditions and
482 compositions (crystal and melt). It can be concluded that the role of melt chemistry is to reduce the
483 number of melt sites onto which REE can be accommodated. Thus, the melt structure can

potentially control the partitioning of trace elements over a wide spectrum of melt compositions (Fig. 6). However, for an isolated bulk melt composition, the final value of the REE partition coefficient is also determined by the relative (rival) effects of pressure, temperature and mineral chemistry.

Using a calibration dataset specific to basaltic compositions, Wood and Blundy (1997) found that *P* and *T* closely describe the variance of *E* according to the regression equation (3), whereas X_{Al}^{M1} and X_{Ca}^{M2} are the best predictors for r_0, as provided by the best fitting equation (4). Further nonlinear regression calculations performed by Sun and Liang, (2012) and Yao et al. (2012) on a more recent basaltic dataset provided that X_{Mg}^{M2} and X_{Al}^{M1} can also be suitable predictors for r_0. Due to the strong relationship between *E* and r_0, Wood and Blundy (1997) preferred to estimate the value of Young's modulus using only *P* and *T*. Conversely, an intrinsic trade-off between *E* and r_0 was also found by Sun and Liang, (2012) that favoured calculating *E* as a linear function of r_0. The authors demonstrated that the dependence of *E* and r_0 on the same clinopyroxene components does not weaken the predictive power of the lattice strain model. However, in multiple linear regression analyses some variables may closely describe the variance of the dataset, whereas some others may generate a set of predictions with low degrees of freedom that lead to strong data overfitting. Therefore, variables that do not improve the fit must be identified and removed from a model. Through an algorithm based on the Mallows' *Cp* statistic, we have performed systematic permutations of a number of independent variables to derive the best predictive models for r_0, and *E*. Mallows' *Cp* is expressed as (Hair et al., 1995):

$$Cp = \frac{RSS_k}{RSS_p} - n + 2p \tag{10}$$

RSS_k is the ratio of the residual sum of squares of all predictors *k*, RSS_p is the residual sum of squares of only *p* of the k predictors, and *n* is the number of observations. Mallows' *Cp* is a measure

of the bias in a model: if the type and number of selected predictors *p* (including the constant term in linear regression) are sufficient to provide a good description of the data, then *Cp* has values as close as possible to *p*. The independent variables used for permutations were X_{Al}^{iv}, X_{Al}^{M1}, X_{Ca}^{M2}, X_{Na}^{M2}, X_{Mg}^{M1}, X_{Mg}^{M2}, $[Ca^{2+}/(M^{+}+M^{2+})]^{melt}$, $[NBO/T]^{melt}$, *P* and *T*. Results are reported in Table 6S together with the mean squared error (*MSE*), R^2, *p*, and *Cp*. The Mallows' *Cp* statistic indicates that *E* and r_0 are both primary influenced by the same variables (i.e., X_{Ca}^{M2} and X_{Mg}^{M2}), corroborating the observation of Sun and Liang (2012) that *E* is indeed linearly correlated to r_0 (R^2 = 0.968). In contrast, the temperature, pressure and melt composition have minor effects on these parameters, as would be expected given (a) these are crystal-chemical parameters and (b) that the thermal expansivity of the M2 site is relatively small for the temperature range considered here (Nimis, 1999). Therefore, using X_{Ca}^{M2} and X_{Mg}^{M2} as independent variables, we have performed a multiple linear regression analysis of the data from the Campi Flegrei to derive an improved predictive model for *E* (Fig. 8a):

$$E = -82.35 + 636.56X_{Ca}^{M2} - 253.29X_{Mg}^{M2} \quad (11)$$

The statistics (R^2 = 0.967 and SEE = 4.72) of the equation (11) are much better than those observed for the original equation (3) when *T* and *P* of trachy-phonolitic magmas are used as input data (R^2 = 0.495 and SEE = 17.78). Through the same approach, we have also derived a predictive model for r_0 (Fig. 8b):

$$r_0 = 1.0231 + 0.0278X_{Ca}^{M2} - 0.0101X_{Mg}^{M2} \quad (12)$$

The equation (12) produces an improved fit to the data of the Campi Flegrei (R^2 = 0.954 and SEE = 0.002). Conversely, clinopyroxene compositions from trachytes and phonolites provide low

534 statistics for X_{Al}^{M1} and X_{Ca}^{M2} (R^2 = 0.552 and SEE = 0.007), as predictors of the original equation
535 (4).

536 It is apparent that the uncertainty measured for the recalibrated equations (11) and (12) is
537 reasonably low due to the restricted bounds of the calibration dataset that, in turn, closely describe
538 the crystallization conditions and compositions of magmas at Campi Flegrei (Fig. 1 and Table 1S).
539 On the other hand, the original equations (3) and (4) of Wood and Blundy (1997) were calibrated
540 using primitive compositions obtained prevalently at high-temperatures that, in turn, do not
541 reproduce the variability internal to the trachy-phonolitic dataset. For example, the percentage error
542 of *E* predicted by the equation (3) increases as the temperature decreases (Fig. 9a) due to the fact
543 that thermal conditions below 1,100 °C are not adequately represented into the calibration dataset of
544 Wood and Blundy (1997). Fig. 9a shows that this is valid either to natural alkaline differentiated
545 magmas from this study or to experimental basaltic compositions equilibrated at relatively low
546 temperatures (data from experiments of Green et al., 2000 and Adam and Green, 2006). Conversely,
547 Fig. 9b shows that the equation (11) has a very low percentage error of *E* at temperatures below
548 1,050 °C, but the error progressively increases with temperature, although T > 1,100 °C are rarely
549 recorded by alkaline differentiated products. This simple test clearly makes the recalibrated
550 equations (11) and (12) not suitable for high-temperature primitive magmas. We also observe that
551 values of *E* and r_0 from basaltic and more differentiated compositions are scattered through the
552 literature, consequently, the global regression analysis of these data did not provide statistically
553 significant parameters applicable over a wide range of temperatures, pressures, and compositions.

554 In the online supplementary material, we provide an Excel spreadsheet in which equations
555 (9), (11), and (12) are incorporated, and that can be used to predict D_{REE} and D_Y through major
556 element analyses of clinopyroxene in equilibrium with trachy-phonolitic magmas. In Fig. 10a we
557 have compared the standard error of estimate of each partition coefficient predicted by (i) the
558 original model of Wood and Blundy (1997), (ii) the Excel spreadsheet from this study, and (iii) the
559 parameterized model of Sun and Liang (2012). It is worth noting that this latter model was

560 calibrated specifically to basaltic systems. With respect to the original model of Wood and Blundy
561 (1997), our recalibrated model offers little improvements in the prediction of D_{LREE}, whereas its
562 accuracy is remarkably high for most of the D_{HREE} values. Conversely, the model of Sun and Liang
563 (2012) is affected by a systematic uncertainty in the prediction of D_{LREE}. This is not surprising if we
564 consider that the model was parameterized over crystallization conditions and compositions rather
565 different to those presented in this study. However, in the case of D_{Tm}, D_{Yb} and D_{Lu}, the standard
566 error of estimate is found to be lower than that of other models. This is due to the fact that the
567 model of Sun and Liang (2012) tends to overestimate the value of *E* that, in turn, reduces the width
568 of the partitioning parabola with minor effects on trace elements having low ionic radii. For
569 example, measured vs. predicted values for D_{Ce} (Fig. 10b) and D_{Yb} (Fig. 10c) show that partition
570 coefficients for larger LREE cations predicted by the model of Sun and Liang (2012) deviate
571 significantly from the one-to-one line, whereas partition coefficients for smaller HFSE cations
572 approach to the one-to-one line much better than those predicted by other models (see also Table 7S
573 for the whole dataset).
574
575 Applications to the Campanian Ignimbrite
576
577 As anticipated from the preceding discussion, the dependence of trace element partitioning on *P*, *T*,
578 and composition (crystal and melt) results in a variety of D_i values. However, most of the
579 petrological models from literature assume for simplicity that D_i is independent on the
580 physicochemical conditions of system, despite such an assumption is unlikely during crystallization
581 of natural magmas. In order to clearly demonstrate the importance of considering the change of D_i
582 for a better understanding of magmatic differentiation, we have selected four natural clinopyroxene-
583 melt pairs representative of the internal compositional variability of the Campanian Ignimbrite
584 eruption (data from Civetta et al., 1997 and Arienzo et al., 2009). These data yield ΔDiHd between
585 0.01 and 0.12 suggestive of near-equilibrium crystallization conditions (Mollo et al., 2013a), but are

586 also characterized by distinct features in terms of *P*, *T*, and composition (Table 8S). In particular,
587 thermometers and barometers of Masotta et al. (2013) suggest that the natural clinopyroxene-melt
588 pairs equilibrated at 100-300 MPa and 914-982 °C, in agreement with previous estimates from
589 petrological (e.g., Fulignati et al., 2004; Marianelli et al., 2006; Fowler et al., 2007) and geophysical
590 (e.g., Zollo et al., 2008) studies. As discussed above, the effect of pressure on trace element
591 partitioning between clinopyroxene and melt can be considered negligible at shallow crustal depths.
592 On the other hand, there is a well-documented inverse correlation between the concentration of
593 water dissolved in the melt and D_{REE} (cf. Blundy et al., 2002; Gaetani, 2004; Sun and Liang, 2012).
594 For trachytic and phonolitic compositions, it is not clear to what extent H_2O can influence D_0^{3+}
595 during magma differentiation. Undoubtedly, the macroscopic effect of increasing water is to depress
596 the liquidus temperature of the melt (Putirka, 2008). However, we have already tested that a water
597 change of ±2 wt.% in trachytic and phonolitic magmas corresponds to a negligible temperature
598 variation of ±12 °C. According to Mollo and Masotta (2014), low ΔDiHd values allow to (1)
599 minimize significantly the uncertainty of barometers and thermometers, and (2) find a good
600 correspondence between the crystallization temperature of magma and the geochemical evolution of
601 clinopyroxene. This latter point is better explained in Fig. 11a where $Mg\#^{cpx}$ correlates positively
602 with *T*, evidencing the relative effects of temperature and clinopyroxene composition on trace
603 element partitioning. Only when magnitudes of these two opposing effects are reciprocally
604 compensated, a set of nearly constant partition coefficients can be expected. Otherwise, temperature
605 and clinopyroxene composition dominate over the final value of D_i, hence controlling the
606 partitioning of trace elements during magma crystallization (e.g., Sun and Liang, 2012). Each
607 symbol plotted on Fig. 11a refers to the value of D_0^{3+} predicted using the Excel spreadsheet from
608 this study. D_0^{3+} increases from 0.67 to 0.91 with decreasing both *T* and $Mg\#^{cpx}$. In this view, the
609 whole range of values calculated for D_{REE} and D_Y has been used as input data for the Rayleigh
610 fractional crystallization equation (FC):
611

612 $C_l^{FC} = C_0 F^{(Di-1)}$ (13)

613

614 Where C_l^{FC} is the concentration of an element in remaining melt during fractional crystallization, C_0
615 is the concentration of the trace element in parental liquid (starting composition), D_i is the partition
616 coefficient of the trace element of interest whose value changes as a function of the
617 physicochemical conditions of the system (see below), F is the fraction of melt remaining during
618 crystallization. At the beginning of the modelling, low degrees of clinopyroxene fractionation (i.e.,
619 3%, 5%, 7%, and 9%) have been considered to constrain its early effect as liquidus phase on the
620 geochemical signature of magma. Stepwise calculations were performed changing the
621 clinopyroxene composition and temperature at each step of fractionation (Fig. 11a), in order to
622 derive a set of four different partition coefficients rather than one single value. In Fig. 11b,
623 modelled Ce and Y concentrations are compared with those of rock samples from the Campanian
624 Ignimbrite. Notably, the ratio of Ce/Y for the Campanian Ignimbrite eruption changes significantly
625 from 0.21 to 0.33, in contrast to what would be expected for igneous products sharing a common
626 parental magma. This discrepancy is reconciled by the nonlinear trajectory of the ^{cpx}FC vector that
627 is controlled by the variation of the partition coefficient. Thus, at the early stage of clinopyroxene
628 crystallization, the incorporation of variable proportions of Ce and Y into the crystal lattice provides
629 explanation for the strong variability of the natural dataset. According to Civetta et al. (1997), the
630 internal differentiation of the Campanian Ignimbrite can be addressed to the fractionation of <10%
631 and ~50% of clinopyroxene and feldspar, respectively. Considering that Ce and Y are highly
632 incompatible in feldspar (D_{Ce} = 0.039 and D_Y = 0.017; Larsen, 1979), further fractional
633 crystallization steps have been developed accounting for the segregation of 50% of feldspars from
634 the solidifying magma. Notably, due to the highly incompatible behaviour of Ce and Y, feldspar
635 fractionation may only increase the REE content in magma but cannot control the internal REE
636 variability of the Campanian Ignimbrite eruption. Modelling results are aligned along four different
637 FC trajectories (i.e., from ^{kfs}FC1 to ^{kfs}FC4) that faithfully reproduce the entire differentiation path of

638 the Campanian Ignimbrite, from lowest to highest Ce/Y ratios (Fig. 11a). Clearly, the constancy of
639 the clinopyroxene-melt partition coefficient would yield only one single FC trend that, in turn, is
640 inadequate to reproduce in full the complex trace element pattern of natural products. Therefore, the
641 process responsible for the heterogeneous REE concentrations of the Campanian Ignimbrite
642 products is twofold: (1) the early fractionation of clinopyroxene at relative high temperature and (2)
643 the subsequent fractionation of feldspars during the final stage of magma cooling (cf. Fowler et al.,
644 2007). Additional complexities, including crystallization of other phases (oxides, biotite, apatite)
645 and partial cumulate mush remelting (e.g., Wolff et al., 2015) can further explain some of the trace
646 element variations observed in the Campanian Ignimbrite .
647
648 **Conclusions**
649
650 Coherently with previous natural and experimental studies, we documented that the partitioning of
651 trace elements between clinopyroxene and trachy-phonolitic melts can be addressed to (1) the entry
652 of REE+Y and HFSE in the M2 and M1 sites, respectively, due to substitution of Si^{4+} with Al^{iv}, (2)
653 the increased net charge on the M1 site that causes divalent TE to become less compatible within
654 clinopyroxene crystal lattice, (3) a charge-balanced cation substitution reaction reflecting an
655 increased ease of locally balancing the excess charge as the number of surrounding tetrahedrally-
656 coordinated aluminium atoms increases, and (4) the effect of changes in melt structure that increase
657 the number of large sites critically important to accommodating large REE cations. On the other
658 hand, we tested that the incorporation of additional crystallochemical parameters (assuming local
659 charge balance between REE in the M2 site and adjacent Al^{iv}) and melt structure parameters (given
660 as the ratio of non-bridging oxygens to tetrahedral cations and/or the ratio of molar calcium to the
661 sum of monovalent and divalent cations) into the lattice strain model of Wood & Blundy (1997) did
662 not provide any improvement for its ability prediction. This is due to the strong rival effects of
663 pressure, temperature, and crystal/melt parameters. Therefore, over a broad range of crystallization

conditions and crystal/melt compositions, it is not possible to differentiate between the relative influence of each single parameter on REE+Y partitioning. As a consequence, no obvious correlations are found when the physicochemical conditions of the system change at the same time. According to the lattice strain theory, we observe that, D_0^{3+}, r_0 and E can be successfully predicted once T, P, X_{Ca}^{M2} and X_{Mg}^{M2} are knows for trachy-phonolitic compositions. On this basis, we updated the existing partitioning equations to derive a self-consistent model for trachy-phonolitic magmas. The application of this model to natural products from the Campanian Ignimbrite, the largest caldera-forming eruption at the Campi Flegrei, reveals that the complex REE pattern of magma can be successfully described by the stepwise fractional crystallization of clinopyroxene and feldspar where the clinopyroxene-melt partition coefficient changes progressively as a function of the physicochemical conditions of the system.

Acknowledgments

We are grateful to Yan Liang and an anonymous reviewer for their useful and constructive comments that helped to improve significantly the quality of the paper. We are also indebted to Andrew C. Kerr as Editor-in-Chief of Lithos for his instructive editorial guidance. A. Cavallo is acknowledged for assistance during electron microprobe analysis. Parts of this research were supported by Swiss NSF fund # 200021-146268.S, ERC Advanced Grant (247162-CRITMAG), Wolfson Research Merit Award, and MIUR, Premiale project – NoRth: New hORizons of the Technology applied to experimental researches and geophysical and volcanological monitoring.

References

688 Arienzo I, Civetta L, Heumann A, Worner G and Orsi G (2009) Isotopic evidence for open system
689 processes within the Campanian Ignimbrite (Campi Flegrei, Italy) magma chamber. B. Volcanol.
690 71(3):285–300.
691 Armienti, P, Tonarini, S, Innocenti, F, D'Orazio, M, 2007. Mount Etna pyroxene as tracer of
692 petrogenetic processes and dynamics of the feeding system, in: Beccaluva, L. Bianchini, G., Wilson,
693 M. (Eds.), Cenozoic Volcanism in the Mediterranean, Geological Society of America Special
694 Papers, pp. 265-276.
695 Bennett SL, Blundy J, Elliott T (2004) The effect of sodium and titanium on crystal-melt
696 partitioning of trace elements. Geochim Cosmochim Ac 68(10):2335-2347 doi:Doi
697 10.1016/J.Gca.2003.11.006
698 Blundy J, Wood B (1994) Prediction of Crystal-Melt Partition-Coefficients from Elastic-Moduli.
699 Nature 372(6505):452-454 doi:Doi 10.1038/372452a0
700 Blundy J D, Falloon T J, Wood B J, Dalton J A (1995) Sodium partitioning between clinopyroxene
701 and silicate melts. J Geophys Res 100: 15501-15516.
702 Blundy J, Wood B (2003) Partitioning of trace elements between crystals and melts. Earth Planet Sc
703 Lett 210(3-4):383-397 doi:Doi 10.1016/S0012-821x(03)00129-8
704 Blundy JD, Robinson JAC, Wood BJ (1998) Heavy REE are compatible in clinopyroxene on the
705 spinel lherzolite solidus. Earth Planet Sc Lett 160(3-4):493-504 doi:Doi 10.1016/S0012-
706 821x(98)00106-X
707 Civetta L, Orsi G, Pappalardo L, Fisher RV, Heiken G, Ort M (1997) Geochemical zoning,
708 mingling, eruptive dynamics and depositional processes - The Campanian Ignimbrite, Campi
709 Flegrei caldera, Italy. J Volcanol Geoth Res 75(3-4):183-219 doi:Doi 10.1016/S0377-
710 0273(96)00027-3
711 D'Antonio M (2011) Lithology of the basement underlying the Campi Flegrei caldera:
712 Volcanological and petrological constraints. J Volcanol Geoth Res 200(1-2):91-98 doi:Doi
713 10.1016/J.Jvolgeores.2010.12.006

714 Deino A L, Orsi G, Piochi M, de Vita S (2004) The age of the Neapolitan Yellow Tuff caldera-
715 forming eruption (Campi Flegrei caldera—Italy) assessed by $^{40}Ar/^{39}Ar$ dating method. J Volcanol
716 Geotherm Res 133:157–170 doi:10.1016/S0377-0273(03)00396-2
717 De Vivo B, Rolandi G, Gans PB, Calvert A, Bohrson WA, Spera FJ, Belkin HE (2001) New
718 constraints on the pyroclastic eruptive history of the Campanian volcanic Plain (Italy). Miner Petrol
719 73(1-3):47-65 doi:Doi 10.1007/S007100170010
720 Del Bello E, Mollo S, Scarlato P, von Quadt A, Forni F, Bachmann O (2014) New petrological
721 constraints on the last eruptive phase of the Sabatini Volcanic District (central Italy): Clues from
722 mineralogy, geochemistry, and Sr–Nd isotopes. Lithos 205(0):28-38
723 doi:http://dx.doi.org/10.1016/j.lithos.2014.06.015
724 Dygert N, Liang Y, Sun C, Hess P (2014) An experimental study of trace element partitioning
725 between augite and Fe-rich basalts. Geochim Cosmochim Ac 132:170-186 doi:
726 10.1016/j.gca.2014.01.042
727 Fabbrizio A, Carroll MR (2008) Experimental constraints on the differentiation process and pre-
728 emptive conditions in the magmatic system of Phlegraean Fields (Naples, Italy). J Volcanol Geoth
729 Res 171(1-2):88-102 doi:Doi 10.1016/J.Jvolgeores.2007.11.002
730 Fedele L, Zanetti A, Morra V, Lustrino M, Melluso L, Vannucci R (2009) Clinopyroxene/liquid
731 trace element partitioning in natural trachyte-trachyphonolite systems: insights from Campi Flegrei
732 (southern Italy). Contrib Mineral Petr 158(3):337-356 doi:Doi 10.1007/S00410-009-0386-5
733 Forsythe LM, Nielsen RL, Fisk MR (1994) High-Field-Strength Element Partitioning between
734 Pyroxene and Basaltic to Dacitic Magmas. Chem Geol 117(1-4):107-125 doi:Doi 10.1016/0009-
735 2541(94)90124-4
736 Fowler SJ, Spera F, Bohrson W, Belkin HE, De Vivo B (2007) Phase equilibria constraints on the
737 chemical and physical evolution of the campanian ignimbrite. J Petrol 48(3):459-493 doi:Doi
738 10.1093/Petrology/Egl068

739 Francis D, Minarik W (2008) Aluminum-dependent trace element partitioning in clinopyroxene.
740 Contrib Mineral Petr 156(4):439-451 doi:Doi 10.1007/S00410-008-0295-Z
741 Freda C, Gaeta M, Misiti V, Mollo S, Dolfi D, Scarlato P (2008) Magma–carbonate interaction: an
742 experimental study on ultrapotassic rocks from Alban Hills (Central Italy). Lithos 101(3):397-415
743 Fulignati P, Marianelli P, Proto M, Sbrana A (2004) Evidences for disruption of a crystallizing front
744 in a magma chamber during caldera collapse: an example from the Breccia Museo unit (Campanian
745 Ignimbrite eruption, Italy). J Volcanol Geoth Res 133:141-155
746 Gaetani GA (2004) The influence of melt structure on trace element partitioning near the peridotite
747 solidus. Contrib Mineral Petr 147(5):511-527 doi:Doi 10.1007/S00410-004-0575-1
748 Gaetani GA, Grove TL (1995) Partitioning of Rare-Earth Elements between Clinopyroxene and
749 Silicate Melt - Crystal-Chemical Controls. Geochim Cosmochim Ac 59(10):1951-1962 doi:Doi
750 10.1016/0016-7037(95)00119-0
751 Gaetani GA, Kent AJR, Grove TL, Hutcheon ID, Stolper EM (2003) Mineral/melt partitioning of
752 trace elements during hydrous peridotite partial melting. Contrib Mineral Petr 145(4):391-405
753 doi:Doi 10.1007/S00410-003-0447-0
754 Hair Jr J F, Anderson R E, Tatham R L, Black W C (1995) Multivariate data analysis. 3rd ed, New
755 York, Macmillan, 742p.
756 Hart SR, Dunn T (1993) Experimental Cpx Melt Partitioning of 24 Trace-Elements. Contrib
757 Mineral Petr 113(1):1-8 doi:Doi 10.1007/Bf00320827
758 Hill E, Wood BJ, Blundy JD (2000) The effect of Ca-Tschermaks component on trace element
759 partitioning between clinopyroxene and silicate melt. Lithos 53(3-4):203-215 doi:Doi
760 10.1016/S0024-4937(00)00025-6
761 Huang F, Lundstrom CC, McDonough WF (2006) Effect of melt structure on trace-element
762 partitioning between clinopyroxene and silicic, alkaline, aluminous melts. Am Mineral 91(8-
763 9):1385-1400 doi:Doi 10.2138/Am.2006.1909

764 Kennedy AK, Lofgren GE, Wasserburg GJ (1993) An experimental study of trace element
765 partitioning between olivine, orthopyroxene and melt in chondrules: equilibrium values and kinetic
766 effects. Earth Planet Sc Lett 115(1–4):177-195 doi:http://dx.doi.org/10.1016/0012-821X(93)90221-
767 T
768 Klemme S, Blundy JD, Wood BJ (2002) Experimental constraints on major and trace element
769 partitioning during partial melting of eclogite. Geochim Cosmochim Ac 66(17):3109-3123 doi:Doi
770 10.1016/S0016-7037(02)00859-1
771 Lanzafame G, Mollo S, Iezzi G, Ferlito C, Ventura G (2013) Unraveling the solidification path of a
772 pahoehoe "cicirara" lava from Mount Etna volcano. B Volcanol 75(4) doi:Doi 10.1007/S00445-
773 013-0703-8
774 Larsen, LM (1979) Distribution of REE and Other Trace-Elements between Phenocrysts and
775 Peralkaline Undersaturated Magmas, Exemplified by Rocks from the Gardar Igneous Province,
776 South Greenland. Lithos 12(4): 303-315 doi: 10.1016/0024-4937(79)90022-7.
777 Le Bas MJ, Le Maitre RW, Streckeisen A, Zanettin B, Rocks ISotSoI (1986) A Chemical
778 Classification of Volcanic Rocks Based on the Total Alkali-Silica Diagram. J Petrol 27(3):745-750
779 doi:10.1093/petrology/27.3.745
780 Lemarchand F, Villemant B, Calas G (1987) Trace-Element Distribution Coefficients in Alkaline
781 Series. Geochim Cosmochim Ac 51(5):1071-1081 doi:Doi 10.1016/0016-7037(87)90201-8
782 Liang Y, Sun CG, Yao LJ (2013) A REE-in-two-pyroxene thermometer for mafic and ultramafic
783 rocks. Geochim Cosmochim Ac 102:246-260 doi:Doi 10.1016/J.Gca.2012.10.035
784 Lindstrom DJ (1976) Partitioning of Ferric Iron between Diopside and Silicate Liquid. Eos T Am
785 Geophys Un 57(4):339-339
786 Lofgren GE, Huss GR, Wasserburg GJ (2006) An experimental study of trace-element partitioning
787 between Ti-Al-clinopyroxene and melt: Equilibrium and kinetic effects including sector zoning. Am
788 Mineral 91(10):1596-1606 doi:10.2138/am.2006.2108

789 Lundstrom CC, Shaw HF, Ryerson FJ, Phinney DL, Gill JB, Williams Q (1994) Compositional
790 Controls on the Partitioning of U, Th, Ba, Pb, Sr and Zr between Clinopyroxene and Haplobasaltic
791 Melts - Implications for Uranium Series Disequilibria in Basalts. Earth Planet Sc Lett 128(3-4):407-
792 423 doi:Doi 10.1016/0012-821x(94)90159-7
793 Lundstrom CC, Shaw HF, Ryerson FJ, Williams Q, Gill J (1998) Crystal chemical control of
794 clinopyroxene-melt partitioning in the Di-Ab-An system: Implications for elemental fractionations
795 in the depleted mantle. Geochim Cosmochim Ac 62(16):2849-2862 doi:Doi 10.1016/S0016-
796 7037(98)00197-5
797 Mahood G, Hildreth W (1983) Large Partition-Coefficients for Trace-Elements in High-Silica
798 Rhyolites. Geochim Cosmochim Ac 47(1):11-30 doi:Doi 10.1016/0016-7037(83)90087-X
799 Marianelli P, Sbrana A, Proto M (2006) Magma chamber of the Campi Flegrei supervolcano at the
800 time of eruption of the Campanian Ignimbrite. Geology 34(11):937-940 doi:Doi
801 10.1130/G22807a.1
802 Marks M, Halama R, Wenzel T, Markl G (2004) Trace element variations in clinopyroxene and
803 amphibole from alkaline to peralkaline syenites and granites: implications for mineral-melt trace-
804 element partitioning. Chem Geol 211(3-4):185-215 doi:Doi 10.1016/J.Chemgeo.2004.06.032
805 Masotta M, Gaeta M, Gozzi F, Marra F, Palladino DM, Sottili G (2010) H2O- and temperature-
806 zoning in magma chambers: The example of the Tufo Giallo della Via Tiberina eruptions (Sabatini
807 Volcanic District, central Italy). Lithos 118(1-2):119-130 doi:Doi 10.1016/J.Lithos.2010.04.004
808 Masotta M, Mollo S, Freda C, Gaeta M, Moore G (2013) Clinopyroxene-liquid thermometers and
809 barometers specific to alkaline differentiated magmas. Contrib Mineral Petr 166(6):1545-1561
810 doi:Doi 10.1007/S00410-013-0927-9
811 Matsui Y, Onuma N, Nagasawa H, Higuchi H, Banno S (1977) Crystal-Structure Control in Trace-
812 Element Partition between Crystal and Magma. B Soc Fr Mineral Cr 100(6):315-324
813 McDade P, Blundy JD, Wood BJ (2003) Trace element partitioning between mantle wedge
814 peridotite and hydrous MgO-rich melt. Am Mineral 88(11-12):1825-1831

Mollo S, Giacomoni PP, Andronico D, Scarlato P (2015a) Clinopyroxene and titanomagnetite cation redistributions at Mt. Etna volcano (Sicily, Italy): Footprints of the final solidification history of lava fountains and lava flows. Chemical Geology, 406:45-54 doi:http://dx.doi.org/10.1016/j.chemgeo.2015.04.017.

Mollo S, Masotta M, Forni F, Bachmann O, De Astis G., Moore G, Scarlato P (2015b) A K-feldspar-liquid hygrometer specific to alkaline differentiated magmas. Chemical Geology, 392:1-8, doi:10.1016/j.chemgeo.2014.11.010.

Mollo S, Masotta M, Forni F, Bachmann O, De Astis G, Moore G, Scarlato P (2014) A K-feldspar–liquid hygrometer specific to alkaline differentiated magmas. Chemical Geology, in press.

Mollo S, Blundy JD, Iezzi G, Scarlato P, Langone A (2013a) The partitioning of trace elements between clinopyroxene and trachybasaltic melt during rapid cooling and crystal growth. Contrib Mineral Petr 166(6):1633-1654

Mollo S, Putirka K, Misiti V, Soligo M, Scarlato P (2013b) A new test for equilibrium based on clinopyroxene-melt pairs: Clues on the solidification temperatures of Etnean alkaline melts at post-eruptive conditions. Chem Geol 352:92-100

Mollo S, Iezzi G, Ventura G, Cavallo A, Scarlato P (2012) Heterogeneous nucleation mechanisms and formation of metastable phase assemblages induced by different crystalline seeds in a rapidly cooled andesitic melt. Journal of Non-Crystalline Solids 358(12-13):1624-1628

Mollo S, Lanzafame G, Masotta M, Iezzi G, Ferlito C, Scarlato P (2011a) Cooling history of a dike as revealed by mineral chemistry: A case study from Mt. Etna volcano. Chem Geol 288(1-2):39-52

Mollo S, Masotta M (2014) Optimizing pre-eruptive temperature estimates in thermally and chemically zoned magma chambers. Chem Geol 368:97-103

Mollo S, Putirka K, Iezzi G, Del Gaudio P, Scarlato P (2011b) Plagioclase-melt (dis)equilibrium due to cooling dynamics: Implications for thermometry, barometry and hygrometry. Lithos 125(1-2):221-235

840 Morimoto N (1988) Nomenclature of Pyroxenes. Miner Petrol 39(1):55-76
841 doi:10.1007/BF01226262
842 Muñoz M, Sagredo J (1974) Clinopyroxenes as geobarometric indicators in mafic and ultramafic
843 rocks from Canary Islands. Contrib Mineral Petr 44(2):139-147 doi:10.1007/BF00385786
844 Nagasawa H (1973) Rare-Earth Distribution in Alkali Rocks from Oki-Dogo-Island, Japan. Contrib
845 Mineral Petr 39(4):301-308 doi:Doi 10.1007/Bf00376470
846 Nagasawa H, Schnetzler CC (1971) Partitioning of Rare Earth,Alkali and Alkaline Earth Elements
847 between Phenocrysts and Acidic Igneous Magma. Geochim Cosmochim Ac 35(9):953-& doi:Doi
848 10.1016/0016-7037(71)90008-1
849 Nimis P (1999) Clinopyroxene geobarometry of magmatic rocks. Part 2. Structural geobarometers
850 for basic to acid, tholeiitic and midly alkaline magmatic systems. Contrib Mineral Petrol 135:62–74
851 doi:10.1007/s004100050498
852 Onuma N, Higuchi H, Wakita H, Nagasawa H (1968) Trace Element Partition between 2 Pyroxenes
853 and Host Lava. Earth Planet Sc Lett 5(1):47-& doi:Doi 10.1016/S0012-821x(68)80010-X
854 Orsi G, Dantonio M, Devita S, Gallo G (1992) The Neapolitan Yellow Tuff, a Large-Magnitude
855 Trachytic Phreatoplinian Eruption - Eruptive Dynamics, Magma Withdrawal and Caldera Collapse.
856 J Volcanol Geoth Res 53(1-4):275-287 doi:Doi 10.1016/0377-0273(92)90086-S
857 Orsi G, Di Vito MA, Selva J, Marzocchi W (2009) Long-term forecast of eruption style and size at
858 Campi Flegrei caldera (Italy). Earth Planet Sc Lett 287(1-2):265-276 doi:Doi
859 10.1016/J.Epsl.2009.08.013
860 Pabst S, Worner G, Civetta L, Tesoro R (2008) Magma chamber evolution prior to the Campanian
861 Ignimbrite and Neapolitan Yellow Tuff eruptions (Campi Flegrei, Italy). B Volcanol 70(8):961-976
862 doi:Doi 10.1007/S00445-007-0180-Z
863 Pappalardo L, Mastrolorenzo G (2012) Rapid differentiation in a sill-like magma reservoir: a case
864 study from the campi flegrei caldera. Sci Rep-Uk 2 doi:Artn 712. Doi 10.1038/Srep00712

865 Pappalardo L, Ottolini L, Mastrolorenzo G (2008) The Campanian Ignimbrite (southern Italy)
866 geochemical zoning: insight on the generation of a super-eruption from catastrophic differentiation
867 and fast withdrawal. Contrib Mineral Petr 156(1):1-26 doi:Doi 10.1007/S00410-007-0270-0
868 Pappalardo L, Piochi M, D'Antonio M, Civetta L, Petrini R, (2002) Evidence for multi-stage
869 magmatic evolution during the past 60 ka at Campi Flegrei (Italy) deduced from Sr, Nd and Pb
870 isotope data. J Petrol 43:1415–1434
871 Putirka K, Johnson M, Kinzler R, Longhi J, Walker D (1996) Thermobarometry of mafic igneous
872 rocks based on clinopyroxene-liquid equilibria, 0-30 kbar. Contrib Mineral Petr 123(1):92-108
873 doi:Doi 10.1007/S004100050145
874 Ray GL, Shimizu N, Hart SR (1983) An Ion Microprobe Study of the Partitioning of Trace-
875 Elements between Clinopyroxene and Liquid in the System Diopside-Albite-Anorthite. Geochim
876 Cosmochim Ac 47(12):2131-2140 doi:Doi 10.1016/0016-7037(83)90038-8
877 Scarlato P, Mollo S, Blundy JD, Iezzi G, Tiepolo M (2014) The role of natural solidification paths
878 on REE partitioning between clinopyroxene and melt. B Volcanol 76(3) doi:Artn 810. Doi
879 10.1007/S00445-014-0810-1
880 Schnetzler CC, Philpotts JA (1970) Li, K, Rb, Sr, Ba and Rare-Earth Concentrations to Apollo-12
881 Lunar Soil. Eos T Am Geophys Un 51(7):583-&
882 Shannon RD (1976) Revised Effective Ionic-Radii and Systematic Studies of Interatomic Distances
883 in Halides and Chalcogenides. Acta Crystallogr A 32(Sep1):751-767 doi:Doi
884 10.1107/S0567739476001551
885 Signorelli S, Vaggelli G, Romano C, Carroll MR (2001) Volatile element zonation in Campanian
886 Ignimbrite magmas (Phlegrean Fields, Italy): evidence from the study of glass inclusions and matrix
887 glasses. Contrib Mineral Petr 140(5):543-553
888 Skulski T, Minarik W, Watson EB (1994) High-Pressure Experimental Trace-Element Partitioning
889 between Clinopyroxene and Basaltic Melts. Chem Geol 117(1-4):127-147 doi:Doi 10.1016/0009-
890 2541(94)90125-2

Sun CG, Liang Y (2012) Distribution of REE between clinopyroxene and basaltic melt along a mantle adiabat: effects of major element composition, water, and temperature. Contrib Mineral Petr 163(5):807-823 doi:Doi 10.1007/S00410-011-0700-X

Sun CG, Liang Y (2013) The importance of crystal chemistry on REE partitioning between mantle minerals (garnet, clinopyroxene, orthopyroxene, and olivine) and basaltic melts. Chem Geol 358:23-36 doi:Doi 10.1016/J.Chemgeo.2013.08.045

Tuff J, Gibson SA (2007) Trace-element partitioning between garnet, clinopyroxene and Fe-rich picritic melts at 3 to 7 GPa. Contrib Mineral Petr 153(4):369-387 doi:Doi 10.1007/S00410-006-0152-X

Villemant B (1988) Trace-Element Evolution in the Phlegrean Fields (Central-Italy) - Fractional Crystallization and Selective Enrichment. Contrib Mineral Petr 98(2):169-183 doi:Doi 10.1007/Bf00402110

Watson EB, Muller T (2009) Non-equilibrium isotopic and elemental fractionation during diffusion-controlled crystal growth under static and dynamic conditions. Chem Geol 267(3-4):111-124 doi:Doi 10.1016/J.Chemgeo.2008.10.036

Webster JD, Raia F, Tappen C, De Vivo B (2003) Pre-eruptive geochemistry of the ignimbrite-forming magmas of the Campanian Volcanic Zone, Southern Italy, determined from silicate melt inclusions. Miner Petrol 79(1-2):99-125 doi:Doi 10.1007/S00710-003-0004-6

Wolff JA, Ellis BS, Ramos FC, Starkel WA, Boroughs S, Olin PH, Bachmann, O (2015) Remelting of cumulates as a process for producing chemical zoning in silicic tuffs: A comparison of cool, wet and hot, dry rhyolitic magma systems. Lithos 236-237, 275-286.

Wood BJ, Blundy JD (1997) A predictive model for rare earth element partitioning between clinopyroxene and anhydrous silicate melt. Contrib Mineral Petr 129(2-3):166-181 doi:Doi 10.1007/S004100050330

Wood BJ, Blundy JD (2001) The effect of cation charge on crystal-melt partitioning of trace elements. Earth Planet Sc Lett 188(1-2):59-71 doi:Doi 10.1016/S0012-821x(01)00294-1

Wood BJ, Blundy JD (2002) Trace element partitioning - new developments building on the lattice strain model. Geochim Cosmochim Ac 66(15A):A846-A846

Wood BJ, Trigila R (2001) Experimental determination of aluminous clinopyroxene-melt partition coefficients for potassic liquids, with application to the evolution of the Roman province potassic magmas. Chem Geol 172(3-4):213-223 doi:Doi 10.1016/S0009-2541(00)00259-X

Yao LJ, Sun CG, Liang Y (2012) A parameterized model for REE distribution between low-Ca pyroxene and basaltic melts with applications to REE partitioning in low-Ca pyroxene along a mantle adiabat and during pyroxenite-derived melt and peridotite interaction. Contrib Mineral Petr 164(2):261-280 doi:Doi 10.1007/S00410-012-0737-5

Zollo A, Maercklin N, Vassallo M, Dello Iacono D, Virieux J, Gasparini P (2008) Seismic reflections reveal a massive melt layer feeding Campi Flegrei caldera. Geophysical Research Letters 35(12) doi:Doi 10.1029/2008gl034242

Figure captions

Fig. 1. The compositions of host melts and clinopyroxene phenocryst cores from this study are compared with those of natural products at Campi Flegrei in terms of total alkali vs. silica of the melt (a), ΣHREE vs. ΣLREE of the melt (b), Di vs. Hd of clinopyroxene, and (c) ΣHREE vs. ΣLREE of clinopyroxene. Natural data from Villemant (1988), Civetta et al. (1997), Fulignati et al. (2004), Marianelli et al. (2006), Fedele et al. (2007), Pappalardo et al. (2002; 2008), and Arienzo et al. (2009).

Fig. 2. Example of the textural features of clinopyroxene phenocrysts from this study. (a) Backscattered electron images show that crystals are euhedral and complex zoning patters are absent. Microprobe compositional profiles reveal the occurrence of some chemical heterogeneities

942 at the crystal-melt interface. (b) Diffusive boundary layer occurs into the glass next to
943 clinopyroxene rims showing Al and Na enrichments (see also data in Table 5S).
944
945 Fig. 3. Plots of partition coefficients for HFSE (Ti, Zr, Nb, Ta), REE (La) and TE (Co) vs. Al^{iv}.
946 Data from this study have been compared with those from literature to highlight the dependence of
947 D_i on Al^{iv}.
948
949 Fig. 4. Plots of partition coefficients for REE and Y vs. ionic radii (data from Shannon 1976) for the
950 samples object of this study. The near parabolic dependence found by Onuma et al. (1968) dictates
951 the distribution of the data. The lines show fits to the lattice strain model of Blundy and Wood
952 (1994). Fit parameters are listed in Table 4S. The agreement of our data with the model emphasizes
953 the importance of lattice strain in controlling REE and Y partitioning at equilibrium crystallization
954 conditions.
955
956 Fig. 5. Plots of D_0^{3+} for clinopyroxene-melt partitioning of REE vs. Al^{iv} content in clinopyroxenes
957 from this study and previous works. D_0^{3+} is calculated through the lattice strain model of Blundy
958 and Wood (1994).
959
960 Fig. 6. Plot of D_0^{3+} for clinopyroxene-melt partitioning of REE vs. *NBO/T* of the melt. (a) Our data
961 for trachy-phonolitic melts are compared with those from literature obtained for highly polymerized
962 silicic melts, and moderately-to-poorly polymerized silicic melts. According to Gaetani (2004) and
963 Huang et al. (2006) the melt structure have a significant influence on partition coefficients for
964 $[NBO/T]^{melt}$ values higher than 0.4. (b) Plot of D_0^{3+} for clinopyroxene–melt partitioning of REE vs.
965 $[Ca^{2+}/(M^{+}+M^{2+})]^{melt}$, where M^{+} and M^{2+} are $Na^{+}+K^{+}$ and $Fe^{2+}+Ca^{2+}+Mg^{2+}$, respectively . The
966 negative correlation between D_0^{3+} and $[Ca^{2+}/(M^{+}+M^{2+})]^{melt}$ confirms the reliability of Eqn. (2)

967 favouring large structural sites critically important to accommodating large trace element cations in
968 the melt.
969
970 Fig. 7. Clinopyroxene-melt pairs from this study, Pappalardo et al. (2008) and Fedele et al. (2009)
971 have been used as input data for the original equation for D_0^{3+} derived by Wood and Blundy (1997).
972 New predictors have been also introduced in this equation, i.e., $[REE]^{cpx}/[X^{3+}]$ (after Wood and
973 Blundy, 2001) and $[REE]^{melt}/[Ca^{2+}/(M^{+}+M^{2+})]^{melt}$. The analysis of predicted vs. measured values
974 indicates that these new predictors do not offer improvements for the ability prediction of the
975 original equation of Wood and Blundy (1997).
976
977 Fig. 8. Clinopyroxene-melt pairs from this study, Pappalardo et al. (2008) and Fedele et al. (2009)
978 have been used as input data for the original equations for (a) E and (b) r_0 derived by Wood and
979 Blundy (1997). The analysis of predicted vs. measured values indicates that these equations are
980 affected by a high uncertainty. The best fitting equations have been derived through the regression
981 analysis of trachy-phonolitic data using X_{Ca}^{M2} and X_{Mg}^{M2} as predictors.
982
983 Fig. 9. The predictive equations for E from (a) Wood and Blundy (1997) and (b) this study have
984 been tested using trachy-phonolitic (this study, Pappalardo et al., 2008 and Fedele et al., 2009) and
985 basaltic (Green et al., 2000 and Adam and Green, 2006) data. For the original equation of Wood
986 and Blundy (1997), the percentage error of E increases with decreasing temperature. The opposite
987 occurs for the equation from this study showing low ability prediction for high-temperature basaltic
988 magmas.
989
990 Fig. 10. D_{REE} and D_Y "measured" in this study are compared with those "predicted" by the original
991 model of Wood and Blundy (1997), the parameterized model of Sun and Liang (2012) for basaltic
992 compositions, and the recalibrated model from this study for trachy-phonolitic compositions. (a)

993 Comparison of the standard error of estimate. (b) Comparison of D_{Ce} values as representative of
994 partitioning of larger LREE cations. (c) Comparison of D_{Yb} values as representative of partitioning
995 of smaller LREE cations.
996
997 Fig. 11. Natural clinopyroxene-melt pairs from the Campanian Ignimbrite have been used as input
998 data for the thermobarometer of Masotta et al. (2013) and the trace element model presented in this
999 study. (a) Temperature vs. $Mg\#^{cpx}$ diagram shows that the geochemical evolution of clinopyroxene
1000 parallels the decreasing temperature of magma. Each symbol plotted on the diagram refers to the
1001 value of D_0^{3+} predicted using the Excel spreadsheet from this study. D_0^{3+} is found to increase from
1002 0.60 to 0.85 with decreasing both T and $Mg\#^{cpx}$. (b) Ce vs. Y diagram showing the geochemical
1003 evolution of the Campanian Ignimbrite modelled through the Rayleigh fractional crystallization
1004 equation. At the beginning of the modelling, low degrees of clinopyroxene fractionation (i.e., 3%,
1005 5%, 7%, and 9%) have been considered. Stepwise calculations were performed changing the
1006 clinopyroxene composition and temperature at each step of fractionation. Modelled Ce and Y
1007 concentrations were used to draw the ^{cpx}FC vector. Fractional crystallization calculations were
1008 further developed accounting for the segregation of ~50% of K-feldspar from the solidifying
1009 magma. Modelling results are aligned along four different FC trajectories (i.e., from ^{kfs}FC1 to
1010 ^{kfs}FC4).

Figure1

Click here to download high resolution image

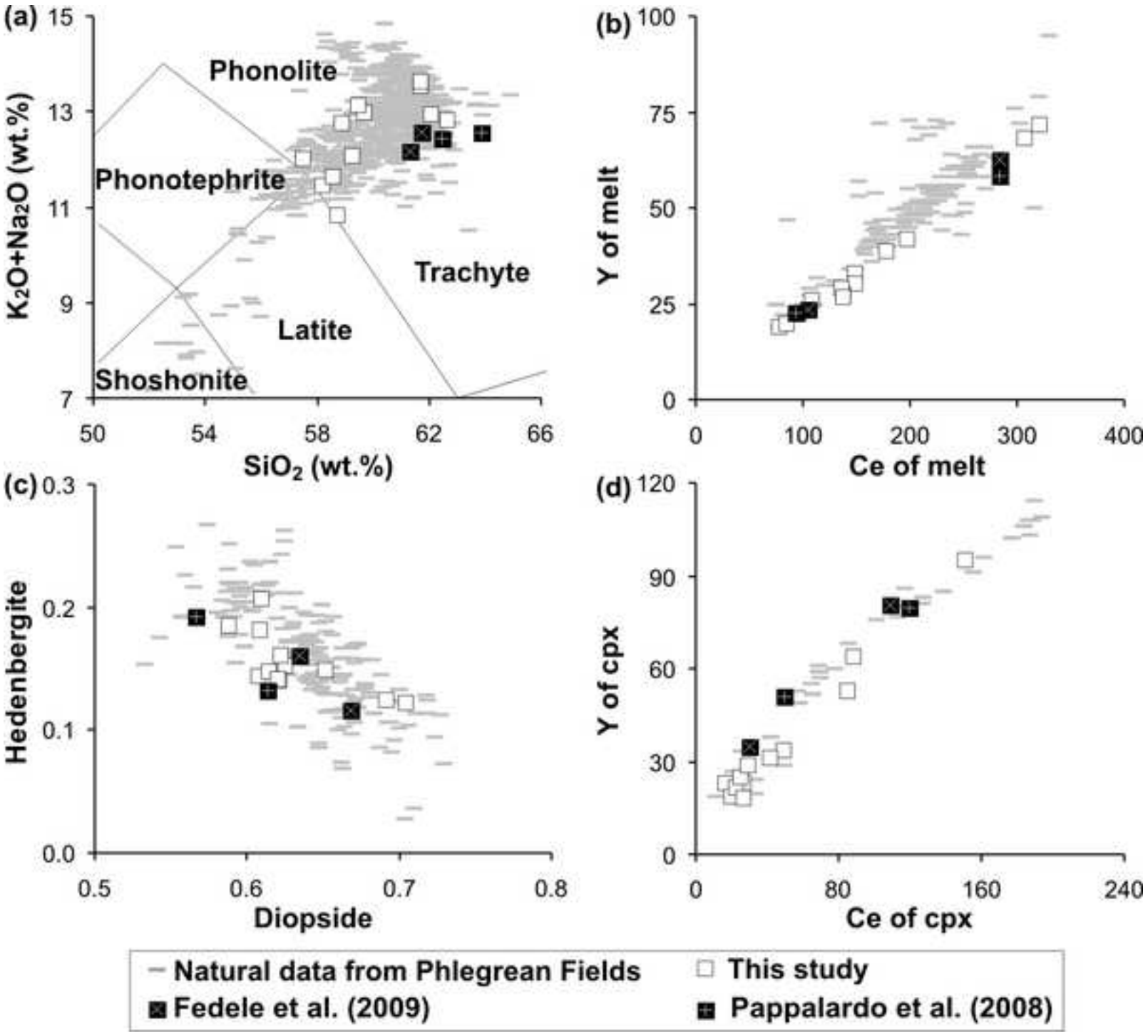

Figure2

Click here to download high resolution image

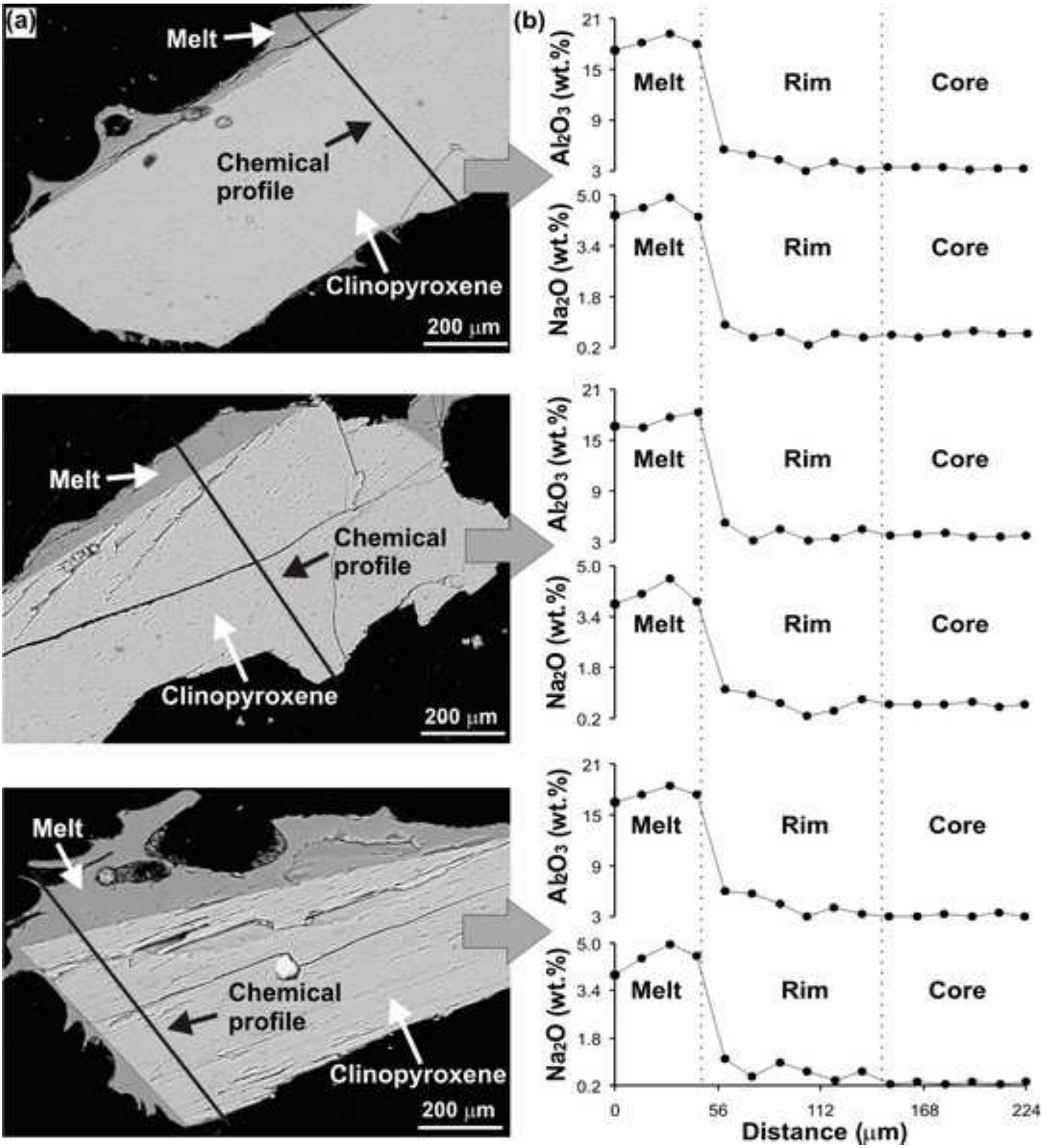

Figure3

Click here to download high resolution image

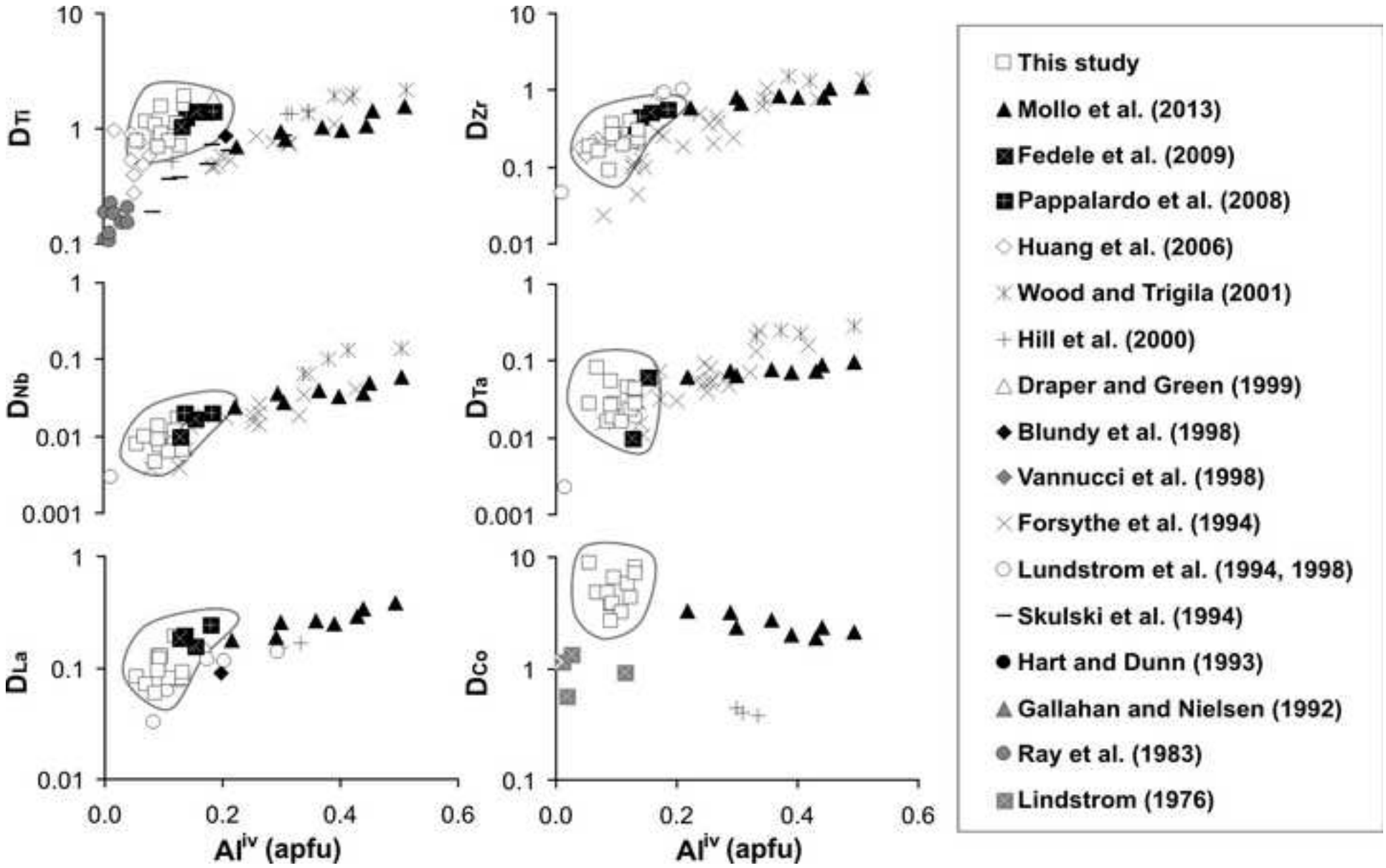

Figure4

Click here to download high resolution image

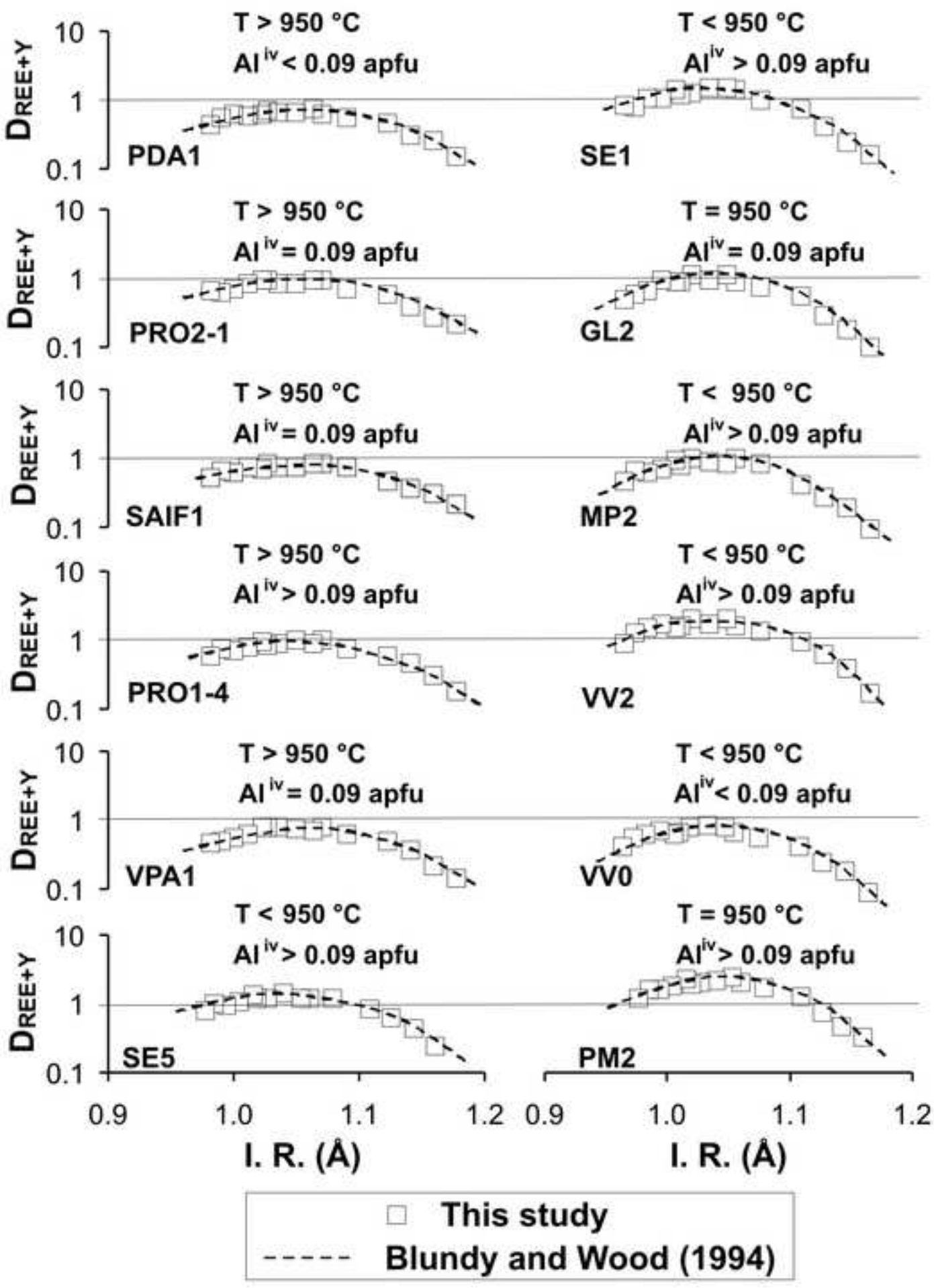

Figure5

Click here to download high resolution image

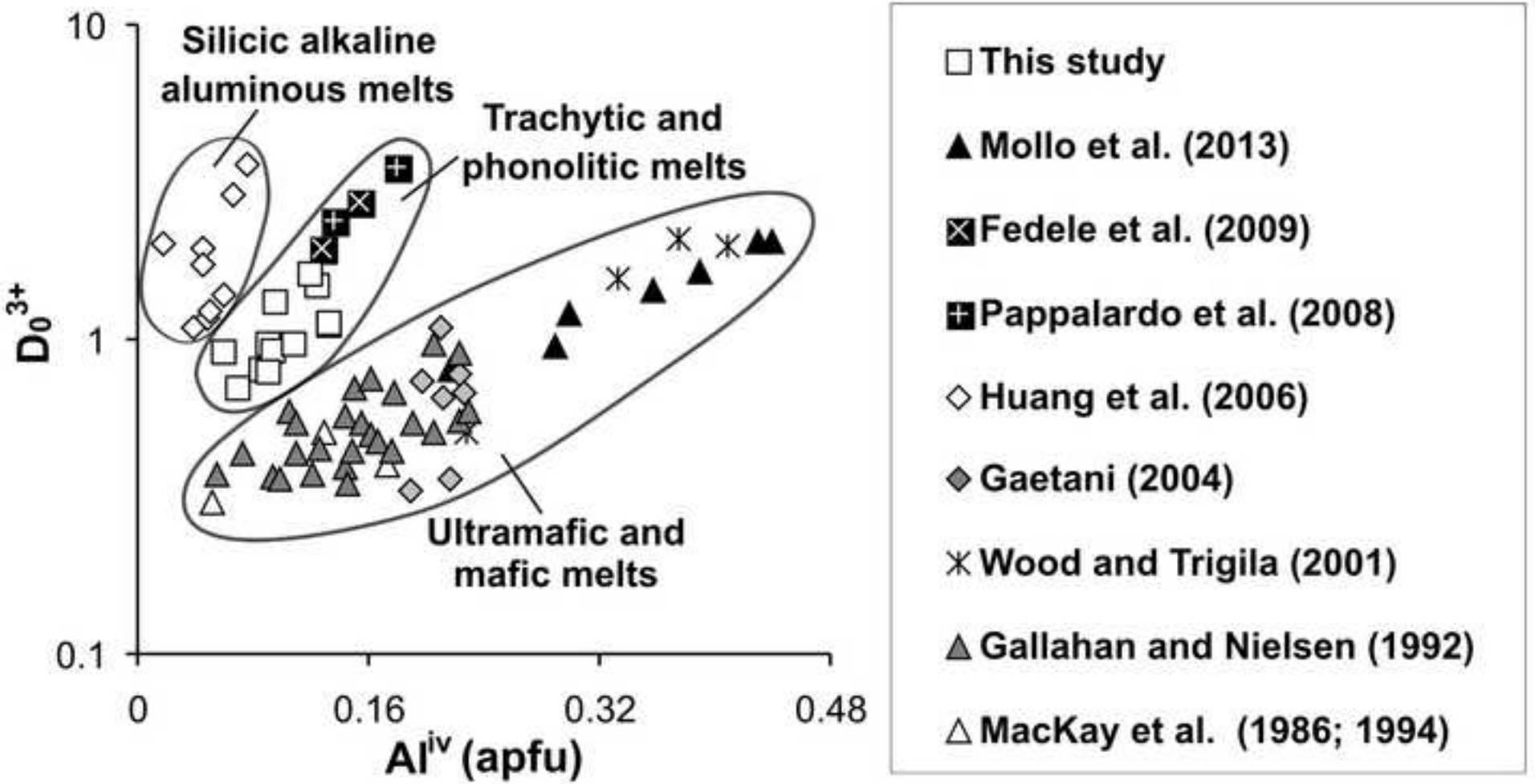

Figure6

Click here to download high resolution image

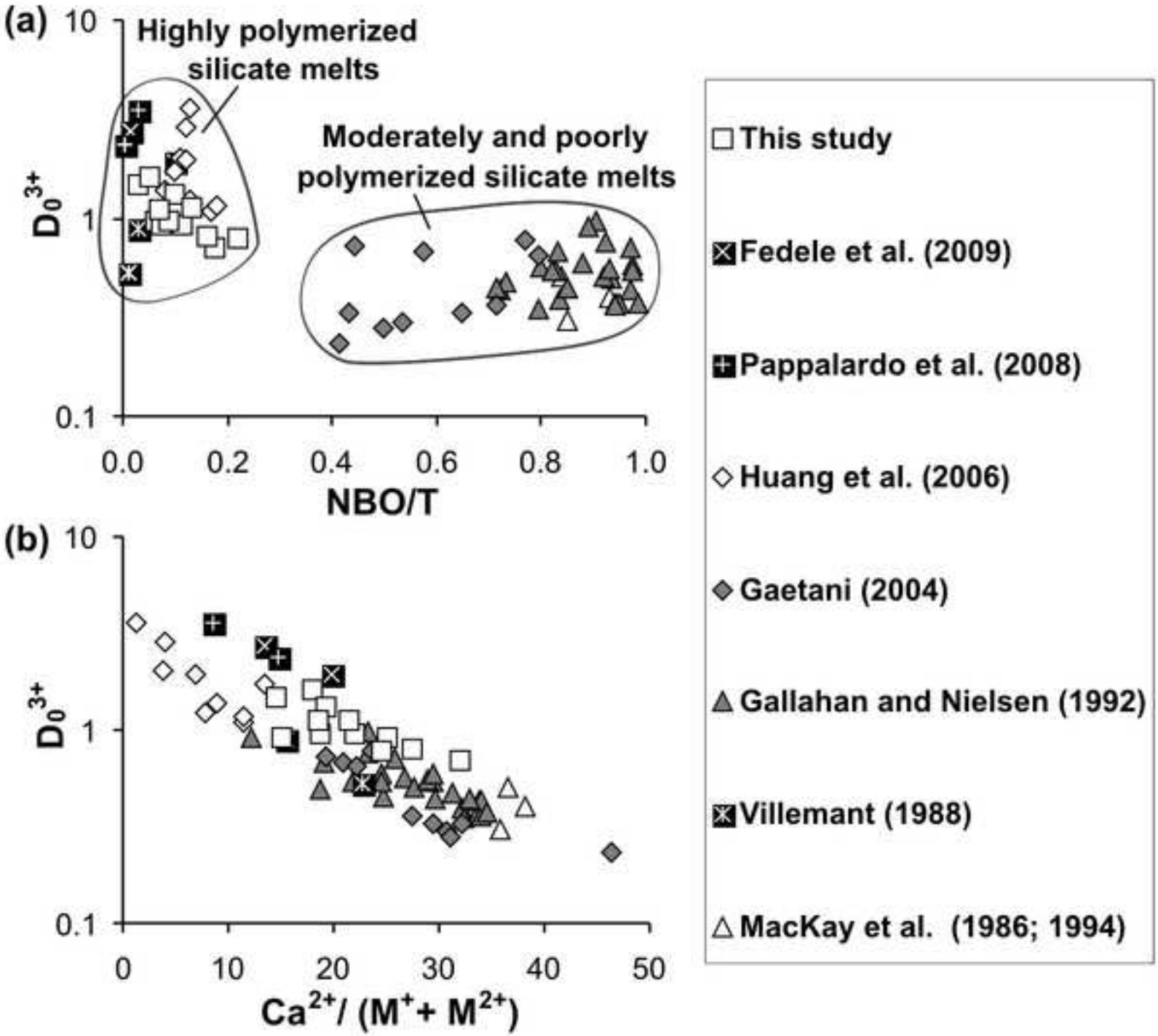

Figure7

Click here to download high resolution image

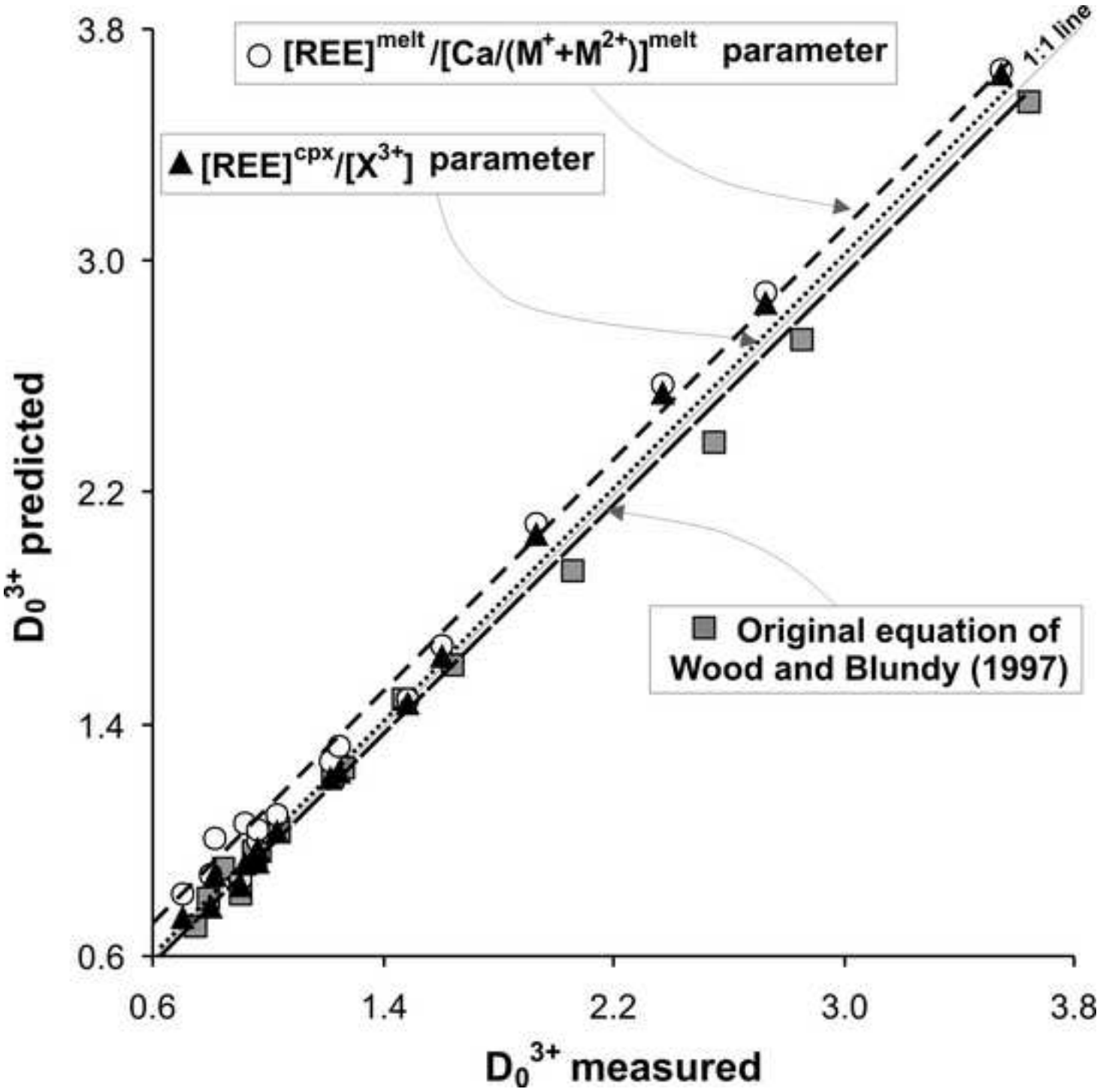

Figure8
Click here to download high resolution image

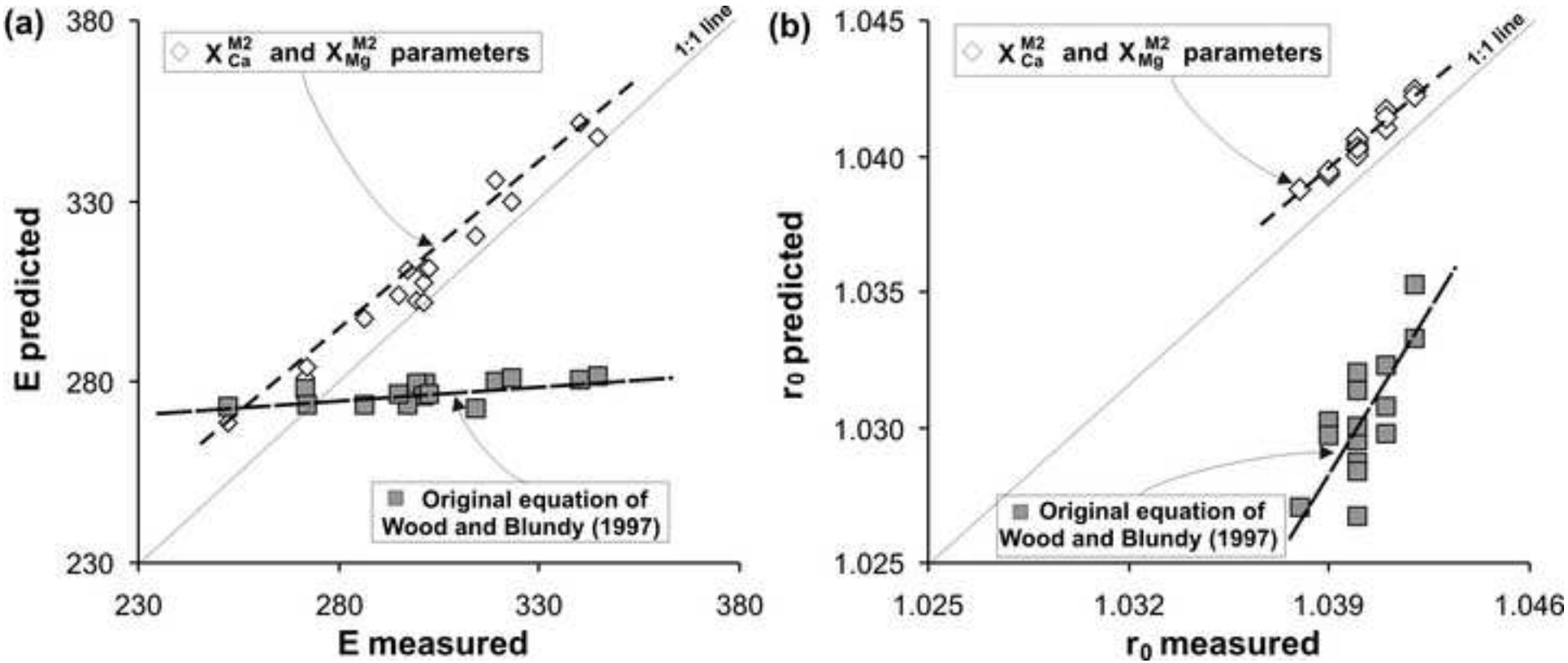

Figure9
Click here to download high resolution image

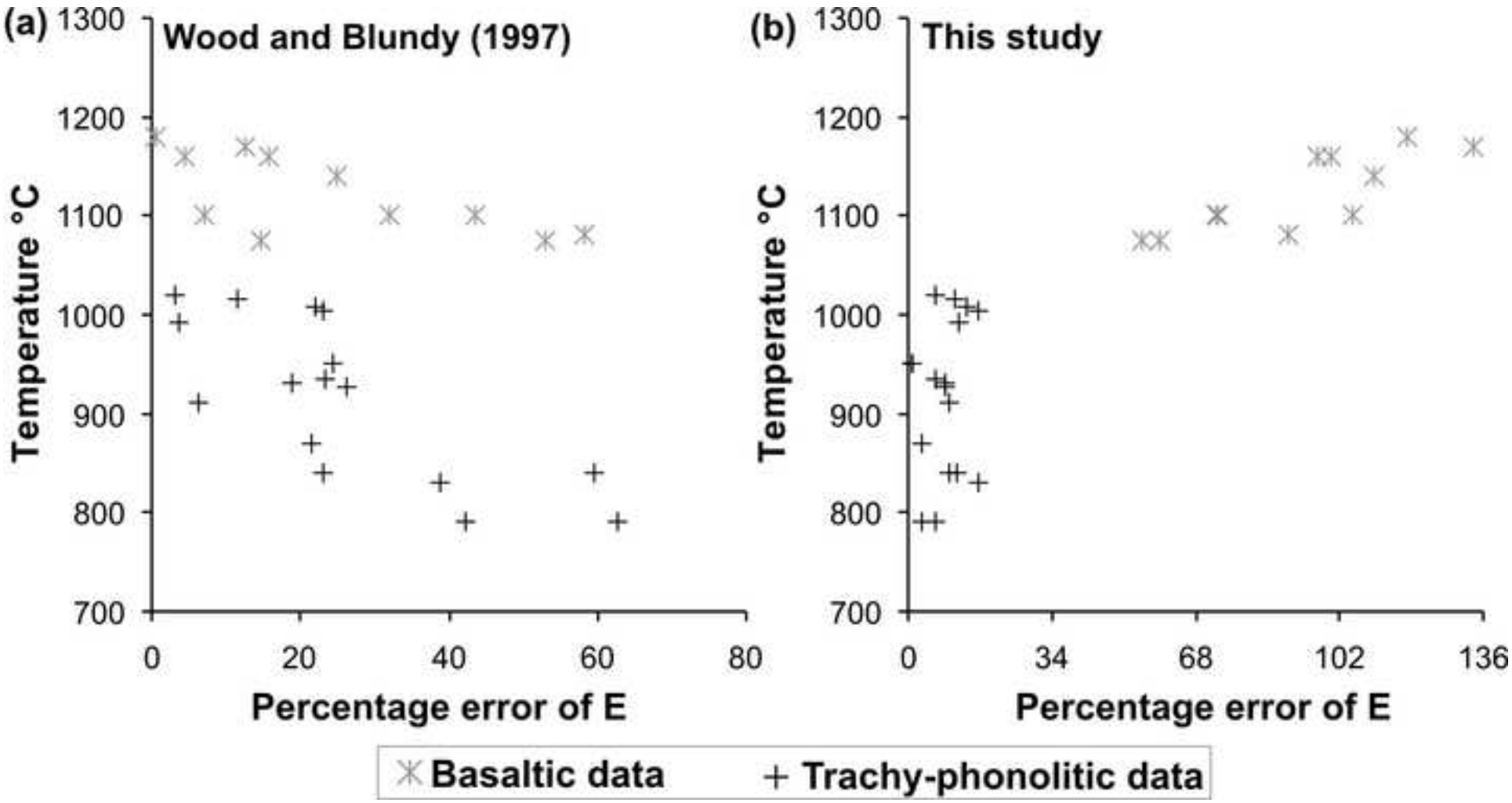

Figure10

Click here to download high resolution image

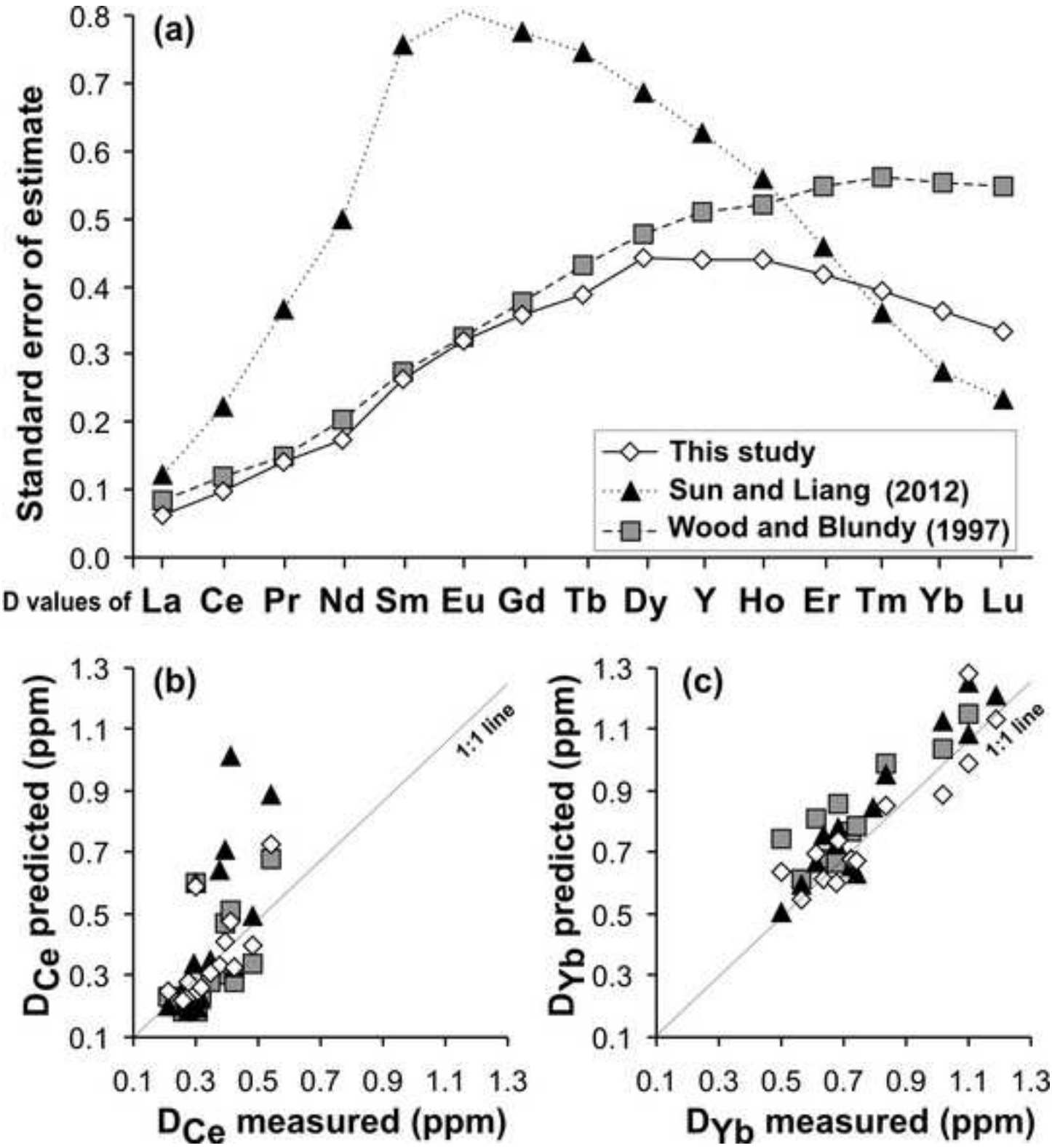

Figure11
Click here to download high resolution image

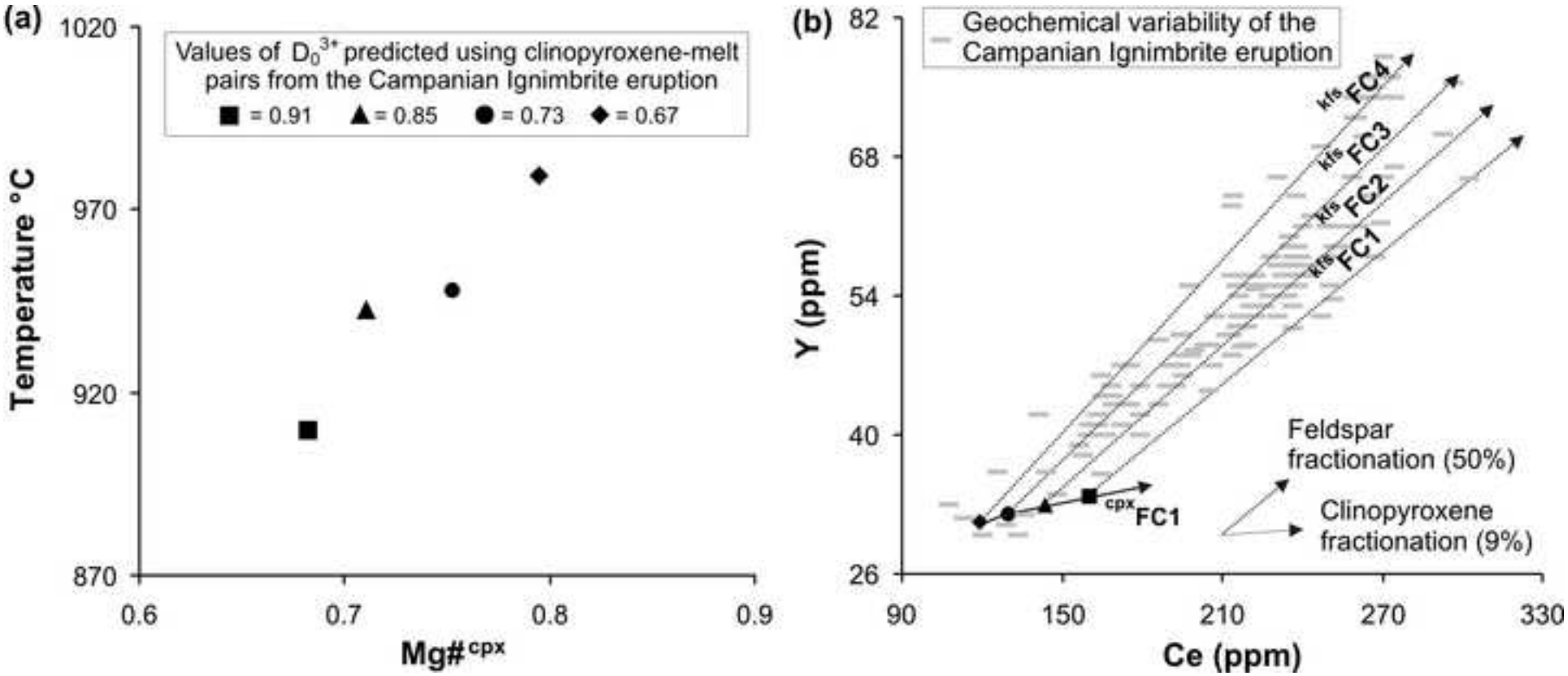

Table1S

Click here to download Background dataset for online publication only: Table 1S.xls

Table2S

Click here to download Background dataset for online publication only: Table 2S.xls

Table3S

Click here to download Background dataset for online publication only: Table 3S.xls

Table4S

Click here to download Background dataset for online publication only: Table 4S.xls

Table5S

Click here to download Background dataset for online publication only: Table 5S.xls

Table6S

Click here to download Background dataset for online publication only: Table 6S.xls

Table7S

Click here to download Background dataset for online publication only: Table 7S.xls

Table8S

Click here to download Background dataset for online publication only: Table 8S.xls

Cpx-melt D model for trachy-phonolitic compositions

Click here to download Background dataset for online publication only: CPX-MELT D MODEL FOR TRACHY-PHONOLITIC COMP